3-D Seismic Evaluation of Fault Control on Quaternary Subsidence Patterns, Rates, and Related Surface Morphology in Southeastern Louisiana

by

Terra Jane George,

B.Sc.

Thesis

Presented to the Faculty of the Graduate School of

The University of Texas at Austin

in Partial Fulfillment

of the Requirements

for the Degree of

Master of Science in Geological Sciences

The University of Texas at Austin

August 2008

3-D Seismic Evaluation of Fault Control on Quaternary Subsidence Patterns, Rates, and Related Surface Morphology in Southeastern Louisiana

Approved by
Supervising Committee:

_____

_____

_____

This thesis is dedicated to my grandmother, Eloyese, who is a constant source of love and encouragement; to my parents, Terry and Kathy, who have sacrificed much to allow me to succeed; and to my sister, Laramie, who has been a help and comfort during this process. This thesis is also dedicated to my extended family and friends, who are too many to list. Thank you all for the prayers and encouraging words, which have made all the difference.

Acknowledgments

The author wishes to express her sincere gratitude to Dr. David Mohrig for his valuable support and accurate supervision of this thesis and through-out the past two years at U.T., and to thank Drs. William L. Fisher and Ronald J. Steel for serving on this thesis committee.

Also, I would like to thank Dr. Elizabeth J. Catlos and Mr. Mark Falk for their encouragement, advice, and guidance in the preparation of this document, as well as Mr. Aymeric-Pierre B. Peyret for many hours of LaTeX-formatting assistance. Further, I would like to thank the faculty and staff of the Jackson School of Geosciences for their guidance, especially Mr. Thomas E. Hess for many hours of help with seismic processing. Additional thanks to Mr. Jeffrey Nittrouer for miscellaneous help and advice during my career at U.T.

This project was made possible by: Western Geco®, OpendTect®, Seismic Micro-Technology®, the National Center for Earth-surface Dynamics (funded by the Office of Integrative Activities, N.S.F., under agreement Number EAR-0120914), and ConocoPhillips Co.

Finally, I would like to thank God for the opportunity to work with an amazing dataset and so many talented individuals.

TERRA JANE GEORGE

The University of Texas at Austin

August 2008

3-D Seismic Evaluation of Fault Control on Quaternary Subsidence Patterns, Rates, and Related Surface Morphology in Southeastern Louisiana

Terra Jane George, MS. GeoSci.
The University of Texas at Austin, 2008

Supervisor: David Mohrig

Throughout the past century, the Louisiana coastline has been deteriorating at an alarming rate. Fault induced subsidence has been suggested to be one of the likely drivers of this land loss. I directly addressed the control of faulting on Quaternary delta subsidence using subsurface architectural data. I carried out a systematic process for evaluating fault movement on individual faults in the subsurface by using an industry grade 3-D seismic survey to evaluate the interaction of complex fault patterns and shallow substrate ($< 1s$ or $1,000m$). Using amplitude data, as well as a coherency algorithm, horizons and faults were mapped in $\sim 1400km^2$ of data in southeastern Louisiana. Measurements of fault displacement were obtained by determining time offset of

synchronous horizons. Down-to-the-basin and counter-regional growth faulting was observed. Both styles of faulting are associated with movement of Jurassic-age salt deposits and display measurable offset at depths as shallow as $\sim .450s$ (roughly $380m$). Fault displacements increase roughly linearly with burial depth. The displacement data together with well-log data provide a tentative Quaternary rate for the normal faulting of $0.1mm \cdot yr^{-1}$ to $1mm \cdot yr^{-1}$.

I have assessed the possible control of subsurface faulting on surface topography using co-registered maps of fault traces and orthophoto quadrangles. This analysis has revealed a number of instances where faulting affects modern surface morphology. Often, the up-thrown sides of growth faults are capped by marshland, whereas the downthrown blocks are drowned by $\sim .7m$ of surface water (Snedden et al., 2007). Further, the influence of faulting extends to the modern planform of the lower Mississippi River, as data indicate that growth faults control the position of a major bend near the river's outlet.

Contents

List of Tables

List of Figures

Chapter 1

Introduction

In 2005, Hurricanes Katrina and Rita brought national attention to a long-standing problem in southern Louisiana. Wetlands and barrier islands, critical for protection from storm surges, have been inundated by seawater due to rapid subsidence during the 20^{th} century (Gagliano et al. (1981); Turner and Cahoon (1988); Morton et al. (2005)). While this issue has been documented for decades by scientists and engineers (Morgan and Larimore (1957); Gagliano et al. (1981); Williams et al. (1992); Beall et al. (2005); Morton et al. (2005)), it has recently drawn the attention of political leaders due to the region's population and prominence as a major economic center for a variety of industries and commerce, including fisheries, petroleum production, and natural gas distribution (Turner and Cahoon (1988); Gagliano (2005b); Morton et al. (2005)). Further coastal deterioration increasingly subjects Louisiana to catastrophic flood events that endanger lives, in addition to the nation's economy; therefore, an understanding of the driving forces behind subsidence, and measures necessary to prevent further degradation of wetlands and barrier islands are critically important.

A considerable number of theories have been proposed concerning the fundamental causes of subsidence on the Mississippi delta (Törnqvist et al., 2006), including natural compaction of sediments (Meckel et al. (2006); Meckel et al. (2005); Törnqvist et al. (2008)), removal of hydrocarbons and formation water (Morton et al. (2001); Morton et al. (2005)) and structural deformation with associated faulting (Gagliano (2005c); Dokka et al. (2006); Dokka (2006)), leading to significant debate as to the primary drivers of land loss. Many of these studies have utilized surface measurements (GPS elevation data) and shallow sediment cores; however few have incorporated subsurface architectural data to evaluate the causes of land subsidence and coastal deterioration. This study does so by using a recently collected, 3-D seismic volume from greater Breton Sound, Louisiana. With this data I have been able to identify subsurface features, such as faults and mobile substrate (salt), which allow me to better determine the control of structural deformation and growth faulting on the patterns of delta-top subsidence.

Chapter 2

Geologic Setting

In order to comprehend how modern subsidence in coastal Louisiana is driven, it is necessary to understand the geologic history and framework of the greater Gulf of Mexico basin. Evolution of the gulf influences the contemporary processes of sedimentation and growth faulting that impact southern Louisiana today.

2.1 Mesozoic

Initial formation of the Gulf of Mexico basin is tied to early Mesozoic crustal extension and break up of the super continent, Pangaea. This rifting took place near the modern-day southern margin of the North American Plate (Dunbar and Sawyer (1988); Salvador (1991a)). By the Early Jurassic, several developing grabens were flooded with seawater, creating a restricted seaway that ran all of the way across Mexico and was connected to the Pacific Ocean. An arid climate led to the development of a hyper-saline environment in this seaway and to the widespread accumulation of salt deposits (Humphris (1978); Buffler et al.

(1980); Salvador (1991a); Diegel et al. (1995)). Roughly $1,500m$ of Jurassic-age Louann Salt was deposited during this time (Andrews (1960); Maione (2001)).

Continued rifting resulted in emplacement of oceanic crust by the Late Jurassic, marking the completion of Pangaea break up. Thermally driven subsidence of the Gulf of Mexico basin associated with the cooling oceanic crust, dominated basin development until the Cretaceous when sediment loading became the predominant subsidence mechanism (Salvador, 1991a).

The Early Cretaceous Gulf of Mexico basin experienced increased tectonic stability. Terrigenous sediments continued to be deposited into the basin, leading to mobilization of the Jurassic-age salt deposits and associated development of growth faulting (Sohl et al. (1991); Salvador (1991a); Yurewicz et al. (1993)).

A marine transgression during the Cretaceous allowed the Atlantic Ocean to finally link to the waters of the gulf. This transgression, combined with a greenhouse climate, led to the formation of many carbonate reefs throughout the basin and created a well-defined shelf margin which prograded into the basin over time (Salvador (1991a); Yurewicz et al. (1993)). The Mississippi Embayment, future site of the greater Mississippi delta, experienced varying episodes of clastic and carbonate sedimentation until the late Cretaceous when the Laramide Orogeny produced a tremendous influx of clastic sediment to the northern gulf. This sedimentation further drove salt movement and growth faulting and salt movement (Salvador, 1991a).

2.2 Early Cenozoic

The Early Cenozoic Gulf of Mexico continued to experience the delivery of large volumes of Laramide-derived terrigenous sediment to the basin. Siliciclastic sedimentation was most pronounced during the Paleocene and Early Eocene,

causing the shelf margin to prograde 240 to $290km$ from its inherited Cretaceous position (Salvador (1991a); Galloway et al. (2000)). An avenue of terrigenous sediments deposited in what is now western Mississippi, southeastern Arkansas, and northwestern Louisiana is cited as evidence for establishment of the lower Mississippi River system by the Late Paleocene/Early Eocene (Galloway et al., 2000).

Tectonic activity in the hinterland kept rates of sediment delivery to the basin relatively high until the Late Oligocene when the region experienced a long term systems-tract retreat which shrank the Mississippi Delta and allowed coastal and shelfal deposits to be reworked by longshore drift. (Salvador (1991a); Galloway et al. (2000)).

Increased arrival of sediments in the early Miocene renewed the progadation of the Mississippi River Delta, which grew larger than its Oligocene predecessor. Additional shore-zone systems were created, but were affected by sub-regional, geologically ephemeral episodes of hyper-subsidence and collapse from growth faulting and salt movement (Galloway et al., 2000). By the Late Miocene/Early Pliocene, the Mississippi River had become the principle conduit for sediment off of the craton. Nearly $4,000m$ of terrigenous clastics were deposited over 4 million years during the Pliocene, the highest sedimentation rate observed for the Cenozoic. This large volume of fluvial-deltaic sediments prograded the shoreline and continued activating growth faulting and movement of Jurassic-age salt (Salvador, 1991a).

2.3 Quaternary

Pleistocene climate changes dramatically altered the sedimentation patterns in the gulf. The last major continental glaciation lowered mean sea level by $\sim 150m$ relative to today, exposing large areas of the northern shelf. Previously

deposited shelf sediments were eroded and entrenched by channels traversing this exposed surface. The re-eroded sediment was deposited at the shelf edge and on the continental slope, off the shore of modern-day Louisiana (Fisk (1944); McFarlan (1961); Salvador (1991a); Galloway et al. (2000), Kulp et al. (2002)) and the contemporary Mississippi Delta.

During this time, nearly $3,800m$ of sediments were deposited, triggering additional gravity slumping, growth faulting, and salt movement. As the Jurassic-aged salt mobilized, it further influenced the distribution and deposition of clastic sediments. These features are still active processes in the contemporary basin (Salvador, 1991a).

Another affect of salt movement and growth faulting is the occurrence of mini-basins. These basins, which are found between allochtonous salt diapirs, have some of the highest subsidence rates recorded, and are found throughout the Quaternary (Worrall and Snelson (1989); Salvador (1991a); Jackson et al. (1994b) or Jackson et al. (1994a); Schuster (1995); Gras et al. (1998)). These salt bodies, mobilized in the early Cenozoic, have moved horizontally through the basin as much as $150km$ from their original site of deposition (Salvador, 1991a).

The Holocene history of the Gulf of Mexico is characterized by sea-level rise from deglaciation. The Mississippi River acted as a conduit for delivering large volumes of glacial meltwater to the basin (Ruddiman and Wright (1987); Salvador (1991a); Kulp et al. (2002)). Incised areas created during the previous sea-level fall were flooded, and sediments began to fill these canyons (Fisk (1944); Fisk et al. (1954); Coleman et al. (1991); Kulp et al. (2002)). Sedimentation associated with the Mississippi River substantially prograded its delta, creating surface features such as barrier islands, wetlands, lagoons, beaches, and dunes that are still seen today (Fisk (1944); Morgan and Larimore (1957);

Salvador (1991a); Williams et al. (1992); Kulp et al. (2002)). Syn-depositional growth faulting and salt movement continued as a result of sediment loading and still persists today (Coleman et al. (1991); Gagliano (2005a); Dokka et al. (2006)).

Landforms, which were created by an influx of Quaternary sediment, (Coleman et al. (1991); Salvador (1991a); Williams et al. (1992)) are maintained by sediment supplied predominately by the Mississippi River (Fisk (1944); Coleman (1988); Coleman et al. (1991); Williams et al. (1992); Kulp et al. (2002)). The continued addition of new sediment is necessary to counteract land-surface subsidence (Penland *et al.,* 1992) associated with natural compaction (Meckel et al. (2007); Törnqvist et al. (2008)), salt movement, and growth faulting (Worrall and Snelson (1989); Salvador (1991a), Diegel et al. (1995)). Traditionally, flood events and avulsions have provided the sediment to replenish subsiding coastal landforms such as barrier islands (Fisk (1944); Coleman (1988); Boyd et al. (1989); Penland et al. (1988); Williams et al. (1992)). Avulsions of small distributaries and of the larger channel have occurred throughout the history of the river, with at least three events taking place on the main channel during the Holocene (Aslan et al., 2005). It has been estimated that avulsions of the Mississippi River have happened roughly every $1,000$ years during the Holocene, and its further been suggested that the river was experiencing an incipient avulsion into the mid-twentieth century that was averted by construction of the Old River Control Structure (Fisk et al. (1954); Aslan et al. (2005)).

2.4 Human Influence on Delta

Various other engineering efforts have been implemented on the river under the authority of the Mississippi River and Tributaries Project (MR&T) (Biedenharn et al., 2000). Artificial features such as meander cutoffs, levees, and river-

training dikes were constructed to steady the main channel and its distributaries (Biedenharn et al., 2000), reducing the natural process of avulsion which is critical for maintaining subsiding coastal landforms (Fisk et al. (1954); Coleman (1988); Williams et al. (1992); Beall et al. (2005)). The stabilization of the Mississippi River, while intended to quell flooding events, has resulted in the efficient transport of sediment all of the way to the shelf edge. Because of this new depositional regime, coastal features that rely on sediment to overcome the effects of subsidence are steadily drowning (Williams et al. (1992); Day et al. (2007)).

Reduction of wetlands, barrier islands, and other coastal landforms has been occurring at rates as high as $100km^2 \cdot yr^{-1}$ (Gagliano et al. (1981); USGS (2003); Day et al. (2007)). It is estimated that from 1932-2000, Louisiana lost approximately $3,050km^2$ of land, while an additional $1,100km^2$ is projected to be inundated during the next 50 years (USGS, 2003). This loss is significant because these shore-zone features provide essential protection for Louisiana's wide variety of commerce and its increasing population from damaging, high-energy waves and storm surges (Williams et al. (1992); Stone et al. (2004); Day et al. (2007); Törnqvist et al. (2008)). The need for the protection was quite apparent in 2005 when Hurricanes Katrina and Rita pummeled the coast, creating wide-spread destruction and loss of life.

Overall, the Cenozoic history of the Gulf of Mexico, particularly in the Mississippi Delta region, has been marked by high sedimentation rates, which in turn have driven growth faulting and Jurassic-age salt movement. These processes, coupled with natural compaction, have led to well documented areas of hyper-subsidence. Large volumes of sediment, historically deposited on the coast through processes such as avulsion and regional-scale flooding, minimized the effects of subsidence and maintained shore-zone features critical for

protection against storm surges. Artificial stabilization of the Mississippi River has limited its ability to effectively disperse sediments, allowing wetlands and barrier islands to succumb to the effects of on-going subsidence.

It is evident that both human interaction and natural geologic phenomena are influencing the modern surface morphology of coastal Louisiana. This study seeks to delineate the location, frequency, and severity of subsurface features, namely faults, using industry seismic data with well control. A more complete knowledge of fault controlled subsidence is necessary input data for any program designed to restore wetlands.

Chapter 3

Previous Work

For decades, researchers have attempted to quantify the drivers of subsidence in Mississippi River delta and to understand their influences on wetland loss in coastal Louisiana. Subsidence is most often measured by radiocarbon dating buried peat deposits or by recording vertical displacement of benchmarks on surface structures (Morton et al. (2001); Gagliano (2005a); Gagliano (2005c); Gagliano (2005b); Dokka et al. (2006); Törnqvist et al. (2008)). Other methods used to obtain subsidence measurements include: satellites, tide gage records, movement of historical and archeological features, and total area of land loss (Gagliano (2005a); Gagliano (2005c); Gagliano (2005b)). Some 2D seismic lines have been used to identify faulting related subsidence (Lopez et al., 1997), but no comprehensive studies have been completed using modern-day 3-D seismic data.

3.1 Measured Subsidence Rates

Subsidence rates in coastal Louisiana have been studied by many researchers over roughly the past century. The results of several of those studies are pre-

sented in Table 3.1 (located at the end of the chapter). A variety of methods have been employed to estimate subsidence rates, yielding values that range from $0 - 30mm \cdot yr^{-1}$.

The approaches taken in previous work are problematic because of heavy reliance on surface or very shallow subsurface data to make claims about deep seated subsurface processes. Few workers have incorporated any seismic data (Lopez et al., 1997) into their interpretations creating a situation with vast amounts of generated values, but little understanding about the subsurface components that influence those values. This problem is reflected not only in the table, but in many of the controversies that have been stirred as political leaders look to scientific studies to evaluate proposed solutions for combating the subsiding Louisiana coastline.

3.2 Proposed Drivers of Subsidence

Many different explanations have been offered to account for the highly variable subsidence rates measured in southern Louisiana. Three of the most commonly cited explanations for this subsidence are: 1) natural compaction of shallowly buried sediments; 2) compaction via pore-space reduction associated with withdrawal of groundwater and hydrocarbons (oil and natural gas); and 3) faulting. Each of these causes has been the subject of multiple papers, special reports, and in some cases, political hearings.

3.2.1 Subsidence from Natural Compaction

Shallow compaction refers to the thinning of a column of sediment due to natural mechanical reorganization of grains that leads to a reduction in porosity (Meckel et al., 2006). This process increases the bulk density of the sedimentary deposit and causes an overall decrease in its volume. It has been proposed

that shallow compaction is the primary force causing subsidence in southeastern Louisiana (Törnqvist et al., 2008).

Subsidence attributed to natural compaction has been measured at rates up to $5mm \cdot yr^{-1}$ using C-14 dating of buried peat deposits (Törnqvist et al., 2008) and $2.2mm \cdot yr^{-1}$ using stochastic numerical models (Meckel et al., 2006). Morton et al. (2005) and Meckel et al. (2006) provide values for 104 measurements of subsidence using buried peats. The average subsidence rate for this data set is $1.4mm \cdot yr^{-1}$. This rate is associated with a time averaging interval of $100+$ to 1000 years and should be thought of as a long-term value. Subsidence rates associated with only natural compaction are significantly less than the unusually high rates recorded in some places (Table 3.1). Because the measurements are taken near the surface, the shallow substrate methods often record total subsidence acting upon an area, limiting the ability to independently evaluate this component.

3.2.2 Subsidence from Removal of Subsurface Fluids

Southern Louisiana has long been a site of substantial hydrocarbon and groundwater extraction since the 1940s. Observed wetland decline around well sites has created suspicion that subsidence is induced as subsurface fluids are extracted (Morton et al., 2001). Studies conducted on benchmarks and sediment cores within multiple production areas have shown subsidence rates as high as roughly $30mm \cdot yr^{-1}$ (Morton et al. (2001); Table 3.1). This high rate suggests accelerated subsidence in areas where subsurface liquids are being pumped out. However, use of shallow borings and benchmarks alone does not allow the subsurface fluid removal component to be tested independently, as these methods of measurement record total subsidence at or near the surface.

3.2.3 Subsidence from Faulting

As previously highlighted in the geologic history section, large volumes of sediment have been deposited in the Mississippi Delta, triggering the movement of the buried, Jurassic Louann Salt. Sediment loading and salt movement has produced a vast network of growth faults. Since the 1970s many of these faults have been mapped in coastal Louisiana (Hickey and Sabate (1972); Lopez et al. (1997)). The presence of these features has led several researchers to propose that movement along growth faults exerts a primary control on subsidence rates (Lopez et al. (1997); Gagliano et al. (2003); Gagliano (2005a); Gagliano (2005c); Gagliano (2005b); Dokka (2006); Dokka et al. (2006)).

The term "growth fault" refers to a style of normal faulting that occurs syn-depositionally. Because fault movement is concurrent with deposition, the downthrown block (hanging wall) is characteristically thicker than the footwall (Suppe, 1985). The listric shape of these faults creates characteristic "rollover" and "depression" features which are sites of enhanced subsidence (figure 3.1). A regional growth fault is oriented with the hanging wall situated towards the basin, while the hanging wall of the counter-regional fault is situated away from the basin (figure 3.2). Counter-regional faults, though they have a similar geometry as regional growth faults, are specifically associated with salt movement.

In southern Louisiana growth faults have generally been detected using aerial photographs, offsets on structures, previously published fault maps, personal interviews, geomorphic alterations, and in some cases, 15 to 30 year old 2-D seismic data consisting of only a few lines (Hickey and Sabate (1972); Lopez et al. (1997); Gagliano et al. (2003); Gagliano (2005b); Dokka et al. (2006)). These data types are pieced together to locate faults in order for subsidence measurements to be obtained. Measurements of fault related subsidence are

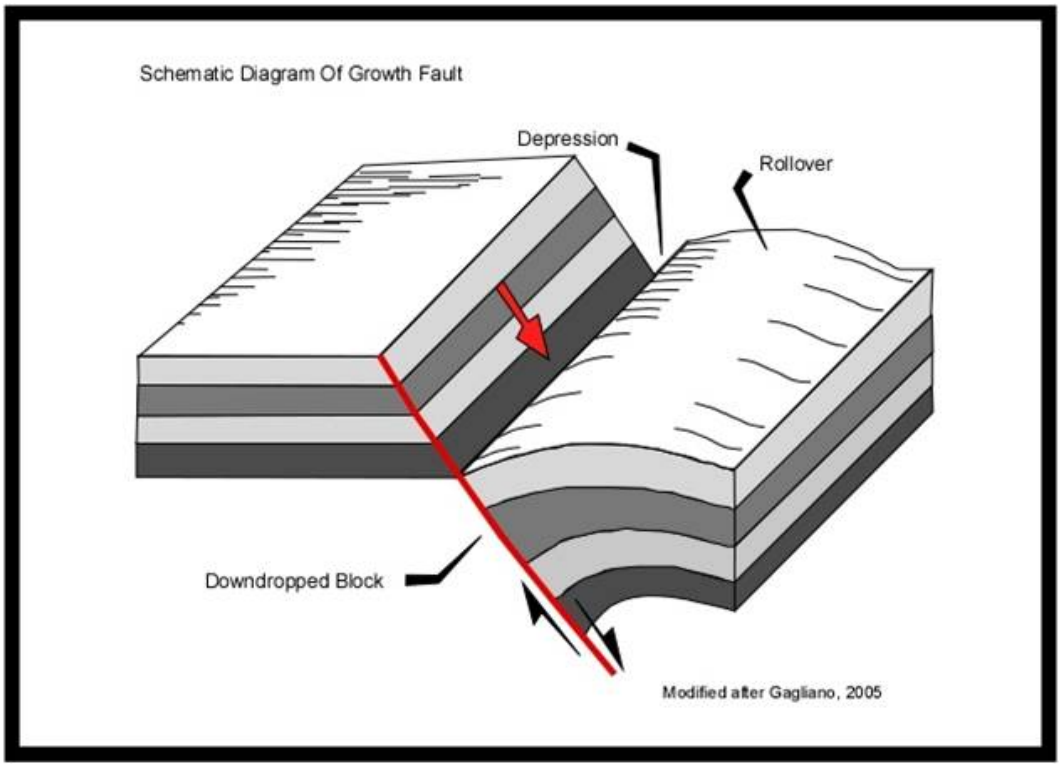

Figure 3.1: Schematic diagram of growth fault, modified after Gagliano (2005b). Subsidence occurs along the depression of a growth fault.

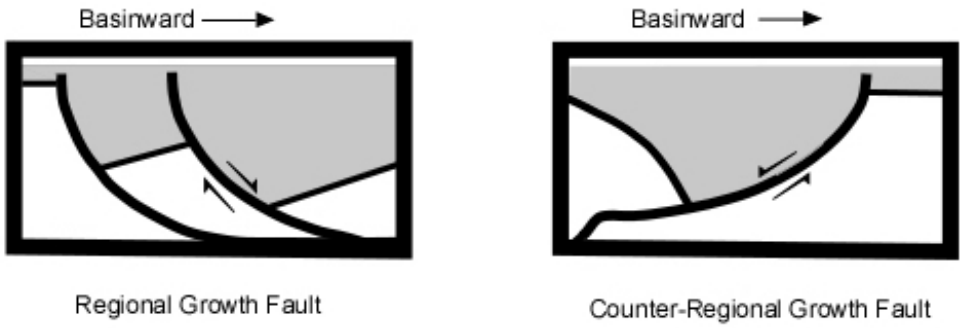

Figure 3.2: Regional growth faults are oriented slipping towards the basin, while counter-regional growth faults slip away from the basin. Modified after Schuster (1995)

frequently made by using vertical displacement on benchmarks and tide gauge records (Gagliano (2005b); Dokka (2006); Dokka et al. (2006)). In some studies, displacements of structures such as roads, buildings, railroads, and bridges have also been utilized (Lopez et al. (1997); Gagliano et al. (2003)). Many different combinations of methods to locate faults and measure displacement have been used, yielding a variety of subsidence rates and in turn, many proposed theories to account for those rates.

3.2.3.1 Fault Related Studies

One of the first studies attempting to quantify growth fault movement in southeastern Louisiana was completed near Lake Pontchartrain (figure 3.3) (Lopez et al., 1997). Using shallow 2D seismic provided by the USGS, two faults were identified in three lines. During a six-year period, offsets on railroad bridges which crossed the faults were recorded. This study reports a range in vertical displacement rates across faults of $2.5mm \cdot yr^{-1}$ to $10mm \cdot yr^{-1}$ (Lopez et al., 1997). These relatively instantaneous or "modern" rates for normal fault displacement are substantially greater than other fault displacement rates collected in the Lake Pontchartrain area. Averaged over $1,000,000+$ years, these reported long-term or "geologic" rates range between $0.003mm \cdot yr^{-1}$ to $0.064mm \cdot yr^{-1}$ (Lopez et al., 1997). Lopez et al. (1997) suggested that this discrepancy in rates is a consequence of longer term geologic rates including both times of fault motion and times of quiescence, while the "modern" rates include only active fault displacement.

In 2004, the U.S. Department of Commerce, along with the National Oceanic and Atmospheric Administration released a study which measured subsidence using leveling lines and GPS data on roadways, buildings, and other structures located in Louisiana, Mississippi, Alabama, Florida, Texas, and Ten-

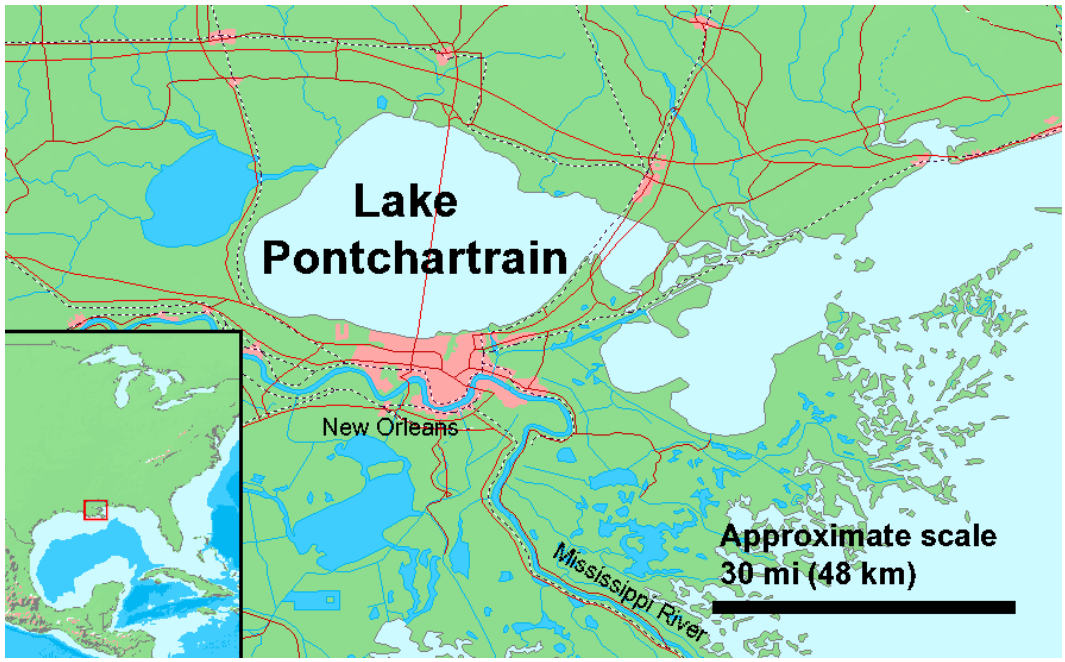

Figure 3.3: The Lake Pontchartrain area served as a site for early fault related subsidence studies by Lopez et al. (1997). GNU Free Documentation Image License.

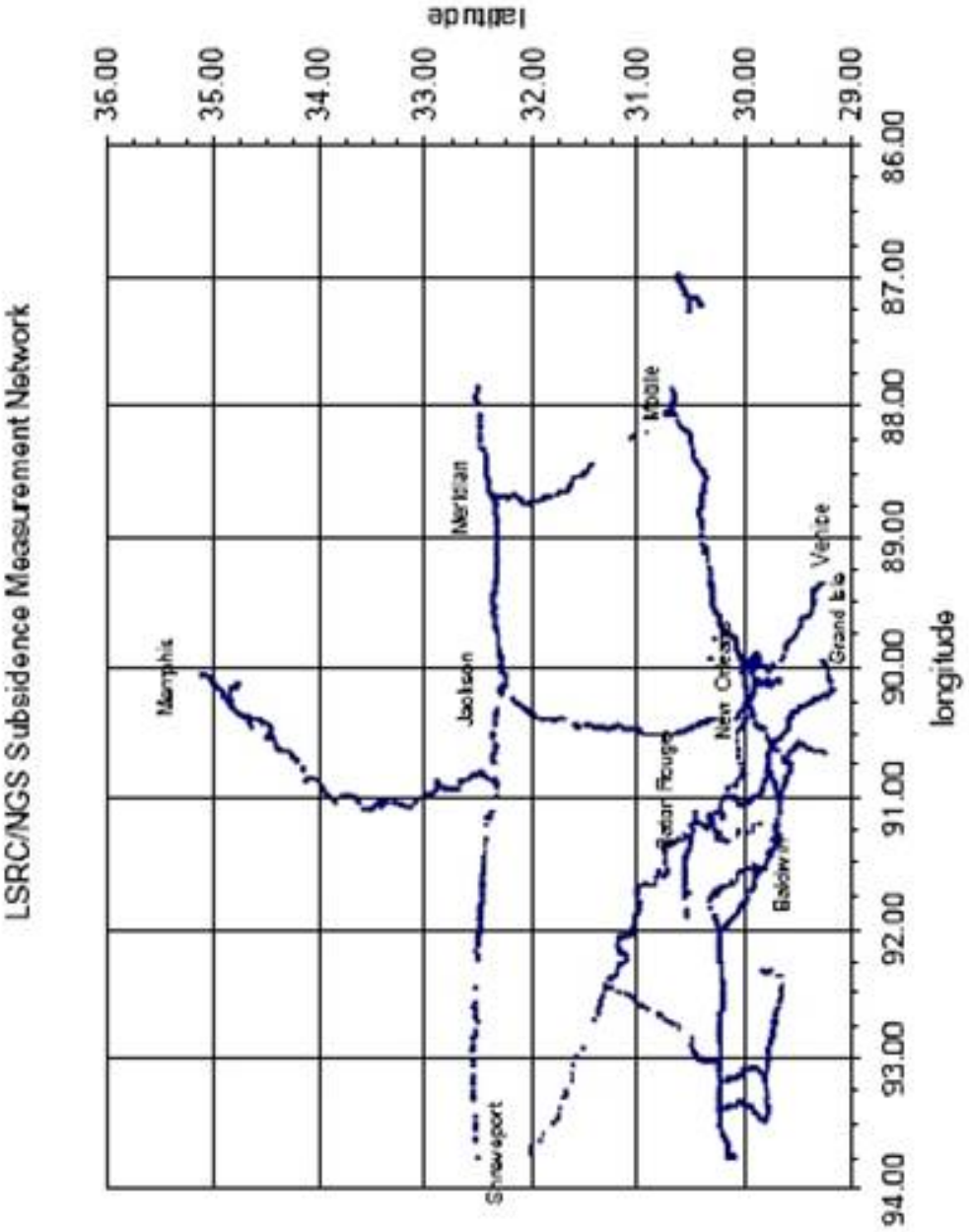

Figure 3.4: First-order benchmarks are usually located on roadways or railroads, which have significant traffic (Shinkle and Dokka, 2004).

nessee (Shinkle and Dokka, 2004). Although this study did not explicitly study faulting, it has been the catalyst for subsequent research (Dokka et al. (2006); Dokka (2006)) on fault induced subsidence using similar methods. Figure 3.4 shows the locations of the first-order benchmarks that were used by Shinkle and Dokka (2004) to calculate subsidence. The "roadmap" likeness of this network (Shinkle and Dokka, 2004) is due to the benchmarks being placed along prominent highways and railways. These measurements were tied to the North American Vertical Datum of 1988 (NAVD 88).

A subsidence rate network was determined by comparing first-order leveling data on benchmarks during the past ~ 80 years. In southeastern Louisiana subsidence network values range from $0 - 25mm \cdot yr^{-1}$, with an average rate of $11mm \cdot yr^{-1}$. Figure 3.5 represents the measured subsidence rate on each benchmark by color, while figure 3.6 is a graphical representation of these values. According to the authors, "a great many assumptions, judgments, and choices went into assembling the network and computing the vertical displacement rates for each benchmark".

Shinkle and Dokka (2004) assessed the validity of the subsidence network numbers by comparing them to information from tide records and continuously operated reference stations (CORS). Unfortunately, they found that no legitimate NAVD 88 elevation reference points were located across a substantial portion of the lower Mississippi Valley and that historical leveling data was unreliable for establishing current elevations. Because the previous elevation data was thought to be invalid, other surficial methods of determining subsidence were deemed useless. However, the authors propose that "ongoing vertical displacement must be monitored at a few fundamental locations and propagated through a base network using periodic reobservations" because elevations on benchmarks are not stationary. It was further concluded that be-

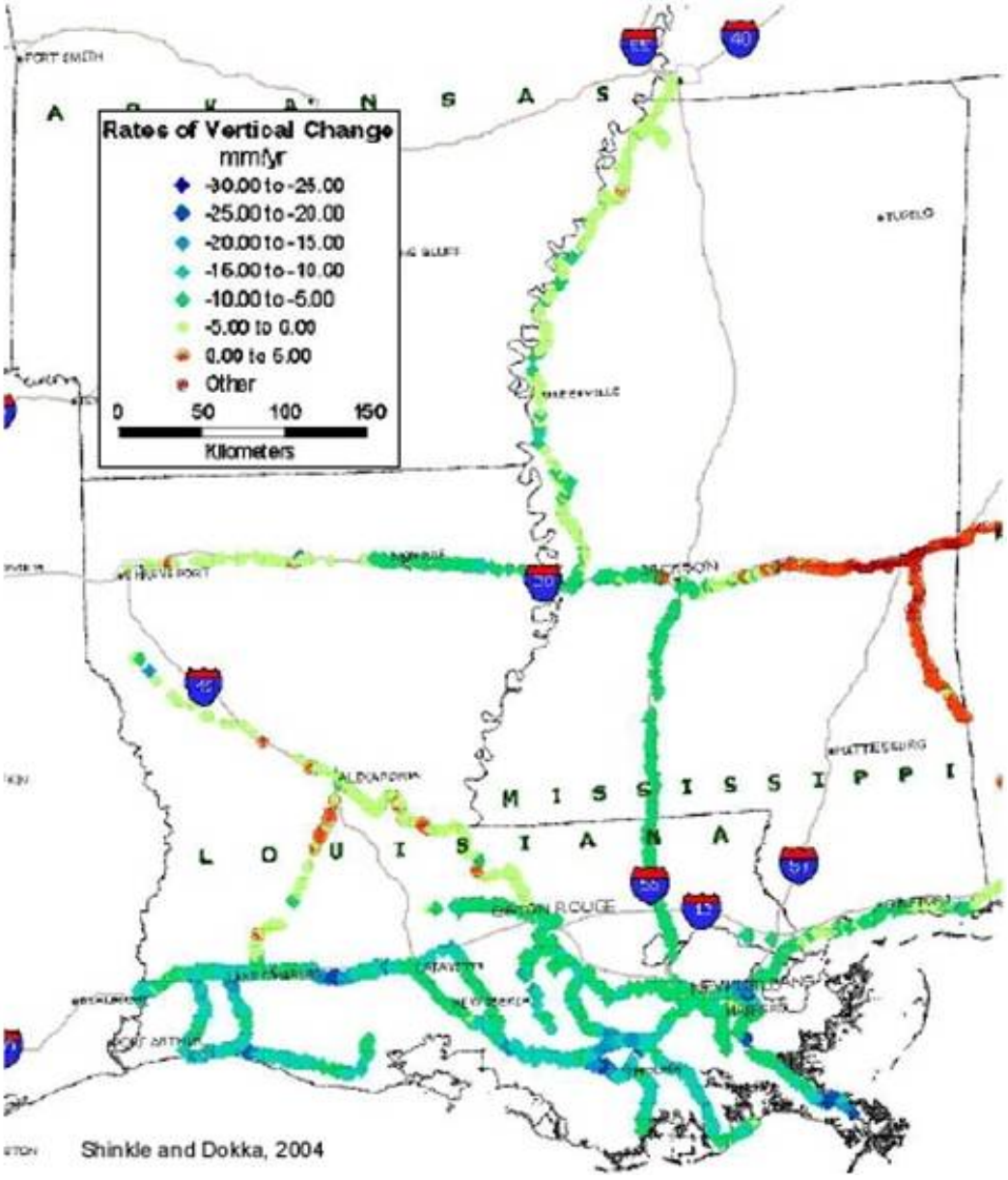

Figure 3.5: Colored representations of subsidence rates measured from first-order benchmarks. High subsidence rates ($10 - 30mm \cdot yr^{-1}$), seen in cool colors, are located through out coastal Louisiana (Shinkle and Dokka, 2004).

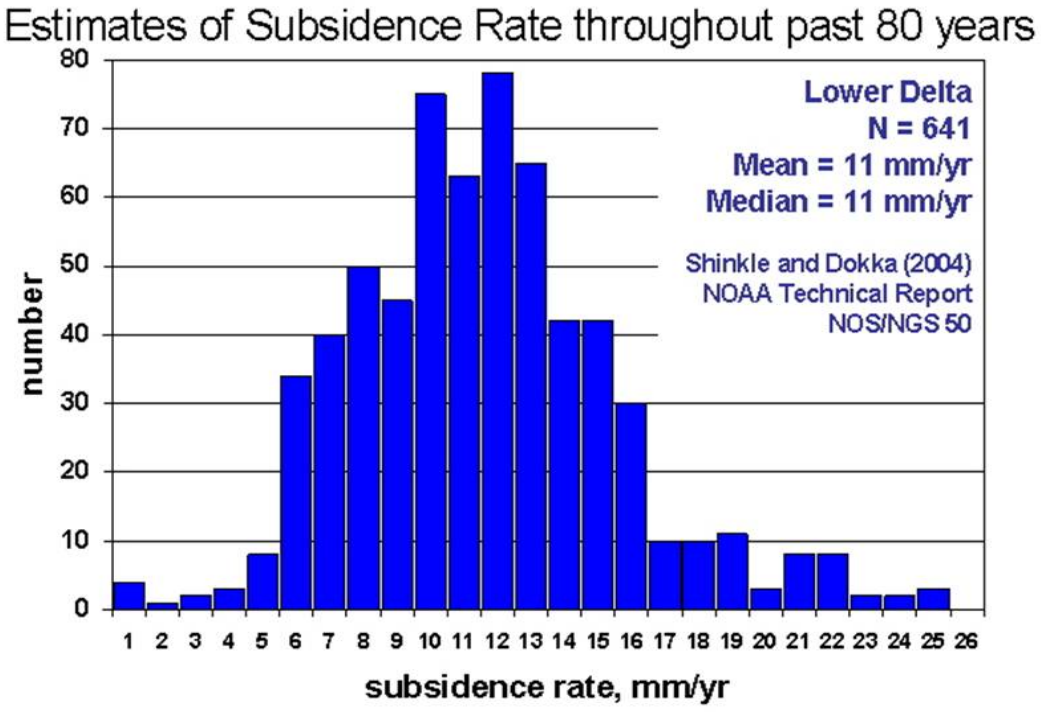

Figure 3.6: Graphical representation of subsidence rates measured from leveling data off first-order benchmarks.

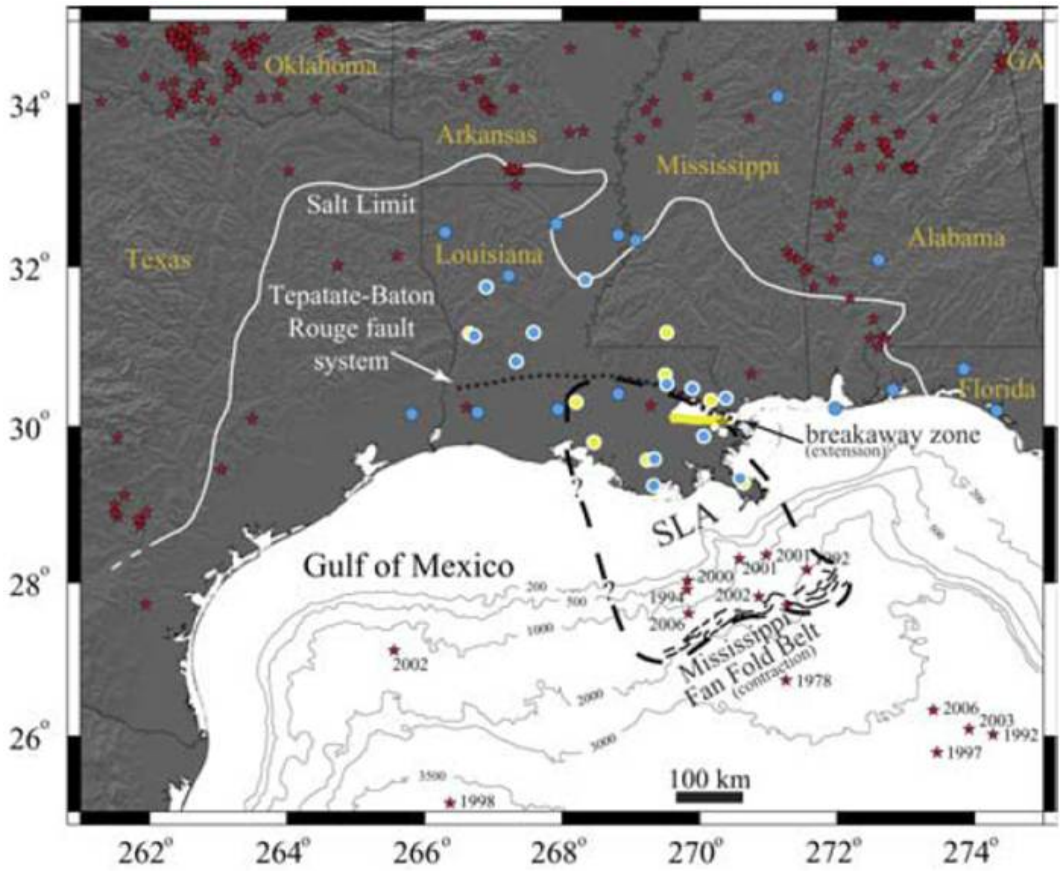

Figure 3.7: Results from leveling data led Dokka to propose a slump block known as the South Louisiana Allochthon as the cause of fault-related subsidence in coastal areas (Dokka et al., 2006).

cause subsidence rates at individual points vary through time and over considerable spatial extents, vertical displacement rates may not change according to a linear function. Therefore, predictive models must take spatial and temporal rate variations into account (Shinkle and Dokka, 2004).

Shinkle and Dokka (2004) was followed by two similar studies, Dokka et al. (2006) and Dokka (2006). These two studies focused specifically on measuring subsidence from fault movement by expanding on the GPS data evaluated during the 2004 study. Dokka et al. (2006) applied GPS data obtained from 1995-2006 in order to evaluate subsidence from tectonic processes in the Mississippi Delta region. Both episodic observations (EGPS), which measures elevation changes over the course of a few days every one to two years, and continuously observed sites (CGPS), which constantly records elevation changes over 2-11 years, were used.

Individual faults along the coast are difficult to identify. Marshland, which is pervasive in many areas of southern Louisiana, mars clear surface expression of faults. This issue is reflected in the author's statement "proof that well-mapped subsurface faults are currently active and disrupt the surface is elusive" (Dokka et al., 2006). In light of this challenge, the Michoud fault system (located in close proximity to the northern margin of the Mississippi River at the northern structural edge of the basin), which had been identified and mapped using well cut-off and seismic reflection surveys (Hickey and Sabate (1972); McBride (1998)) was selected for study by Dokka et al. (2006).

Areas north and south of the Michoud and Tepatate-Baton Rouge fault system were measured using EGPS and CGPS on benchmark locations ranging from $14m$ to $30m$ deep rods to masonry buildings with stable foundations. This data was compared to previous leveling data (deemed invalid by the 2004 study) in the area. Results showed insignificant differential subsidence and

horizontal motion in sites north of the fault system; however areas to the south exhibited a subsidence rate of $5.2 \pm 0.9 mm \cdot yr^{-1}$ and moved southward relative to North America at velocities of $2.2 \pm 0.6 mm \cdot yr^{-1}$. Using this data, Dokka et al. (2006) suggested that southeast Louisiana is a regional coupled extentional-contractional complex with rates similar to the east-west extension of the contemporary central and eastern Basin and Range province. A large portion of southwestern Louisiana and the Gulf of Mexico, termed the South Louisiana allochthon (SLA), is thought to be detaching and moving south-southeast (Figure 3.7).

The second study (Dokka, 2006) looked at historical leveling data on benchmarks using the NAVD88 vertical datum. Once again using various benchmark locations near the Michoud Fault, velocities for years $1955 - 1969$, $1969 - 1971$, $1971 - 1977$, $1977 - 1995$, and 2005 were evaluated. Subsidence was broken into three categories: shallow, intermediate, and deep. The deep component, which specifically evaluated tectonism, was measured from the motions of benchmark BH1089, attached to a $2011 - m$ well. According to this study, subsidence rates from tectonic processes were $16.9 mm \cdot yr^{-1}$ $(1969 - 1971)$ and $7.1 mm \cdot yr^{-1}$ $(1971 - 1977)$, and accounted for 73% and 50% of the total subsidence measured during these time periods. It was suggested that these subsidence rates coincided with slip on the Michoud Fault, part of the proposed southern Louisiana allochthon, that occurred from $1969 - 1995$.

Other efforts have been made to systematically evaluate the significance of fault-induced subsidence. Gagliano et al. (2003) used previously published maps, including Wallace (1966), Hickey and Sabate (1972), and available mega-regional seismic cross sections from McBride (1998) and Strover et al. (2001) to identify 100 fault traces (Fig. 3.8) and create a regional structural framework for southeastern Louisiana. Figure 3.9 illustrates a cross section of the struc-

tural framework that was developed by overlaying surficial fault maps with mega-regional seismic lines.

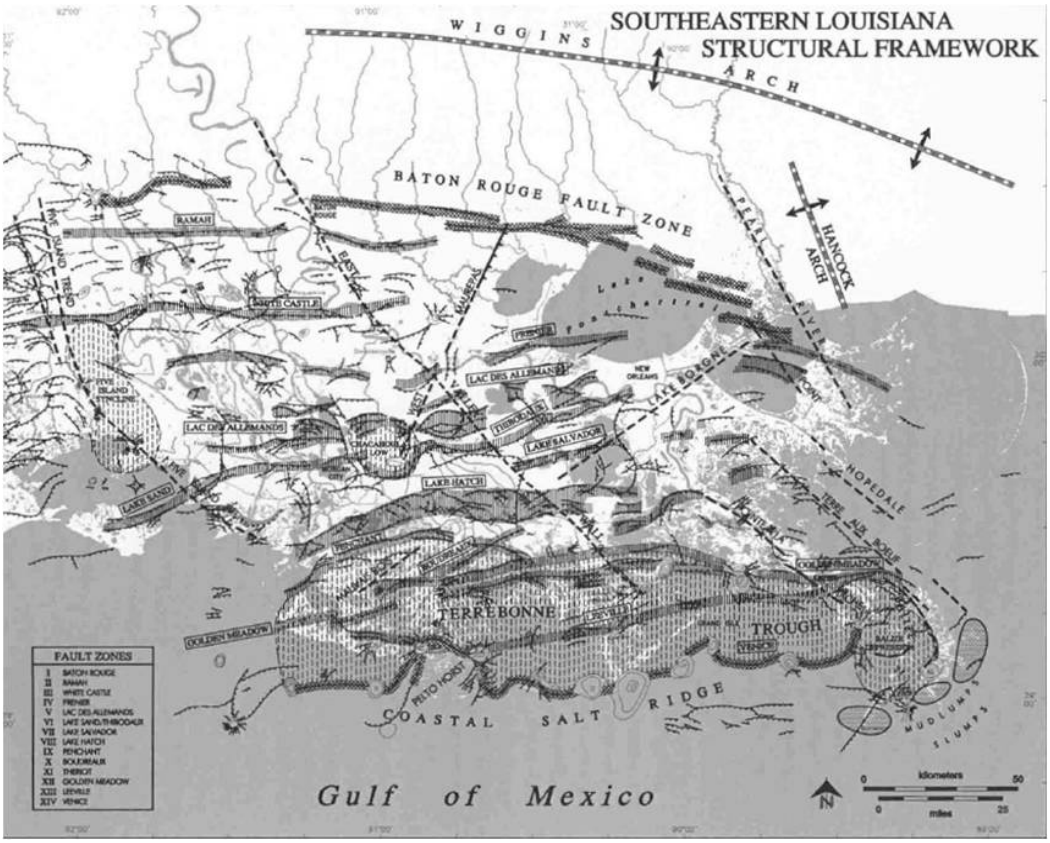

Figure 3.8: Using maps and mega-regional seismic cross sections, Gagliano identified 100 fault traces making up the structural framework of Southeastern Louisiana. Gagliano et al. (2003)

Surface expressions of faults were identified using maps, aerial images, published descriptions, and personal interviews. This surface data was fitted to a north-south mega-regional cross section from McBride (1998), with a 61% correlation between surface faults and subsurface faults (Gagliano et al., 2003). The magnitude, rate of movement, and frequency of these faults were measured using maps, aerial imagery, geoarchaelolgical data, tide gauge records,

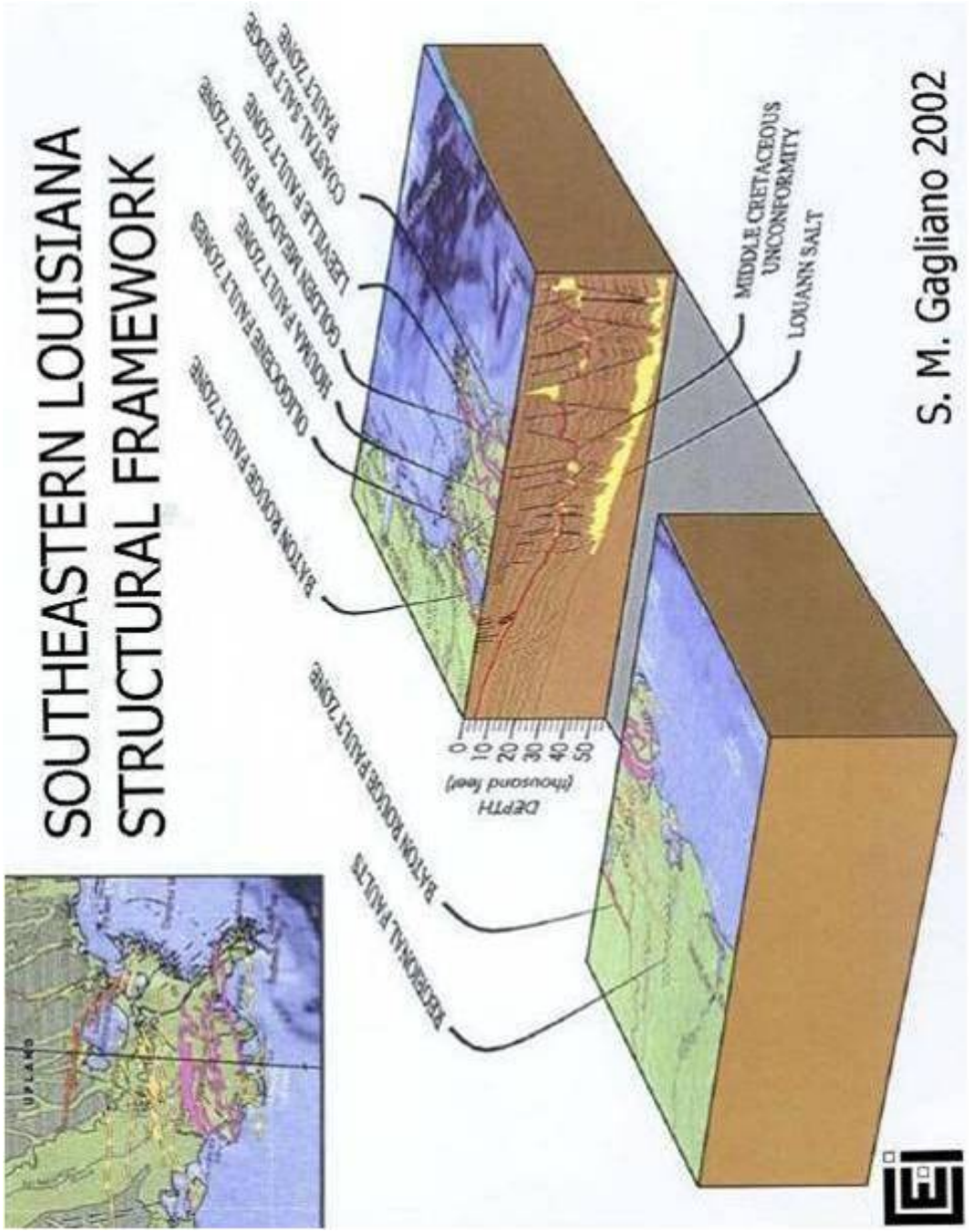

Figure 3.9: Using surficial fault maps and mega-regional seismic lines, this structural framework cross-section was developed for Southeastern Louisiana. Gagliano (2005b)

and measurements from re-leveled benchmarks. Investigations done in six locations using vibracores and McCauley auger samples, were the basis of a north-south cross section (figure 3.10) created to quantify the effects of the Empire Fault, which was shown to have 3.5 ft of vertical displacement along the scarp (Gagliano et al., 2003). Similar works done on other faults in the area have recorded vertical displacements of up to five feet, which over a ~ 30-year period is equivalent to $\sim 40mm \cdot yr^{-1}$(Gagliano et al., 2003). As increased attention is placed on rehabilitating wetlands, it has been suggested that this method allows for effective assessment of fault process in order to adequately design coastal restoration projects (Gagliano et al., 2003).

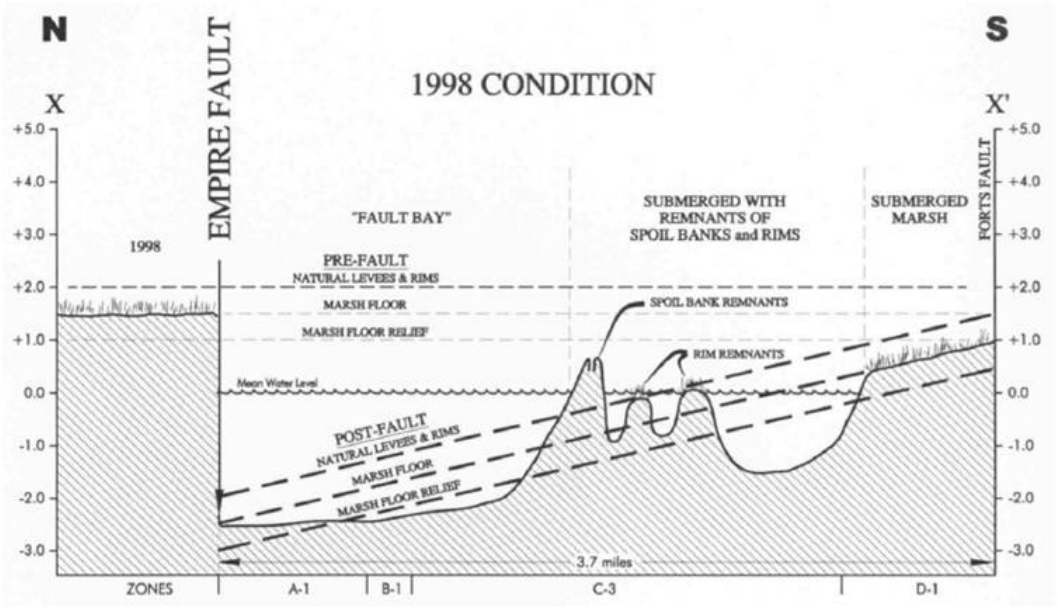

Figure 3.10: North-South cross section from McCauley auger samples. Gagliano et al. (2003)

3.3 Summary/Motivation

Vast areas of valuable wetlands have been lost, and this loss is projected to continue into the future. As models are being developed to curb coastal degradation, it is increasingly important to understand the processes that contribute to subsidence. The layers of complexity must be peeled back, and each individual component must be comprehensively evaluated. Faulting has been pervasive throughout the formation and development of the Gulf of Mexico. Movement of Jurassic-aged salt via continuous sediment loading has created a wide network of faults that are suspected to influence subsidence. While other drivers of subsidence have been proposed, understanding subsidence rates attributed wholly to geologic faults is imperative, as the current methodology used to evaluate subsidence from means such as shallow compaction or fluid removal inevitably measure total subsidence.

A barrage of data has been pieced together in an attempt to assess fault controlled subsidence. This work has primarily focused on using surface measurements, which in some instances, are loosely tied to a few seismic lines. Benchmark data, as well as the datum NAVD88 have not proven to be reliable means to detect fault movement; none-the-less, large-scale tectonic models have been created from releveled data. Previous work has relied heavily on personal opinion or conjecture. As more emphasis is placed on understanding how and why subsidence is happening, it is evident that a truly systematic method must be created to evaluate faulting process in the subsurface.

Rate ($mm \cdot yr^{-1}$)	Duration of Measurement	Location	Method	Reference
$0.06 - 0.12$	$\sim 8k.y.$	Bayou Cypremort, LA	C-14 Dating of Peat	Törnqvist et al. (2006)
$0.69 - 2.2$	$1 - 20kyr$	Numerical Model of MS. Delta	Monte Carlo Approach	Meckel et al. (2007)
$0.9 - 9.4$	1965 & 1982	Bayou Lafourche, LA	Benchmark Measurements	Morton et al. (2002)
$1.5 - 9.4$	$1966 - 1993$	Bayou Petit Caillou, LA		
2.7 & 2.8	$5kyr$	Terrebonne, LA	Peat borings	Roberts et al. (1994)
4.0 & 4.3	$10 - 15kyr$			
~ 5.2	$1995 - 2006$	Southeast LA	GPS Data	Dokka et al. (2006)
$5 - 10$	$1.2 - 1.6kyr$	Bayou Lafourche, LA	Sediment Cores	Törnqvist et al. (2008)
30	$22yrs$	Port Neches, LA	Sediment Cores	Morton et al. (2001)
$0 - 25$	~ 1930's-~ 1980's	Lower MS Valley	Benchmark Measurements	Shinkle and Dokka (2004)
16.9 & 7.1	$1969 - 1971$ & $1971 - 1977$	Southeast Louisiana	Benchmark Measurements	Dokka et al. (2006)
5.6 ave, 29 max	$2002 - 2005$	New Orleans, LA	RADARSAT satellite	Dixon et al. (2006)
Fault related measurements				
.003 to .064	$1,000,000+$ yrs	Lake Pontchartrain, LA	Seismic imagery	Lopez et al. (1997)
2.5 to 10	$1990 - 1996$		Offset on structures	

Table 3.1: *V*arious rates of measured subsidence in coastal Louisiana create many different suggestions as to the causes of subsidence in the Mississippi Delta.

Chapter 4

Research Goal

Understanding the fault-controlled component of Mississippi River delta subsidence is critical to unraveling the complexity of coastal Louisiana's overall land-loss problem. Therefore, my work provides a refined method to measure local and sub-regional variations structural subsidence. Using modern 3-D seismic data, it is possible to provide exact representations of subsurface architecture (fault orientations, salt body locations, channels), as well as relative rates of displacement across individual faults. Local well control, combined with seismic imaging allows for better representation of long-term fault movement and sedimentation rates. Further, this work seeks to compare accurately mapped fault locations with contemporary orthophotos, in order to properly gauge effects on surface morphology.

Chapter 5

Methods

As previously stated, the goal of this project is to provide an unambiguous definition of both regional and counter-regional growth faults using 3-D seismic volume and complimentary well data. Measurements collected from the growth faults are then used to assess spatial and temporal variability in subsidence associated with structural deformation of delta-top deposits.

5.1 Seismic Data

The seismic volume utilized in this study is the multiclient WesternGeco® Grand Lake/Black Bay/Quarantine Bay Emerge1 survey, covering a significant portion of western Breton Sound. The merged 3D survey consists of three individual 3D surveys shot between 1998 and 1999. Aerial extent of the $\sim 1400 km^2$ survey is shown in figure 5.1. Its location is particularly relevant to this study because it encompasses an area that has experienced significant wetland loss during the past 80 years (Fig. 5.2). Because the area is a transition zone between land and shallow marine environments, both Opsesis Eagle and Sercel 368 systems were used to record the data. A 3D Kirchhoff prestack time migra-

tion has been performed on the data to ensure optimal imaging of the complex subsurface structure. Table 5.1 provides a list of acquisition and processing parameters for the survey and its individual components.

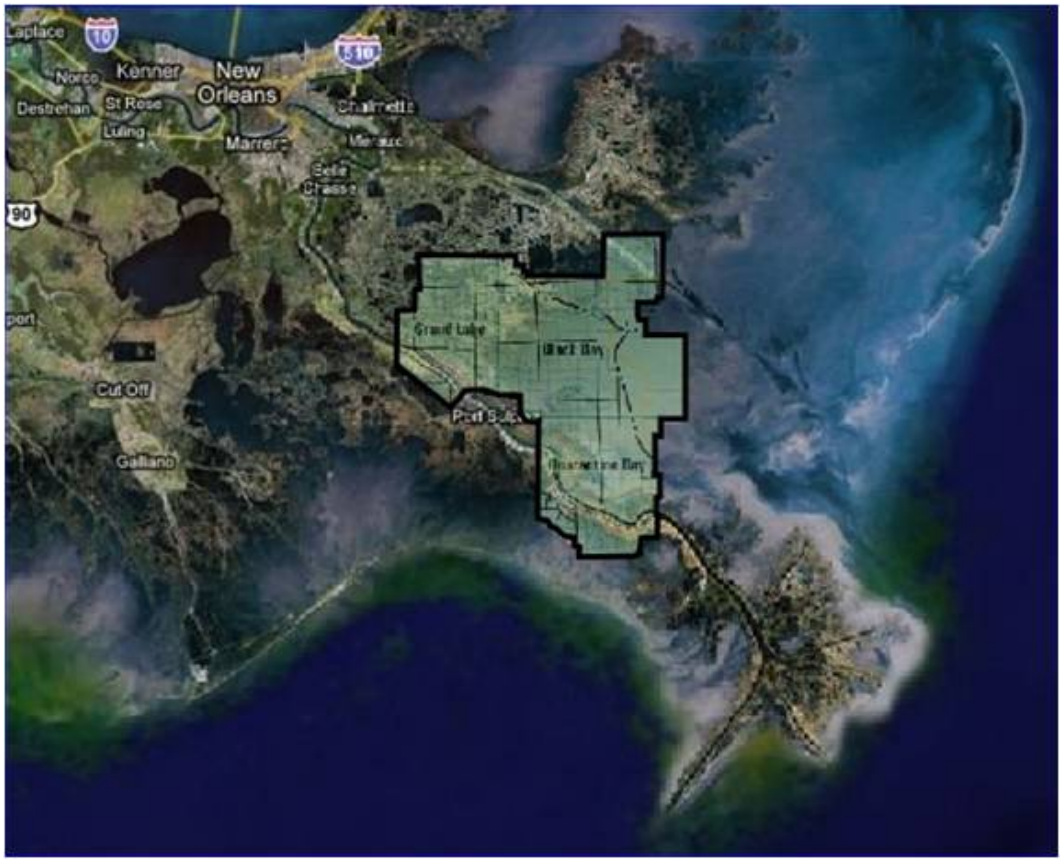

Figure 5.1: Limits of 3D survey outlined on aerial photo.

5.2 Workstation Equipment and Software

SEG-Y data, courtesy of Western Geco™, was loaded into Seismic Micro-Technology (SMT) Kingdom Suite™ as 32-bit floating point data. Data interpretation and analysis relied on two of SMT's "PAKs": TKS 2d/3d PAK and VuPak. TKS -

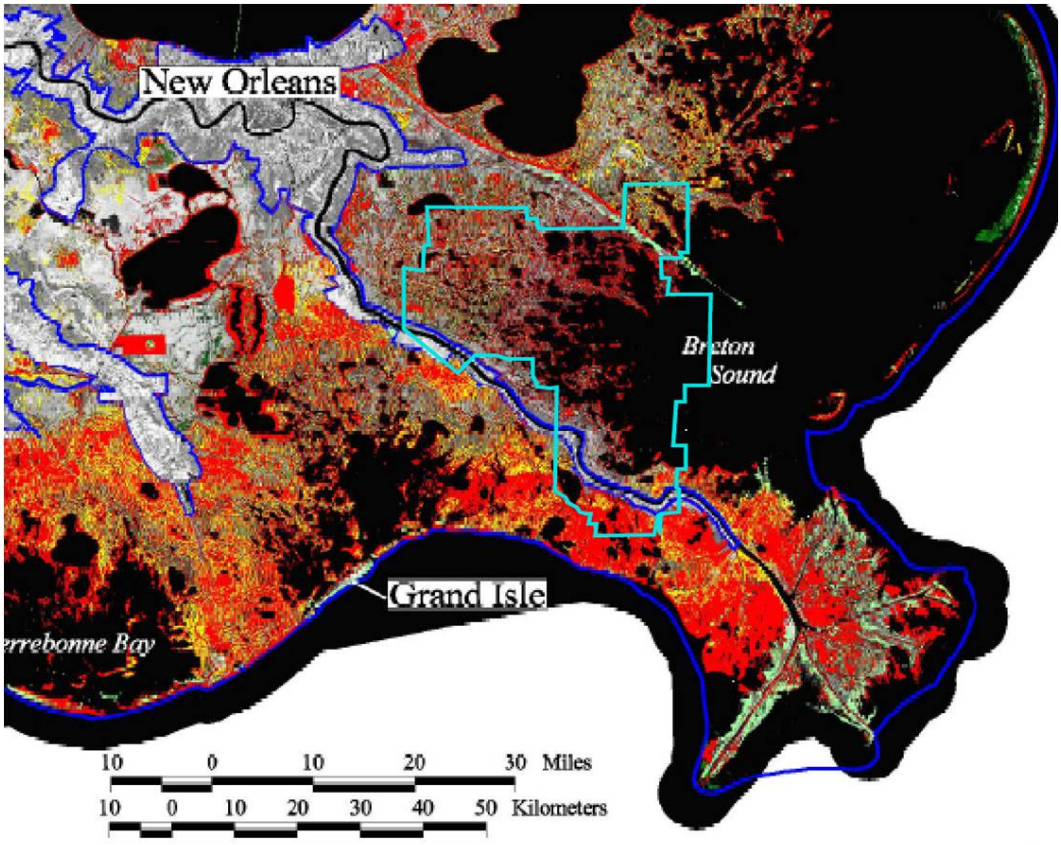

Figure 5.2: Limits of 3D-survey marked on USGS map of coastal land-loss. Red shading indicates areas of land loss during past 80 years. Yellow coloring marks forecasted land lost during next 50 years.

GRAND LAKE	
Recording System	Opseis Eagle
Energy Source	$11lbs$ at $180ft$
Spread Geometry	6 lines of 180 channels
Receiver Lines	$220ft$ intervals; $1980ft$ apart
Source Lines	$220ft$ intervals; $1980ft$ apart
Nominal Fold	30
Cell Size	$110 \times 100ft$
Average Far Offset	$20,000ft$
Survey Completed	1998
BLACK BAY	
Recording System	Sercel 368/ Opseis Eagle
Energy Source	Airgun $640in^3$ and Pentolite $5.5lbs$ at $100ft$
Spread Geometry	2 lines of 180 channels airgun source
	6 lines of 180 channels Pentolite source
Receiver Lines	$220ft$ intervals; $1980ft$ apart
Source Lines	$220ft$ intervals; $1980ft$ apart
	$110ft$ intervals; $1760ft$ apart
Nominal Fold	$30/90$
Cell Size	$110 \times 110ft$
Average Far Offset	$20,000ft$
Survey Completed	1999
QUARANTINE BAY	
Recording System	Sercel 368/ Opseis Eagle
Energy Source	$640in^3$ and $6lbs$ of Dynoseis at $100ft$
Spread Geometry	2 lines of 180 channels (Sercel)
	6 lines of 180 channels (Opseis)
Receiver Lines	$220ft$ intervals; $1980ft$ apart
Source Lines	$110ft$ intervals ; $1760ft$ apart (Sercel)
	$220ft$ intervals; 1980 ft apart (Opseis)
Nominal Fold	$90/30$
Cell Size	$110 \times 100ft$
Average Far Offset	$20,000ft$
Survey Completed	1999

(a) Acquisition Parameters

Table 5.1: *3*D-Survey parameters: Grand Lake/Black Bay/Quarantine Bay EMerge1.

Geometry/Trace editing	Survey Merge
Refraction statistics	Noise attenuation
Surface consistent deconvolution	Velocity analysis (1 mile grid)
Surface consistent amplitude correction	Residual velocity analysis
Kirchhoff prestack time migration	Final stacks (full plus 3 angles
3d Kirchhoff prestack time migration	Datum/Elevation Statistics
Tau-P noise attenuation	Residual statics
Bandpass filter / final scaling	Processing completed 04/2006
Velocity analysis (0.5 mile grid)	

(b) Processing Parameters

Table 5.1: *3*D-Survey parameters: Grand Lake/Black Bay/Quarantine Bay EMerge1.

2d/3dPAK is a fully integrated geophysical and geological interpretation software package for mapping horizons and faults using in-lines, cross-lines and arbitrary lines. VuPAK, an interactive 3D interpretation and visualization package, is completely integrated with TKS. Horizons and faults mapped out in TKS were imaged using VuPAK. All work was carried out on a Dell™ Precision 690 workstation.

5.3 Attributes and Algorithms

Faults can be difficult to detect by using 3-D seismic amplitude data alone. Frequently they appear only as slight changes in the seismic waveform that can be challenging to correlate using traditional seismic cross-sections (Neves et al., 2004). To overcome this problem, I generated a seismic coherency volume from the original amplitude data using a second-generation, semblance-based coherency algorithm available via the OpendTect™ Software, an open-source seismic-processing code. After generating this volume it was loaded in the SMT seismic project for analysis along side the amplitude volume. With the co-

herency attribute volume, the fault locations could be mapped confidently, even in the shallowest interval of the data set. An attribute is simply any measure of seismic data that allows for better visualization of a particular feature (Neves et al., 2004), while an algorithm is the procedure for numerical manipulation of the data in order to achieve the desired attribute.

Seismic coherency is defined as a measure of lateral changes in the seismic response caused by variation in structure, stratigraphy, or other means (Marfurt et al., 1998). A coherence cube is effectively a cube of coherence coefficients produced from the input of a 3-D seismic data volume that exposes features such as faults and channels (Chopra, 2002). This method is superior to traditional shaded relief maps, which only permit 3D visualization of faults and channels based on horizon picks, because seismic coherency operates on the seismic data itself. Therefore, coherency is unfettered by interpreter or automatic picker biases (Marfurt et al., 1998). 3D coherency measurements evaluate trace-to-trace similarity. Because of this, seismic traces with sharp discontinuities, such as those offset by faults, result in low coherence along the fault plane, while continuous areas exhibit high coherence coefficients (Chopra, 2002).

The second-generation coherence algorithm, developed by Marfurt, uses semblance as a coherence estimate (Marfurt et al. (1998); Chopra (2002)). Semblance is defined as a quantitative measurement of the coherence of seismic data from multiple channels that is equal to the energy of a stacked trace divided by the energy of all the traces that make up the stack (Limited, 2008).

A coherency measurement is made by first defining a window of traces around each analysis point to be evaluated. This project defined a temporal analysis window of 56 traces, which is ideal for stacking the discontinuities related with vertical faults (Marfurt et al. (1998); Chopra (2002); Neves et al.

(2004)). Next, the semblance along a set of postulated planar reflectors was completed at a user selected maximum dip of $250ms \cdot m^{-1}$ and a delta dip of $10ms \cdot m^{-1}$.

Figure 5.3 (Marfurt et al., 1998), illustrates a typical calculation of coherency over an elliptical analysis window with arbitrary dips (q, p).

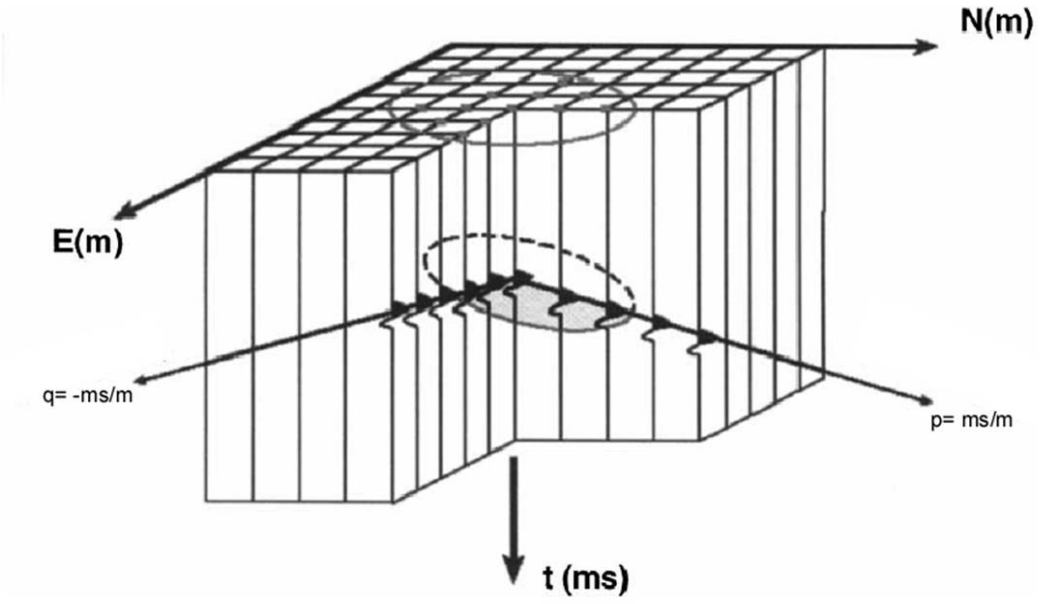

Figure 5.3: Typical coherency calculation over an analysis window using arbitrary dips (p,q). Modified after Marfurt et al. (1998)

5.4 Mapping

Proper assessment of subsidence and structure began with intensive mapping of horizons and faults using the 3-D seismic amplitude and coherency volumes.

5.4.1 Horizons

Roughly 15 horizons were mapped in the amplitude volume at depths between $\sim .450s$ and $\sim 1s$ TWT. Continuous, high-amplitude reflectors were selected as mappable horizons (figure 5.5), and the most laterally continuous horizon was selected as a proxy for total subsidence. Each of these horizons was mapped every $1 - 10$ lines to ensure accurate tracking of the chosen reflector and accurate gridding of the interpreted horizon. Gridding a horizon simply implies that the horizon information has been interpolated to fill in an area between two known values.

The term "proxy subsidence" refers to a distinct horizon seen through out the seismic volume that is representative of total subsidence. As the horizon varies in the time domain, it can be thought of as varying in depth. Because deposition of a certain horizon would occur at time $t = 0$ (the surface), a "deeper" horizon would have a greater time and would therefore have undergone subsidence. It is important to note that this method shows total subsidence in time, but can be a helpful was to visualize subsidence patterns in areas of interest.

5.4.2 Faults

Determining the locations and offsets of faults were key elements of this study. Because faults can be difficult to map in amplitude data, all fault surfaces were mapped using the coherency volume. Incoherent data was assigned a dark color so that fault planes were easily recognized. Figure 5.6 displays three prominent faults imaged in both the amplitude and coherency volumes. Overall, 30 significant faults, both regional and counter-regional were identified in the survey.

Faults identified for thorough analysis were mapped every one to ten inlines depending on the geometric complexity of the structure. After defining the fault plane this way, fault displacement was defined by measuring the off-

set of specific reflectors between the foot- and hanging-wall of the structure. These displacement measurements were collected on each line where the fault surface had been mapped. Roughly 5-10 measurements of reflector offsets were made per line, over a range of survey depths. Measurements of displacement associated with six individual faults is presented in the Data Analysis section and the appendix.

5.5 Well Control

Seismic data is collected in two-way time (TWT), so well data is necessary to develop an algorithm for converting TWT to burial depth and to provide age control for the mapped subsurface horizons.

5.5.1 Velocity Surveys

Correlated values of depth and time were obtained from check-shots in five well bores located within the bounds of the Grand Lake/Black Bay/Quarantine Bay survey. Well information and location for the five velocity surveys is listed in Table 5.2.

A velocity survey allows for an independent assessment of time versus depth, yielding both average and interval velocity measurements (Dobrin and Savit (1988); Limited (2008)). Using geophones, lowered to a number of known depths in the well-bore, the arrival times of waves generated by a charge, vibrosies unit, or air-gun array (used in marine areas) are recorded. Interval velocities, such as those used in this survey, are acquired by dividing the distance between consecutive geophone positions in the well-bore by the difference in arrival times recorded at the two depths after the arrival times are corrected for wave path angularity (Dobrin and Savit, 1988). Average velocities were not used in this study.

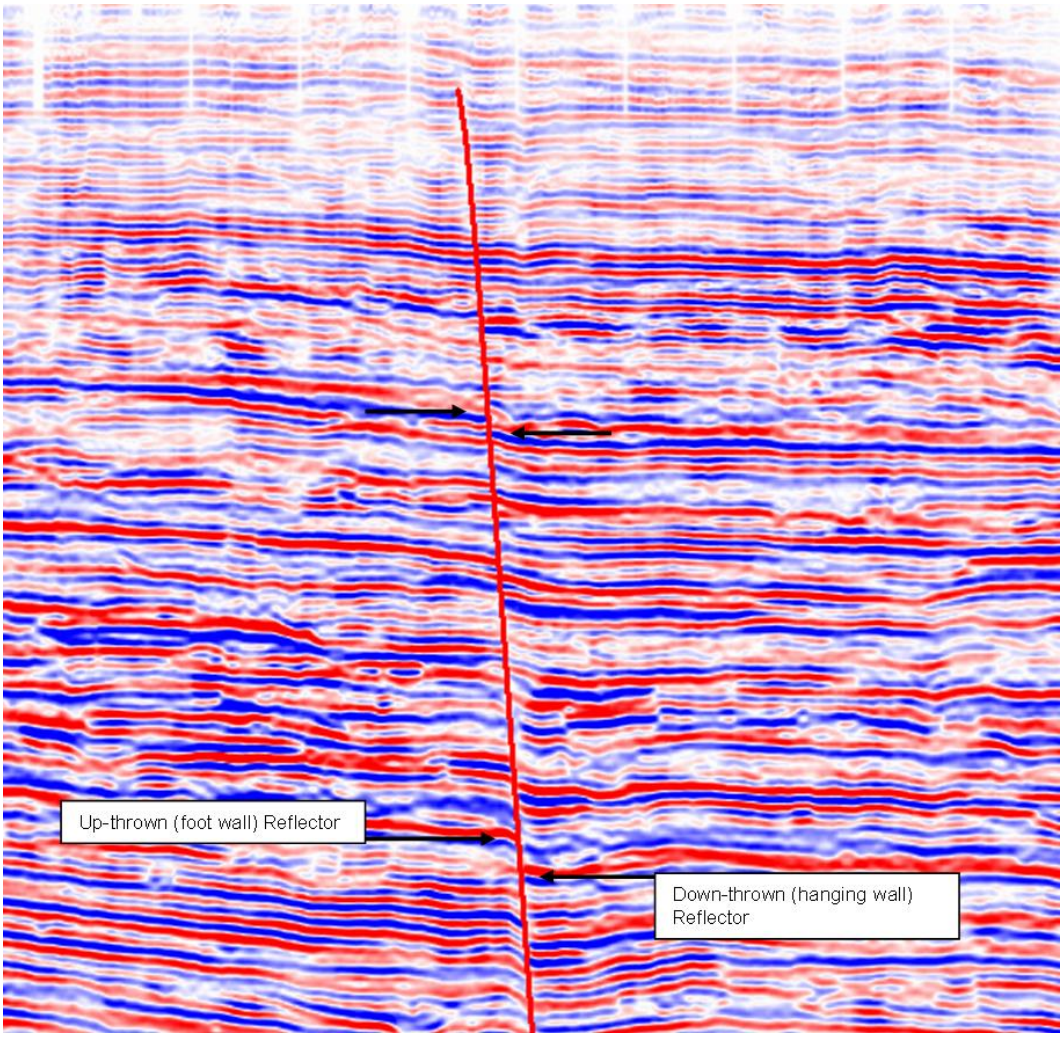

Figure 5.4: Fault displacement was defined by measuring the offset of specific reflectors between the foot- and hanging-wall of the structure.

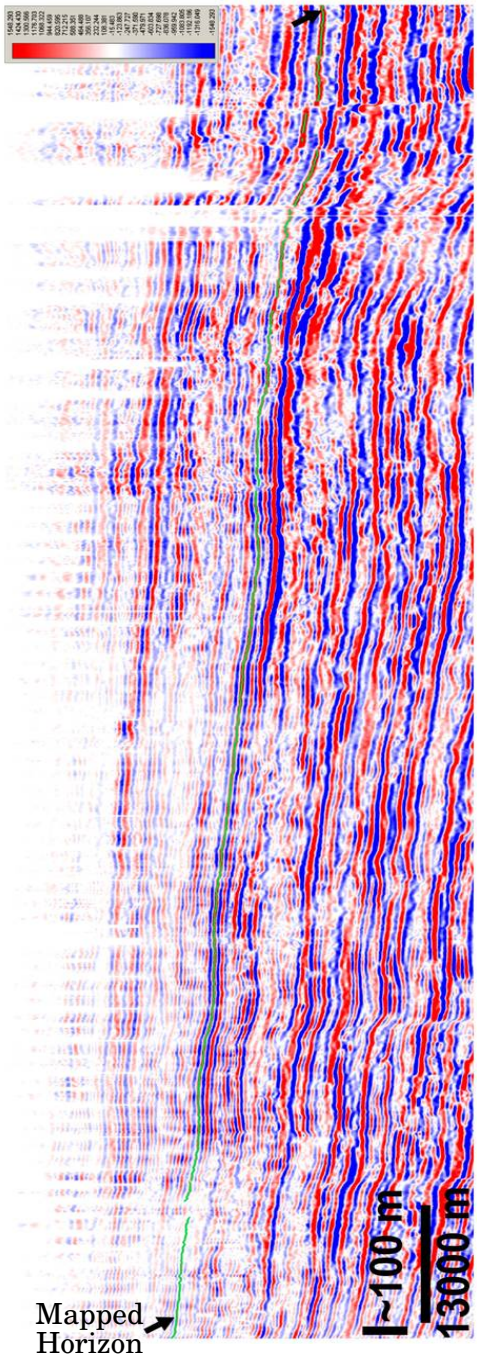

Figure 5.5: A horizon (in cyan), used to determine proxy subsidence, was mapped throughout the survey on a continuous peak reflector.

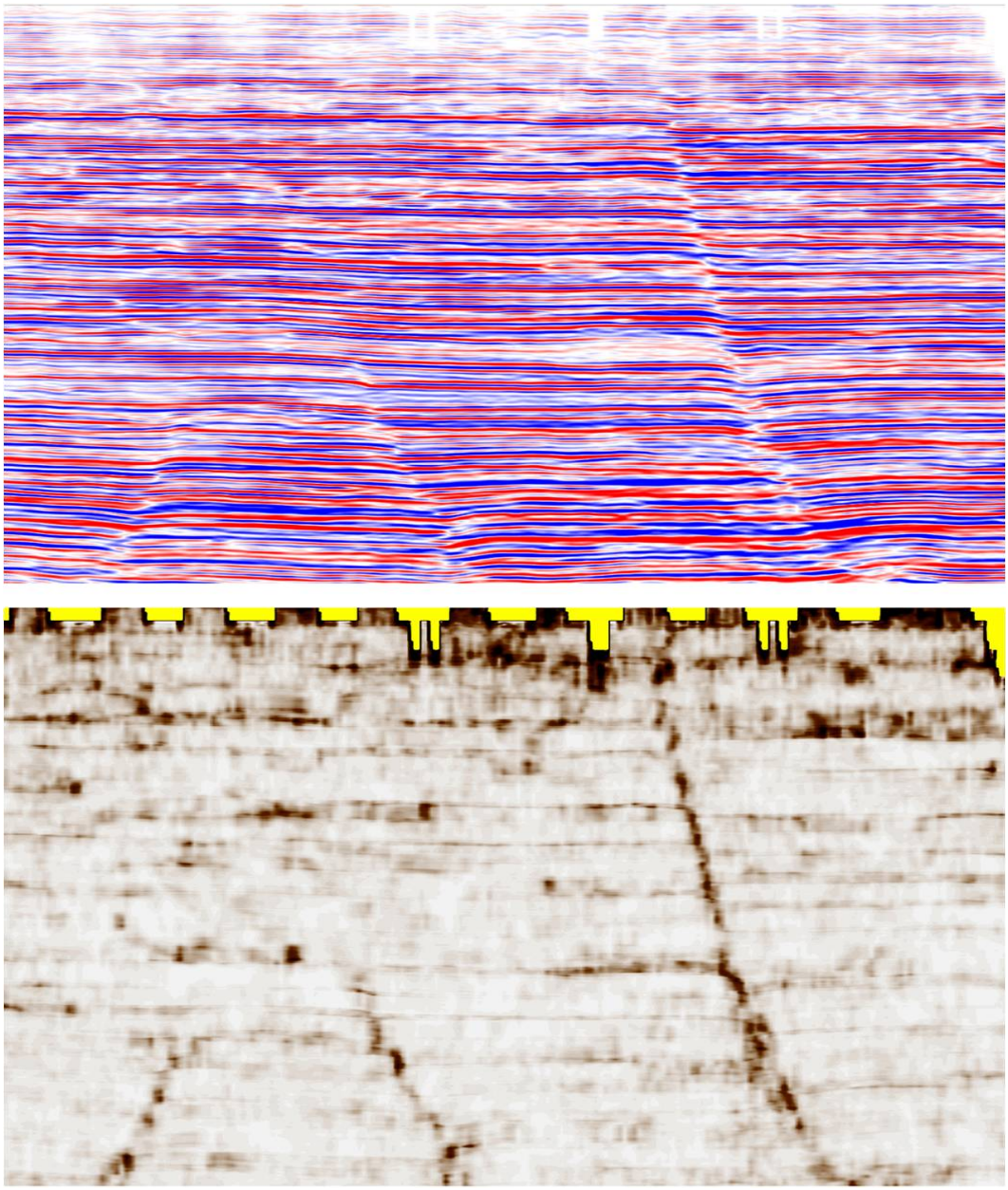

Figure 5.6: Faults imaged in amplitude (top) and coherency (bottom). Using coherency, discontinuous areas offset by faults have much better resolution which is useful for detailed mapping in shallow parts of the 3D volume.

API Number	Well Name and Well Number	Lambert Coordinates	Measured Depth (m)
17075014470000	Richardson Bass ♯26-H	X: 2545784 Y: 297378	3019.653
17075003470000	California Co. ♯ 1	X: 2544486 Y: 350055	3200.4
17075222800000	Atlantic Richfield ♯1	X: 2549649 Y: 340677	4724.4
17075014180000	Humble ♯ 1 New Orleans	X: 2554902 Y: 279550	3959.352
170175001970000	Humble ♯1 John Cutrone	X: 2502529 Y: 325486	4046.22

Table 5.2: *V*elocity surveys from five wells located within the 3D survey were incorporated to convert time (s) to depth (m).

Time versus depth data for the five wells is plotted in Figure 5.7. The best-fit polynomial to this data was used to convert measurement of time into values of burial depth for the 3-D seismic volumes.

The acoustic velocity associated with deposits at specific burial depths was calculated using the time and depth data shown in the upper graph of Figure 5.7. These interval velocities are shown in the lower graph of Figure 5.7, systematically increasing with increasing burial depth.

5.6 Mississippi Surface Data

In order to evaluate the effects of fault-induced subsidence on morphology of the delta surface, I compared high-resolution surface data against the mapped positions of growth faults.

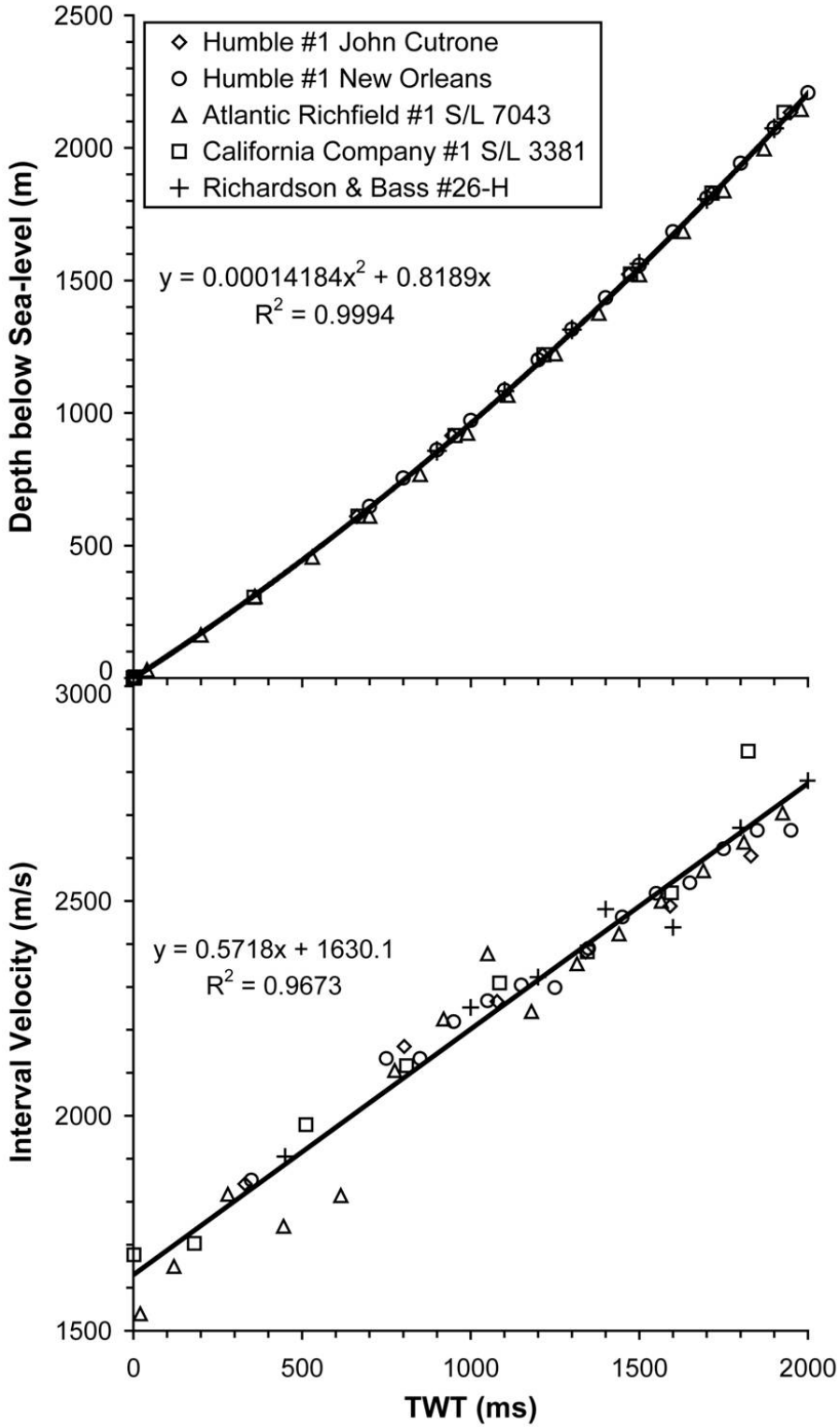

Figure 5.7: Time vs. Depth and interval velocity for wells in 3D-survey

5.6.1 Digital Orthophoto Quarter Quadrangles

Louisiana State University offers hundreds of high resolution Digital Orthophoto Quarter Quadrangles (DOQQ). These images, taken from flyovers and recorded using infrared light, cover an area of about $46km^2$, each pixel representing about one meter. Also, DOQQ photos are georeferenced, meaning they are registered to specific locations on Earth's surface and compatible with other scaled maps. This study used 44 orthophoto quads taken in and around Breton Sound during 2005. All 44 photos were assembled using Adobe Photoshop® to create a large image covering the study area. Surface features displayed on this aerial image were compared to fault structures resolved by high-resolution 3-D seismic time slices (made at $.450s$ and $1s$) to obtain a true sense of how faulting influences contemporary delta-top morphology

Chapter 6

Data Analysis

The methods used to evaluate fault induced subsidence have created a completely new suite of information concerning structural complexity, variation in subsidence rates, fault-slip rates, and delta-surface morphology in southeastern Louisiana.

6.1 Structural Analysis

Extensive mapping identified 30 substantial growth faults in the survey area. Of these faults, 24 are regionally oriented (hanging wall down-to-the-basin, south) and the remaining six are counter-regional (hanging wall down to the north) in nature. Figures 6.1 & 6.2 are base maps which show the locations of each fault visible on $.450s$ and $1s$ coherency time slices. Regional faults are signified on the map in red and counter-regional faults are colored green. Continuous lines indicate a clearly traceable fault, while the dashed lines represent areas of inferred faulting. Faults range in length from .2 km to more than 15 km, and the majority of faults are located in the eastern section of the survey.

Most faults can be mapped to shallow depths that are limited by the seismic resolution ($\sim .300s$) and extend to depths greater than $\sim 1.5s$.

At $t = 1s$, the coherency time slice reveals many clearly defined faults and channels. At $t = .450s$, faults are still clearly visible, however their lateral extents are reduced due to the shallowness of the slice, combined with the listric nature of growth faulting. Collection cones (seen as dots on the surface) are seismic artifacts associated with this shallow map. It is important to note that the cones do not affect the resolution of the faults.

Mapping efforts also revealed a large salt body related to the Jurassic-aged Louann salt. Sediment loading, combined with this salt movement has created the long, complex fault system in the southernmost portion of the survey area. The stratigraphy around the salt body has been dramatically altered. Large mini-basins, known to be areas of hyper-subsidence, are readily seen in conjunction with the mobile salt under the Mississippi River. Because faulting was most intense around salt-structures, it is suspected that these fault networks are induced due to factors related to salt evacuation.

Intertwined counter-regional and regional faults are seen around the salt structure in the southern portion of the survey, which subsequently influence the planform of the Mississippi River near the Jackson Bend. To the west, away from the salt, a stark reduction in frequency of faulting is seen. In that area, one fault (and a small portion of another fault extending from the west) is mappable in shallow substrate. This regional growth fault also interacts with the Mississippi River near a separate bend.

The structural complexity seen in the dataset ($\sim 1400km^2$) appears to be more influenced by localized factors such as salt body movement and sediment loading. No evidence was seen to suggest large-scale tectonic influences such as the proposed SLA (Dokka, 2006).

Figure 6.1: Substantial faults mapped in $.450s$ coherency time slice. Red lines indicate regional growth faulting, green lines indicate counter-regional growth faulting.

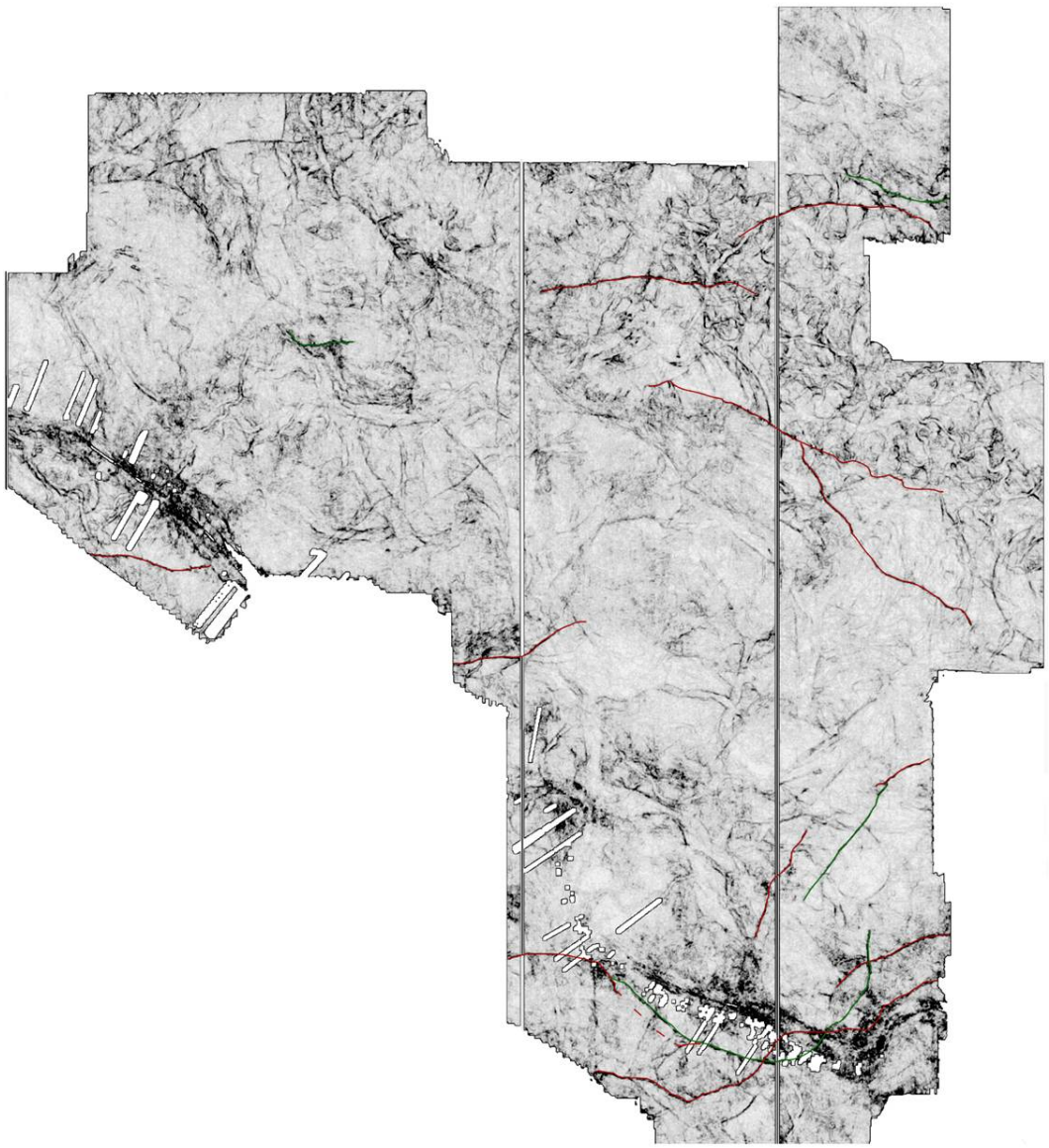

Figure 6.2: Substantial faults mapped in $1s$ coherency time slice. Red lines indicate regional growth faulting, green lines indicate counter-regional growth faulting.

6.2 Proxy Subsidence Map

The pattern of Quaternary subsidence in the survey area has been established through the mapping of a particularly continuous reflector through out most of the 3D survey. Vertical position of this reflector ranged from $.354s$ to $.738s$, depending on location. After fully mapping the reflector, the resulting horizon was gridded so that a time value for the horizon was assigned to each grid point in the survey. Using the velocity survey from LA State 3381, the gridded horizon was converted from time to burial depth (figure 6.3). Since local and regional relief of the delta top is very small, less than $8m$, this map defines the pattern of variable subsidence in the study area.

Expectedly, these map in Figure 6.3 displays an overall increasing subsidence to the south, towards the center of the GOM basin. However, subsidence is locally greatest in those areas exhibiting faulting, especially around the salt structure. A zone of high subsidence parallels the large counter-regional fault in the south, which also coincides with position of the Mississippi River. The proxy subsidence map records the total subsidence acting upon a horizon, and clearly demonstrates that faults influence local subsidence patterns within the bounds of this 3D-survey.

6.3 Individual Fault Measurements

Numerical values of fault movement through time were collected for six select faults. Fault movement is an important component of overall subsidence because a growth fault creates focused accommodation space on the downthrown side of the fault. A description of all 6 faults is presented below. The appendix lists all measurements made above $\sim 1500ft$ on each fault.

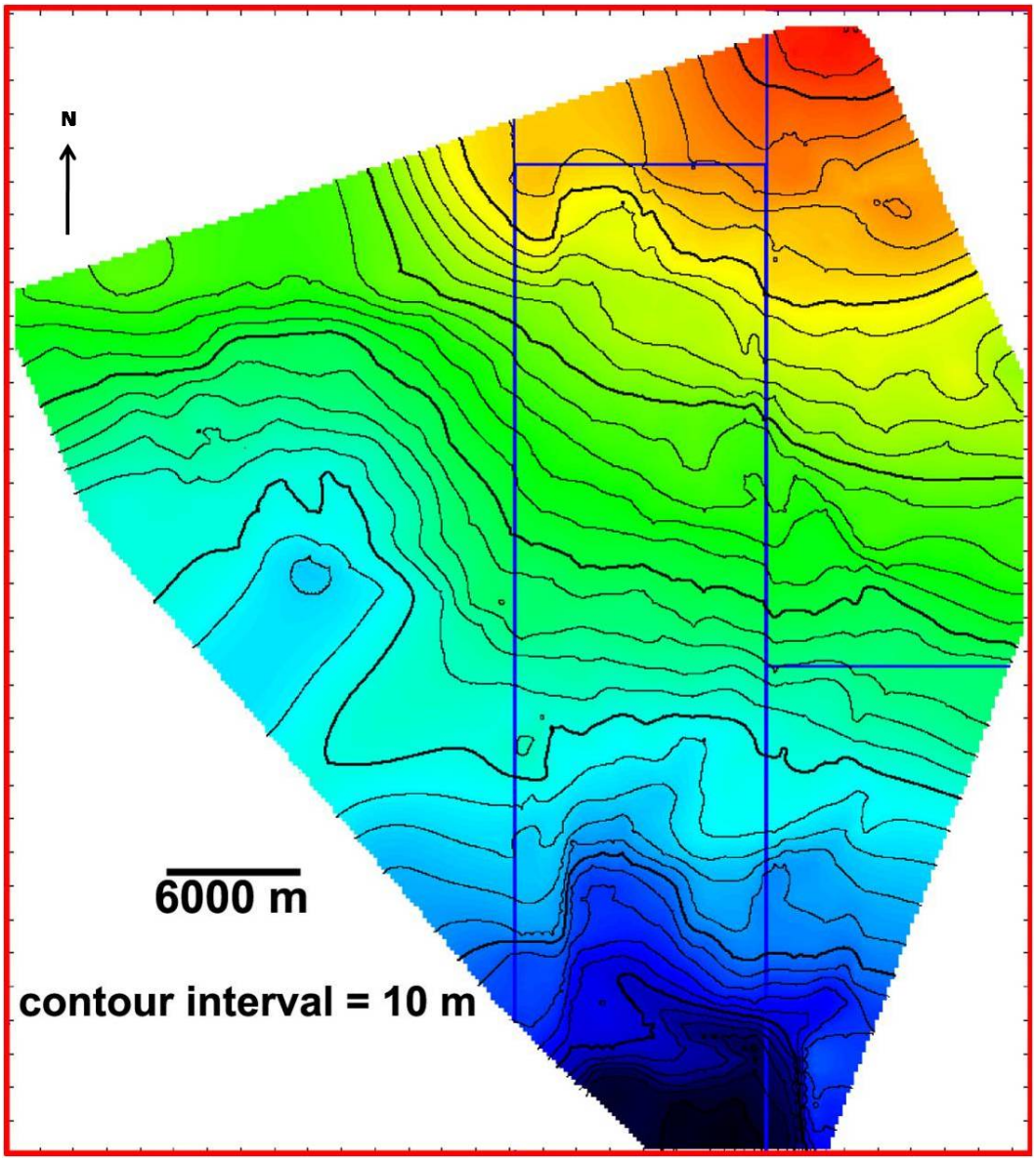

Figure 6.3: Proxy subsidence map converted from time to depth. Higher subsidence areas are shown in cool colors. The “arm” of high subsidence located in the south corresponds to the location of a network of salt-induced growth faults, which also appear to influence the plan-form of the Mississippi River.

6.3.1 Regional Growth Fault "A"

Fault "A" is located between Lambert Coordinates $X : 2553491.3$, $Y : 248536.3$ (western extent) and $X : 2602081.6$, $Y : 262577.3$ (eastern extent) in the southern portion of the survey. This fault is a $\sim 10km$ long, regional growth fault oriented NE-SW and dipping to the S-SE.

Figure 6.4 shows data collected from this fault. The upper graph illustrates fault offset (m) versus depth below delta surface (m), while the lower graph shows the fault offset ratio (local value for fault displacement to burial depth) also plotted against depth below delta surface (m). Maximum fault offset is $120m$ at a depth of $\sim 1300m$, however most offsets range from zero to $\sim 60m$. The wide range in measured values for displacement represents behavior for the entire fault. Displacement values are small near the fault tips where displacement must go to zero. The maximum values for the offset ratio increase with burial depth from roughly 6% at shallowest depths to 9% at greater depths. This means that while total accumulated displacement across this fault is systematically increasing over geologic time, the degree of displacement on this fault is decreasing through geologic time. For example, at $300m$ the maximum fault offset is $18m$ (6% of the depth), while at $900m$ fault offset is 7.5% of the depth or $67.5m$.

6.3.2 Regional Growth Fault "B"

Fault "B" is located between Lambert Coordinates $X : 2562308.9$, $Y : 349699.9$ (western extent) and $X : 25999096.9$, $Y : 335641.8$ (eastern extent) in the east central portion of the survey. This fault is a $\sim 12km$ long, regional growth fault oriented NW-SE and dipping to the S-SW. Data for this fault is seen in figure 6.5.

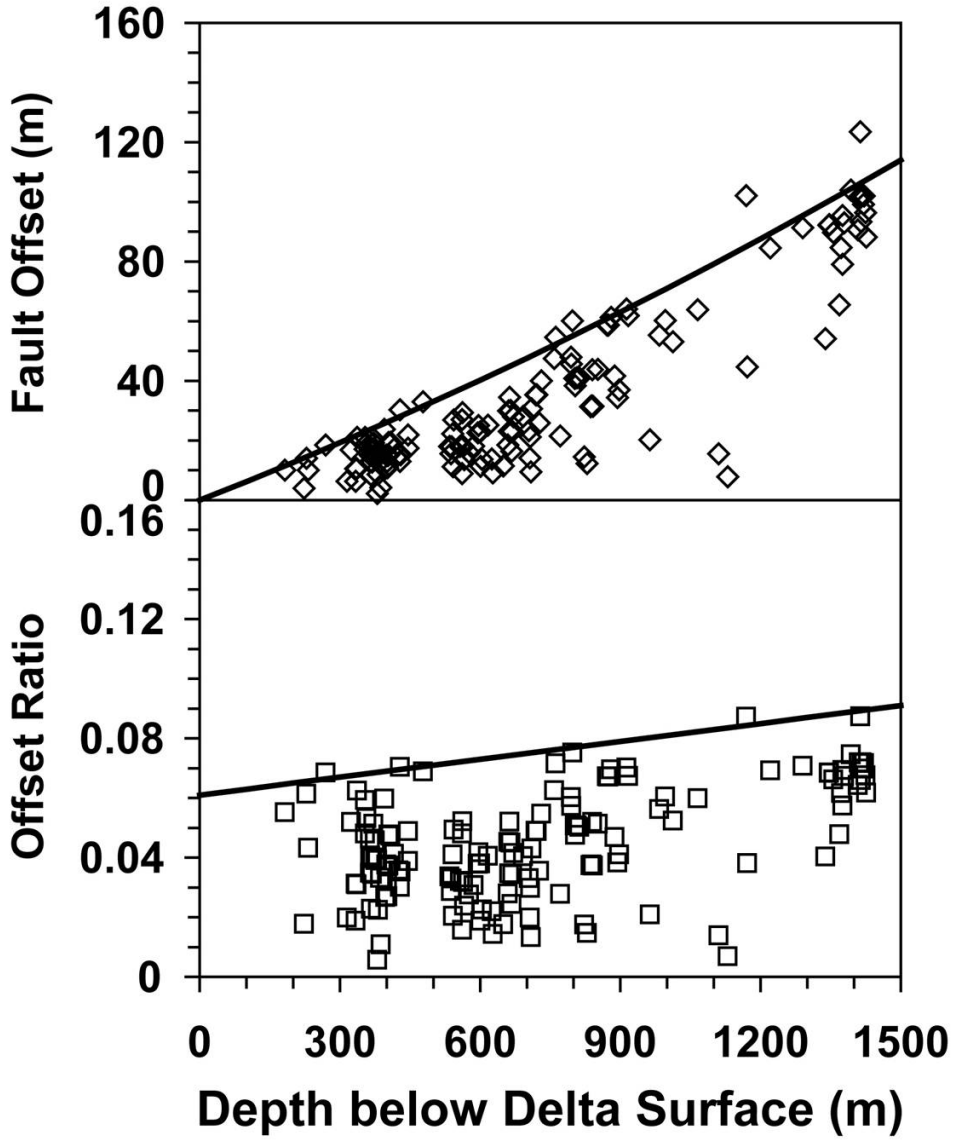

Figure 6.4: Data collected for regional fault "A" shows fault offset (upper graph) and the fault offset ratio (lower graph) plotted against the depth below the delta surface. In this data set, fault offset increases roughly linearly with depth below the delta surface. Maximum fault offset is $\sim\ 120m$, however most faults range from $0-60m$ of offset on a reflector.
The offset ratios (the measured fault offset divided by depth below the delta surface) range from $6-9\%$ of the depth below the delta surface, increasing with depth.

Maximum measured displacement on this fault does not exceed $\sim 50m$ and the maximum values for offset ratio remain a constant 5% with depth below the delta surface. This means that the degree of displacement on this fault is remaining constant over time.

6.3.3 Regional Growth Fault "C"

Fault "C" is located between Lambert Coordinates $X : 2543286.2$, $Y : 362765.2$ (western extent) and $X : 2574540.8$, $Y : 364118.2$ (eastern extent) in the northern portion of the survey. This fault is a $\sim 10km$ long, regional growth fault oriented E-W and dipping to the south.

Values obtained from measuring this fault are presented in figure 6.6. The maximum measured offset on this fault is about $(60m)$ and maximum offset ratio remains a constant 5.5% with depth below delta surface.

6.3.4 Regional Growth Fault "D"

Fault "D" is located between Lambert Coordinates $X : 2539317.8$, $Y : 26569.4$ (western extent) to $X : 2561092.0$, $Y : 254476.4$ (eastern extent) in the southern portion of the survey. This fault is a $\sim 8km$ long, regional growth fault oriented NW-SE and dipping to the S-SW.

Figure 6.7 shows that this fault has a maximum offset of $110m$ at $\sim 1300m$ below the delta top, and that maximum values for the offset ratio values increase from 5.5% to 8% with depths from zero to 1500 m below delta surface.

6.3.5 Regional Growth Fault "E"

Fault "E" is located between Lambert Coordinates $X : 2478851.8$, $Y : 324719.7$ (western extent) and $X : 2495551.6$, $Y : 323357.1$ (eastern extent) in the western

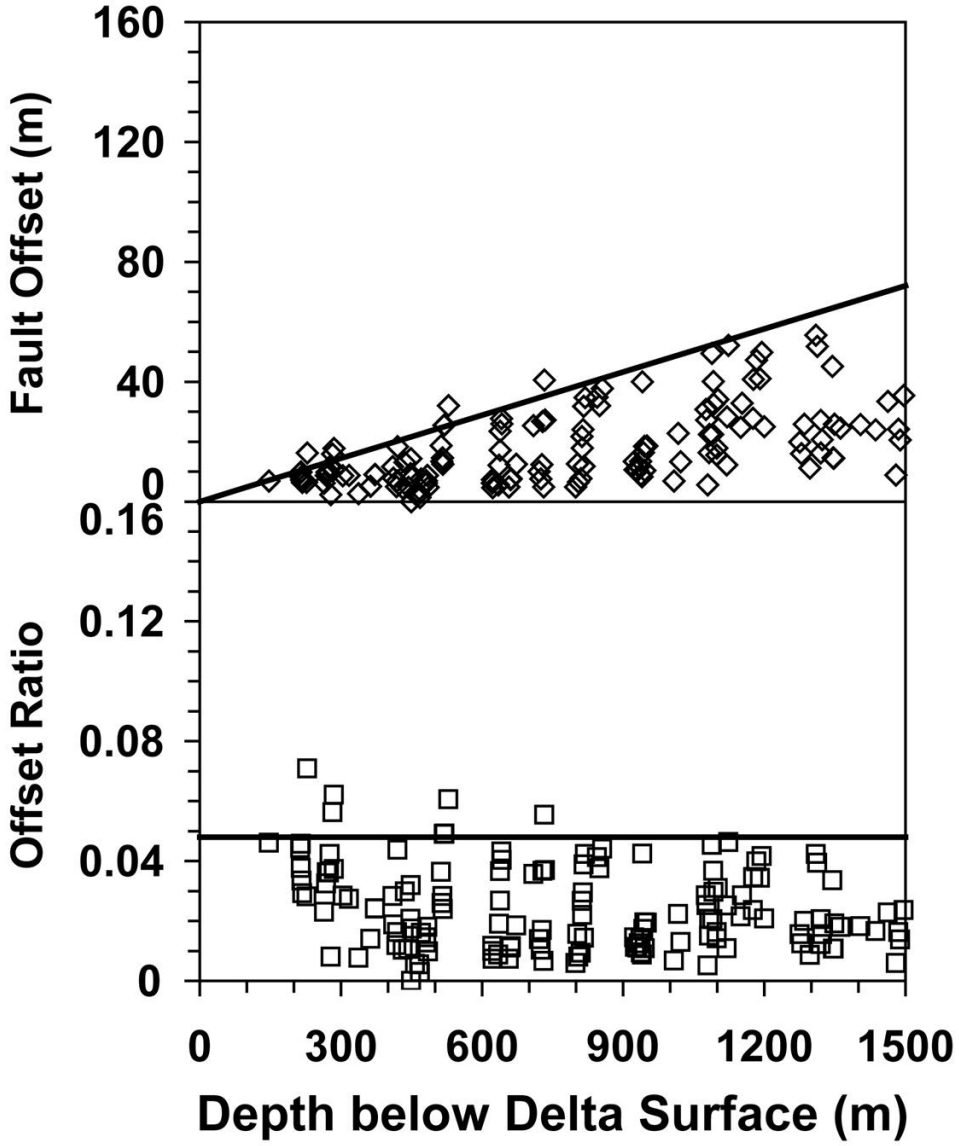

Figure 6.5: Data collected for regional fault "B" shows fault offset (upper graph) and the fault offset ratio (lower graph) plotted against the depth below the delta surface. In this data set, fault offset increases roughly linearly with depth below the delta surface. Faults range from $0 - 50m$ of offset on an n individual reflector.
The offset ratios (the measured fault offset divided by depth below the delta surface) holds constant at approximately 5% of the depth below the delta surface.

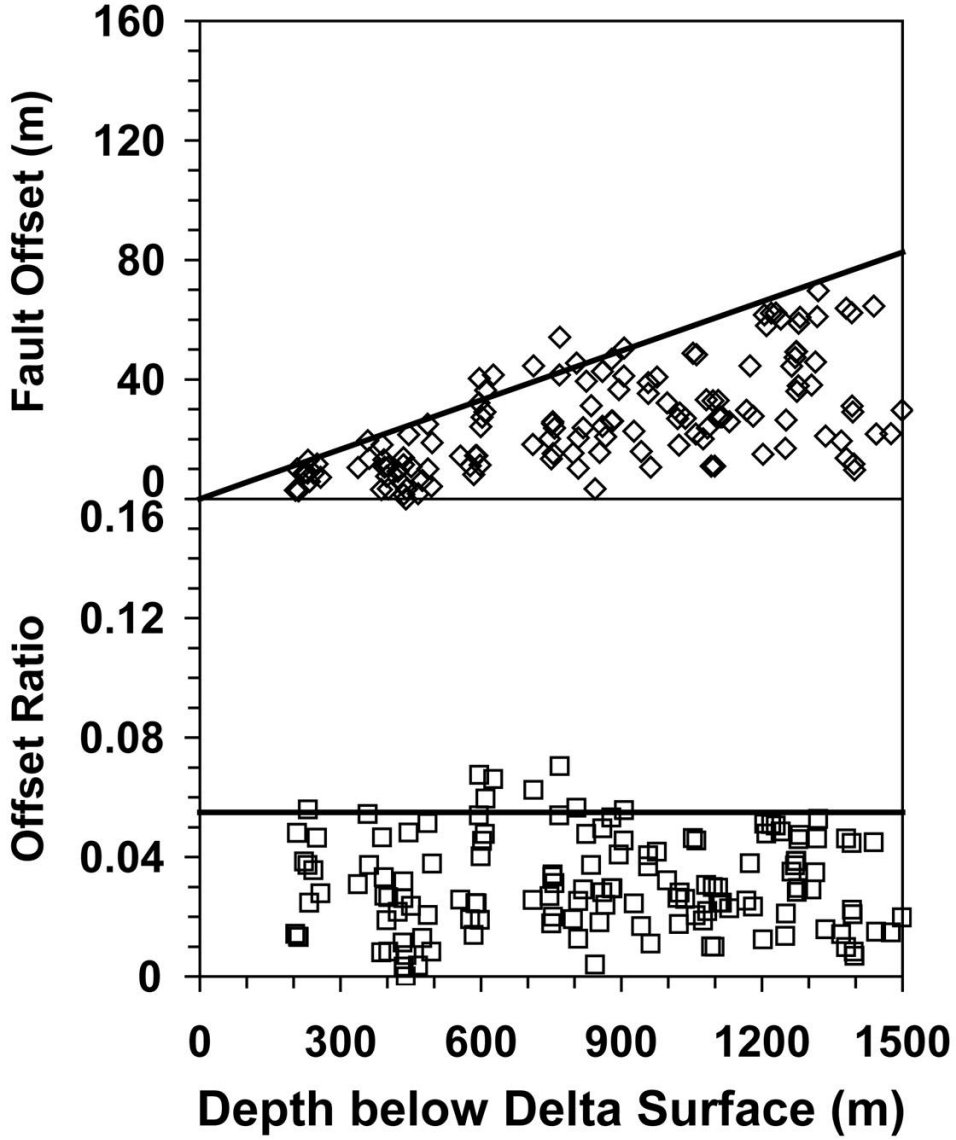

Figure 6.6: Data collected for regional fault "C" shows fault offset (upper graph) and the fault offset ratio (lower graph) plotted against the depth below the delta surface. In this data set, fault offset increases roughly linearly with depth below the delta surface. Maximum fault offset is $\sim 120m$, however most faults range from $0 - 60m$ of offset on a reflector.
The offset ratio (the measured fault offset divided by depth below the delta surface) is consistently 5.5% of the depth below the delta surface.

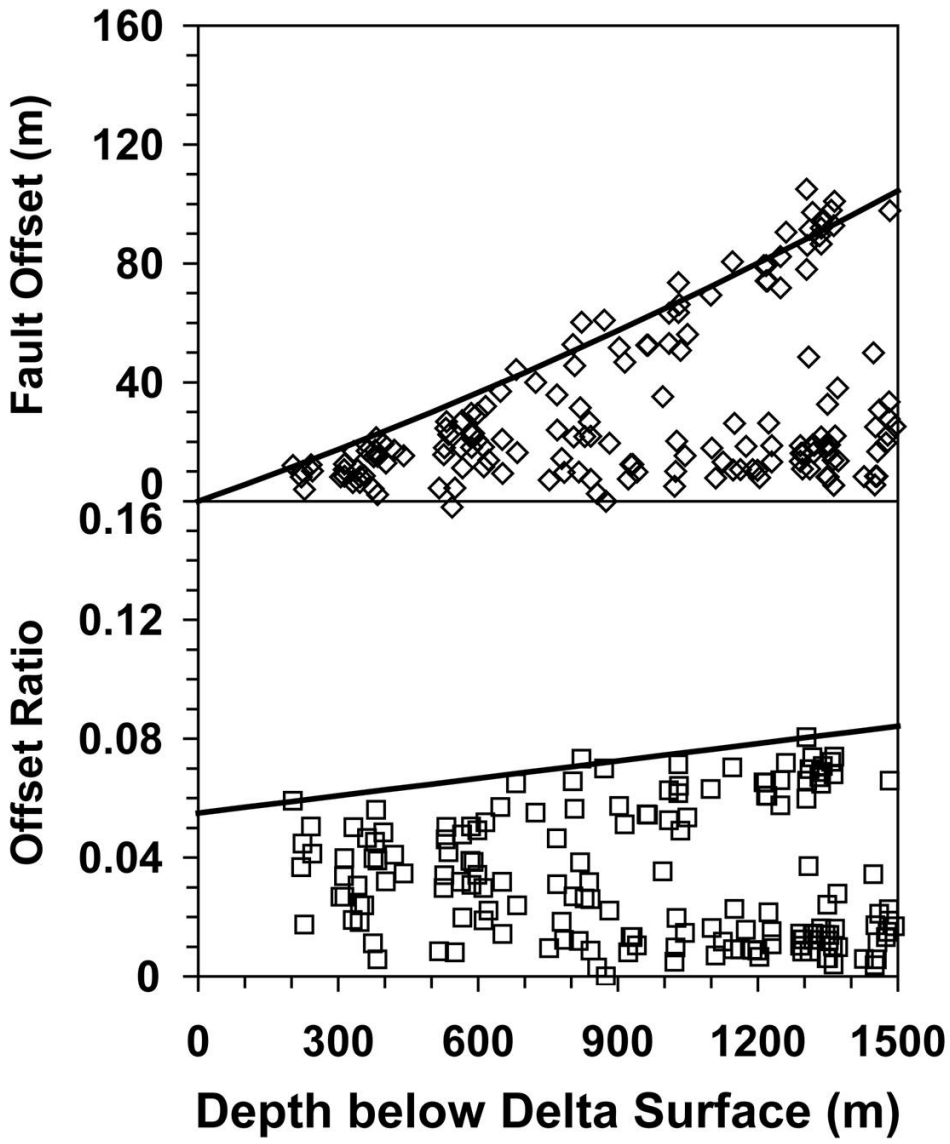

Figure 6.7: Data collected for regional fault "D" shows fault offset (upper graph) and the fault offset ratio (lower graph) plotted against the depth below the delta surface. In this data set, fault offset increases roughly linearly with depth below the delta surface. Maximum fault offset is $\sim 110m$ on an individual reflector.
The offset ratios (the measured fault offset divided by depth below the delta surface) range from $5.5 - 8\%$ of the depth below the delta surface, increasing with depth.

portion of the survey. This fault is a $\sim 3km$ long, regional growth fault oriented E-W and dipping to the south.

Measurements made of this fault are summarized in figure 6.8, which shows offsets ranging from zero to $\sim 100m$ and a constant maximum offset ratio of 8%.

6.3.6 Counter-Regional Growth Fault "F"

Fault "F" is located between Lambert Coordinates $X : 2552857.3$, $Y : 264445.8$ (western extent) and $X : 2588735.9$, $Y : 25437.6$ (eastern extent) in the southern portion of the survey. This fault is a $\sim 12km$ long, counter-regional, salt induced growth fault oriented in an arcing E-W orientation and dipping to the north.

Figure 6.9 shows that this fault has the highest maximum displacement of any fault measured with a value of $\sim 150m$. The maximum values for the offset ratio increase from about 4 to 11% with burial depth. This means that the degree of displacement on this fault is decreasing somewhat over geologic time.

6.4 Estimate of Faulting-Induced Subsidence

The lack of significant reduction in offset ratio through time for the studied growth faults (Figs. 6.4 to 6.9) suggests that these structures are active today. If active, these faults should be producing enhanced or extra subsidence associated with displacements of their hanging walls. I can estimate the magnitude of this enhanced subsidence by combining the near-surface values of fault offset ratio with appropriate measures of deposition rate to calculate a fault-related subsidence rate (FSR), where $FSR = \frac{\text{fault displacement}}{\text{subsurface depth}} \times \frac{\text{depositional thickness}}{\text{time}}$. The near-surface values of offset ratio $\left(\frac{\text{fault displacement}}{\text{subsurface depth}}\right)$ for the six studied faults

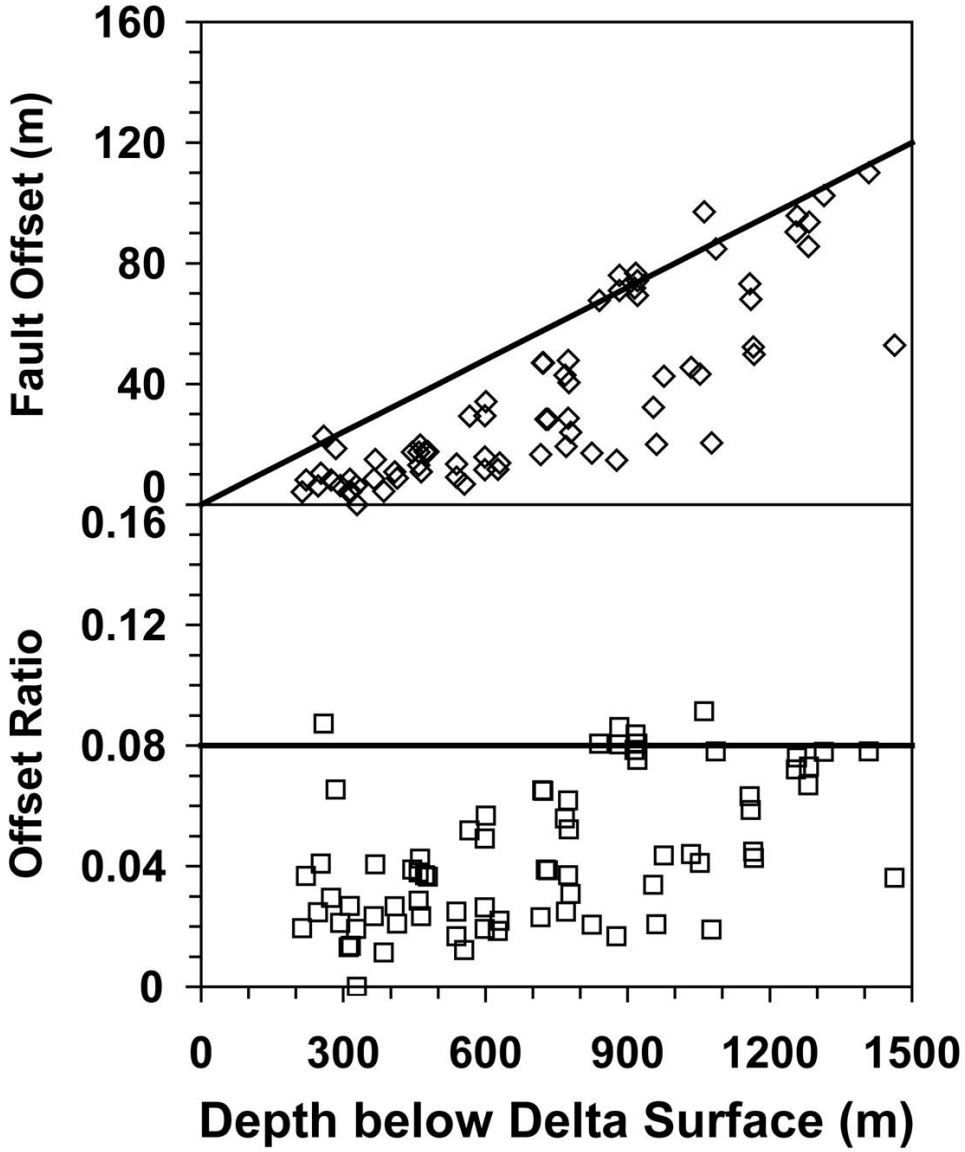

Figure 6.8: Data collected for regional fault "E" shows fault offset (upper graph) and the fault offset ratio (lower graph) plotted against the depth below the delta surface. In this data set, fault offset increases roughly linearly with depth below the delta surface. Maximum fault offset is $\sim 110m$, however most faults range from $0 - 100m$ of offset on a reflector.
The offset ratio (the measured fault offset divided by depth below the delta surface) is 8% of depth below the delta surface.

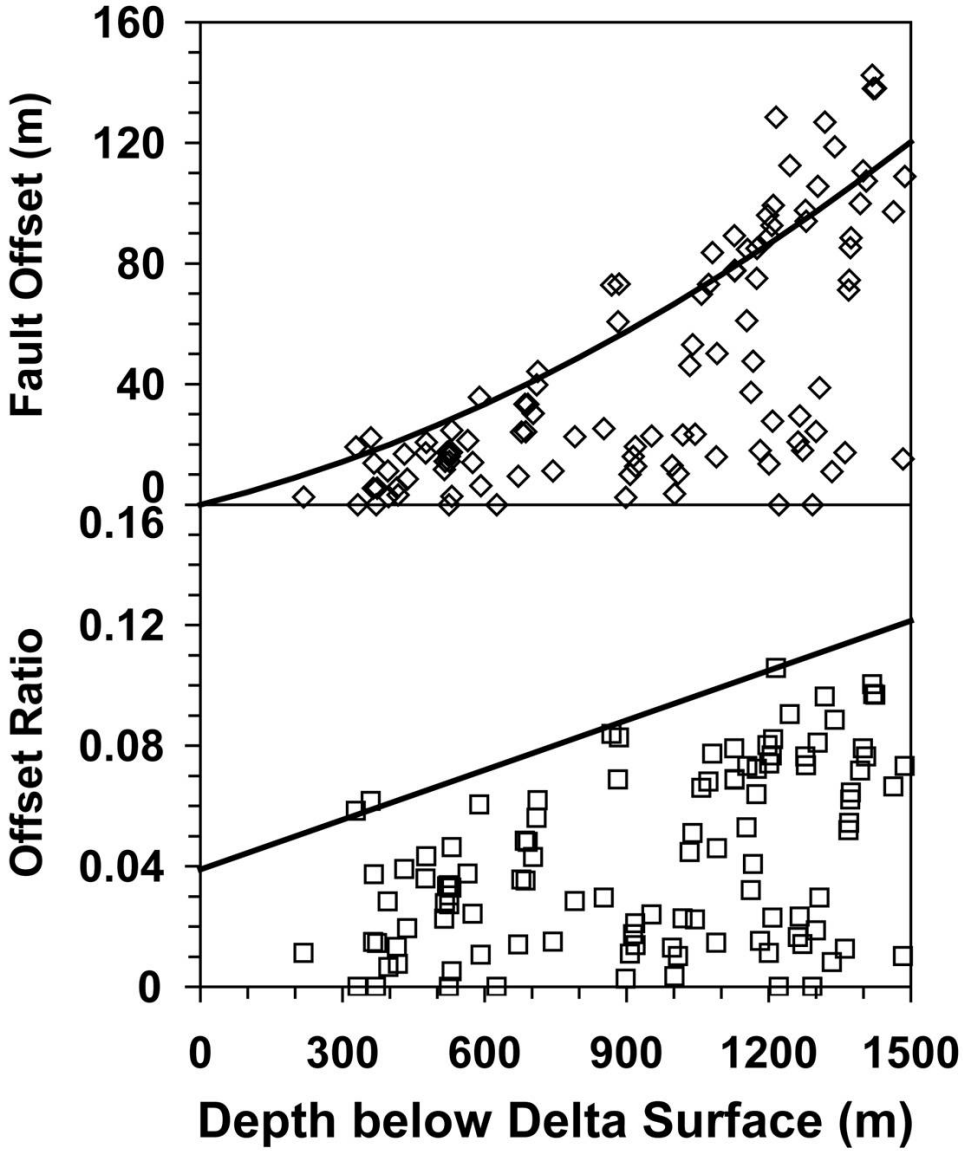

Figure 6.9: Data collected for counter-regional fault "F" shows fault offset (upper graph) and the fault offset ratio (lower graph) plotted against the depth below the delta surface. In this data set, fault offset increases exponentially with depth below the delta surface. Maximum fault offset is $\sim 150m$.
The offset ratios (the measured fault offset divided by depth below the delta surface) range from $4 - 11\%$ of the depth below the delta surface, increasing with depth.

are straightforward to measure (Figs. 6.4 to 6.9) and range between 0.039 and 0.080, with a mean of 0.056.

Generating appropriate values for deposition or burial rate is a little more involved. I assume that deposition rates are roughly equal to the sum of space created by eustatic sea-level rise and land-surface subsidence (Paola, 2000). Based on the tide-gauge record at Pensacola, FL, present-day eustatic sea-level rise is assigned a rate of $2.1mm \cdot yr^{-1}$ (González and Törnqvist, 2006). The mean value for millennial-scale subsidence rates reported by Morton et al. (2005) and Meckel et al. (2006) is $1.4mm \cdot yr^{-1}$ ($n = 104$) and the mean value for decadal-scale subsidence rates reported by Shinkle and Dokka (2004) is $11mm \cdot yr^{-1}$ ($n = 641$). Summing the sea-level rise and subsidence rates yields high and low estimates for deposition rate of $13mm \cdot yr^{-1}$ and $3.5mm \cdot yr^{-1}$. These rates, together with our measurements of offset ratio define the range of calculated values for FSR presented in Table 6.1.

Calculated values of vertical displacement rate for the studied growth faults (Table 6.1) are consistent with measurements previously reported by Lopez et al. (1997). Our calculated values for displacement over decadal to millennial time intervals are less than the annual faulting rates of $2.5mm \cdot yr^{-1}$ to $10mm \cdot yr^{-1}$ and are greater than the very-long term ($1,000,000+$ years) rates that range between $0.003mm \cdot yr^{-1}$ and $0.064mm \cdot yr^{-1}$ (Lopez et al., 1997), which likely includes times of quiescence and movement.

In addition to calculating decadal and millennial time-scale fault displacement values, longer-term movement values for the entire Holocene ($11,550yrs$) were calculated using long-term deposition rates reported by Stanley et al. (1996). The fault-related subsidence rate (FSR) is equal to the offset ratio times the deposition rate. Dividing these thicknesses by the time duration for the

Holocene yields minimum and maximum deposition rates averaged over the past $11,500$ years of $1.7mm \cdot yr^{-1}$ and $6.8mm \cdot yr^{-1}$.

By multiplying upper, lower, and mean offset ratios by the depositional rates, long-term fault displacement versus time values were calculated. Table 6.1 lists the various calculations. The rates of displacement, which are a proxy for fault induced subsidence, range from $0.07mm \cdot yr^{-1}$ to $0.14mm \cdot yr^{-1}$ (lower limit of sedimentation times lower to upper limit of fault offset ratios) to $0.27mm \cdot yr^{-1}$ to $0.55mm \cdot yr^{-1}$ (upper limit of sedimentation times lower to upper limit of fault offset ratios). These values are much lower than values obtained from studies employing surface-based fault measurements, and suggest those measurements are recording other subsidence drivers in addition to fault movement.

Both recent and long-term fault movement values suggest that displacements of active geologic faults in greater Breton Sound, Louisiana are on the order of less than $1mm \cdot yr^{-1}$. These numbers are in direct contrast to higher values, measured via surface or very shallow substrate methods, which suggest that fault movement ranges between $\sim 7.0mm \cdot yr^{-1}$ to $\sim 17.0mm \cdot yr^{-1}$ (Dokka et al., 2006) and $\sim 36mm \cdot yr^{-1}$ (Gagliano et al., 2003).

6.5 Surface Data Comparison

Faults mapped on coherency time slices were co-registered with digital orthophoto quads of the delta top in order to determine if the identified growth faults were influencing the modern-day surface morphology. In keeping with previous figures, red lines indicate regional growth faults, while green lines signify counter-regional faulting. Solid lines represent mapped fault traces and dashed lines define the inferred positioning of faults.

Figures 6.10a & 6.10b, shows the positioning of regional growth fault "C", located in the northern portion of the survey. The hanging wall for this normal fault, a potential site of enhanced subsidence, is on the southern side of its fault trace. There is a remarkable correlation between the exposure of Bayou Lery to the open water of Black Bay and the position of this growth fault. The fault location strongly corresponds with the southern extent of the wetland and cutting of the Lery channel margin. This correlation improves as the burial depth associated with the co-registered fault trace decreases from $1s$ to $.450s$ TWT. The drowned areas of marshland south of the fault trace suggest that the extra subsidence associated with an active hanging wall is sufficient to promote wetland inundation.

Regional growth fault "E", seen in figures 6.11a and 6.11b, is located in the western portion of the survey at Socola, LA. The fault trace defines a boundary between inundated wetlands and the distal Mississippi River levee to the south and relatively emergent topography to the north. There is no obvious topographic expression of the fault on the proximal river levee, suggesting that sites prone to active river sedimentation can overcome the enhanced subsidence associated with the growth faulting or that engineering practices on the proximal levee have masked the fault/surface-morphology interaction. Note that as subsurface depth decreases, the correspondence between fault location and the surface morphology strengthens (6.11b). Inferred faulting areas (dashed lines) are due to gaps in the shallow portions of the seismic. The presence of a discrete fault is suspected in this area, and strong fault signals are observed either side, however because of data gaps this portion must be inferred at $1s$ TWT (no fault evidence is seen at $.450s$ TWT).

Figures 6.12a and 6.12b show regional fault "D" and a small segment of counter-regional fault "F", located near the Mississippi River in the southern

portion of the survey. This fault is also oriented with southerly directed fault movement, and like previous faults, the position of the structure suggests an influence of surface morphology. To the east, a canal seemingly is taking advantage of the fault location. Moving westward, the southerly extent of the wetland also appears to be influence by fault position, a correlation that improves as time decreases. The 3-D seismic coverage does not extend into the far West portion of the orthophoto, but the surface morphology of the wetland suggests some growth fault influence.

On the west side of the photo panel, a wetland is positioned between green counter-regional fault "F" and red regional fault "A". Because these faults are slipping in opposite directions, a high, which directly corresponds to the location of the wetland, is created. Inferred faulting is once again used here because of data gaps over the Mississippi River in the shallow portion of the seismic.

An unnamed regional growth fault and a small piece of counter-regional fault "F" in Breton Sound are seen in Fig. 6.13. These pictures also show a notable connection between the emergent wetland on the footwall and open water over the hanging wall. Notice that crevasse splays of the Mississippi River are actively filling in the space created by hanging-wall subsidence.

A more complex system of faults related to salt movement is seen in Figs. 6.14a & 6.14b, along the Mississippi River. Both regional and counter-regional faults intertwine, creating various overprints on the surrounding morphology. To the east, fault "A" crosses the river and then strongly mimics the curves of the Jackson Bend, further suggesting that faults influence various types of surface processes seen in southeastern Louisiana, including the planform of the Mississippi River itself.

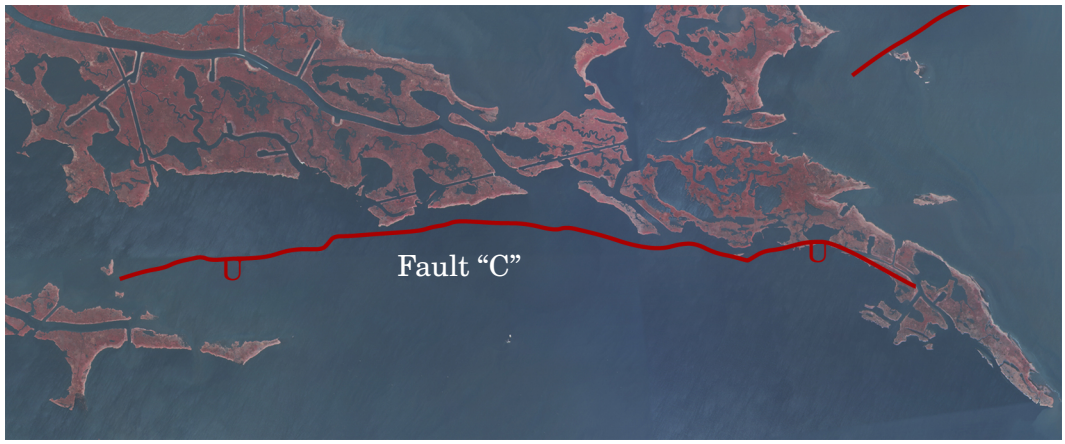

(a) $1.0s$ fault trace, in red, layered over an orthophoto. The location of the fault closely corresponds to the southerly extent of the marsh.

(b) $.450s$ fault trace in red, layered over an orthophoto. Due to the shallow depth of the coherency data and the listic shape of the fault, the fault trace location better correlates to the edge of the wetland than the $1.0s$ trace.

Figure 6.10: Orthophoto Panel 1

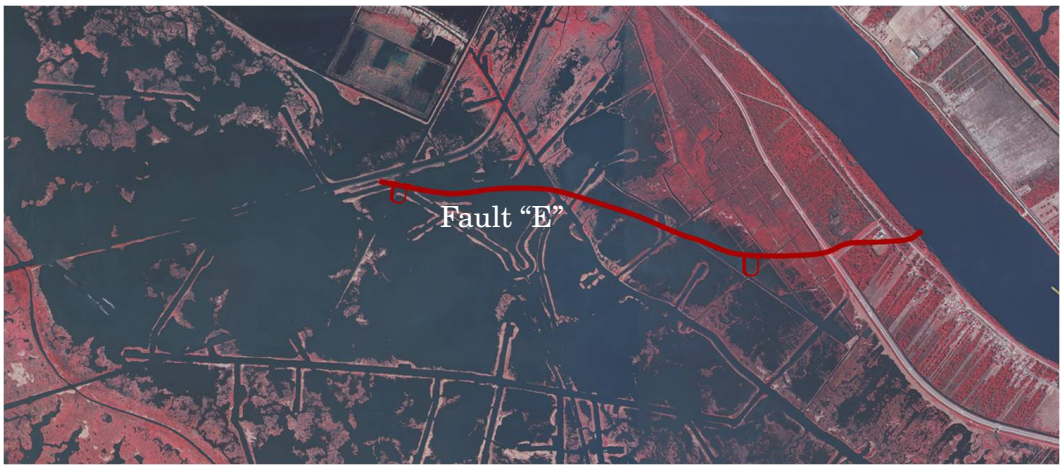

(a) $1.0s$ fault trace, in red, layered over an orthophoto. The location of the fault closely corresponds to the southerly extent of the marsh. Fault is suspected to continue to the West, however no seismic data was available to confirm this.

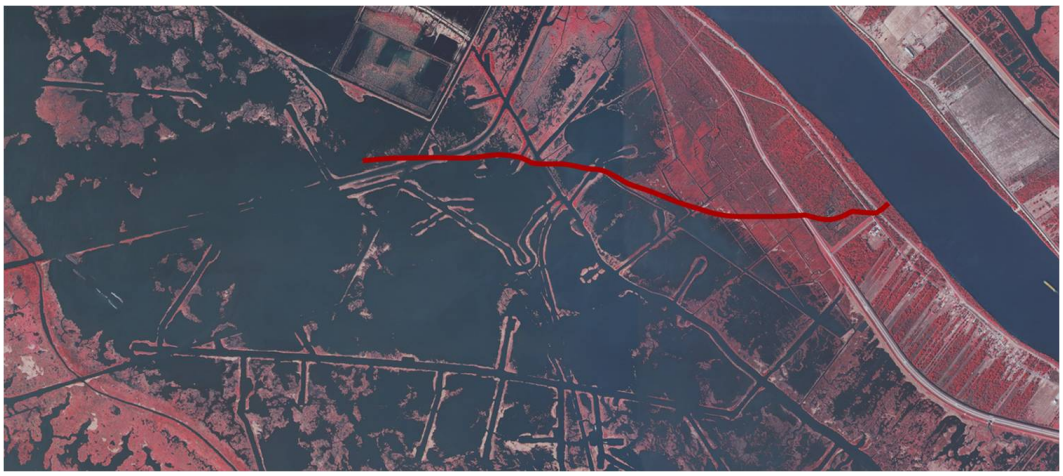

(b) $.450s$ fault trace in red, layered over an orthophoto. Due to the shallow depth of the coherency data and the listic shape of the fault, the fault trace location better correlates to the edge of the wetland than the $1.0s$ trace.

Figure 6.11: Orthophoto Panel 2

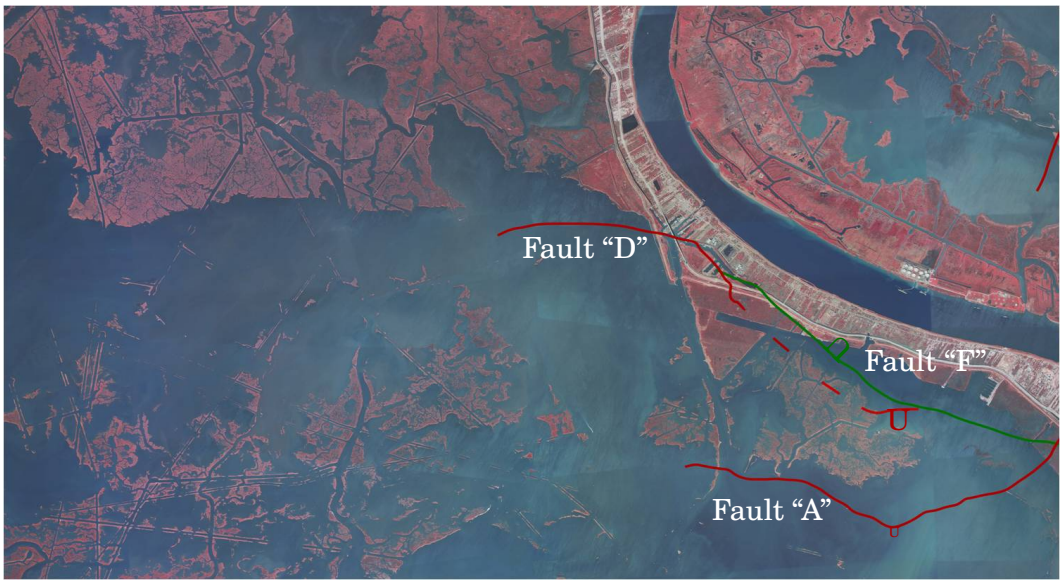

(a) $1.0s$ regional fault trace, in red, and counter-regional fault trace, in green, layered over an orthophoto. The faults seen here closely mimic the spatial extents of several wetlands. Although lack of seismic coverage to the west limits the traceability of fault signatures, it is suspected that fault influence on wetlands continues on west-ward.

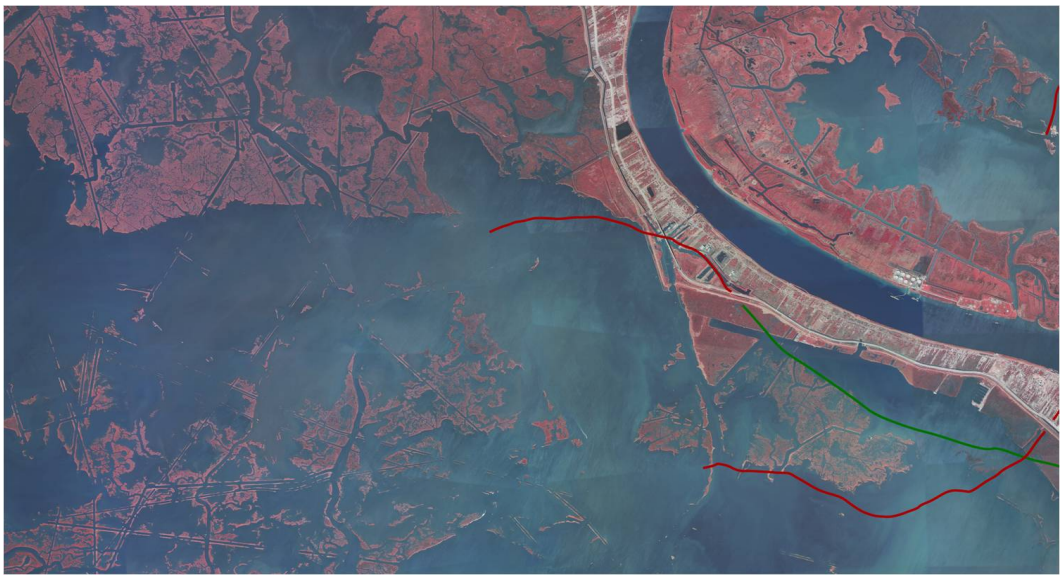

(b) $.450s$ regional fault trace, in red, and counter-regional fault trace, in green, layered over an orthophoto. The faults seen here closely mimic the spatial extents of several wetlands. Although lack of seismic coverage to the west limits the traceability of fault signatures, it is suspected that fault influence on wetlands continues on west-ward.

Figure 6.12: Orthophoto Panel 3

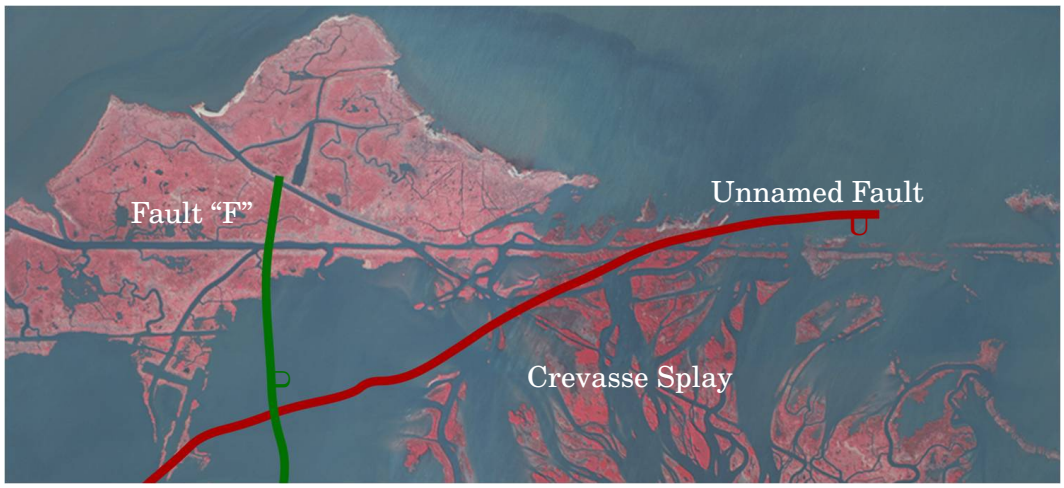

(a) $1.0s$ regional fault trace, in red, and counter-regional fault trace, in green, layered over an orthophoto. The locations of the faults roughly correspond to the location of the wetlands. Note crevasse splays filling space created by the hanging wall subsidence.

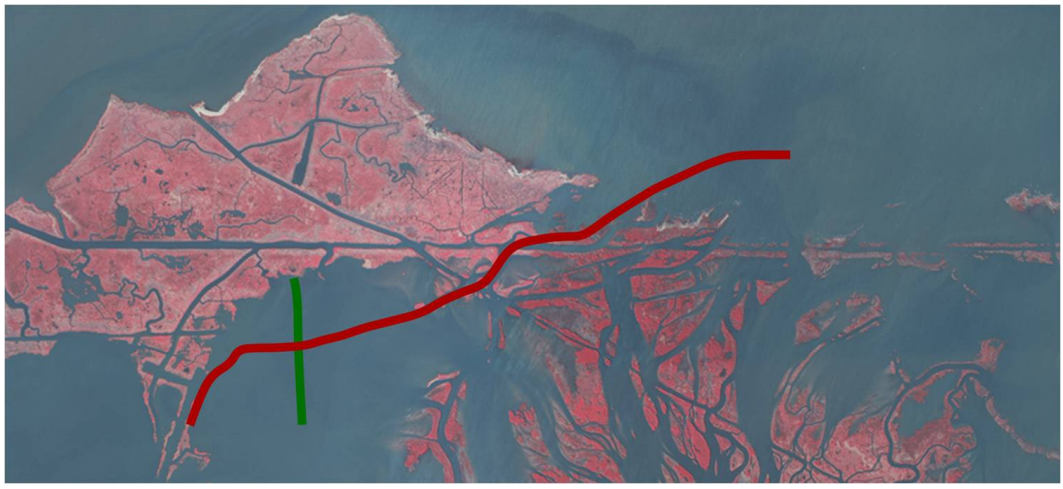

(b) $.450s$ fault trace in red, and counter-regional fault trace, in green, layered over an orthophoto. Due to the shallow depth of the coherency data and the listric shape of the fault, the fault trace location better correlates to the location of the wetland.

Figure 6.13: Orthophoto Panel 4

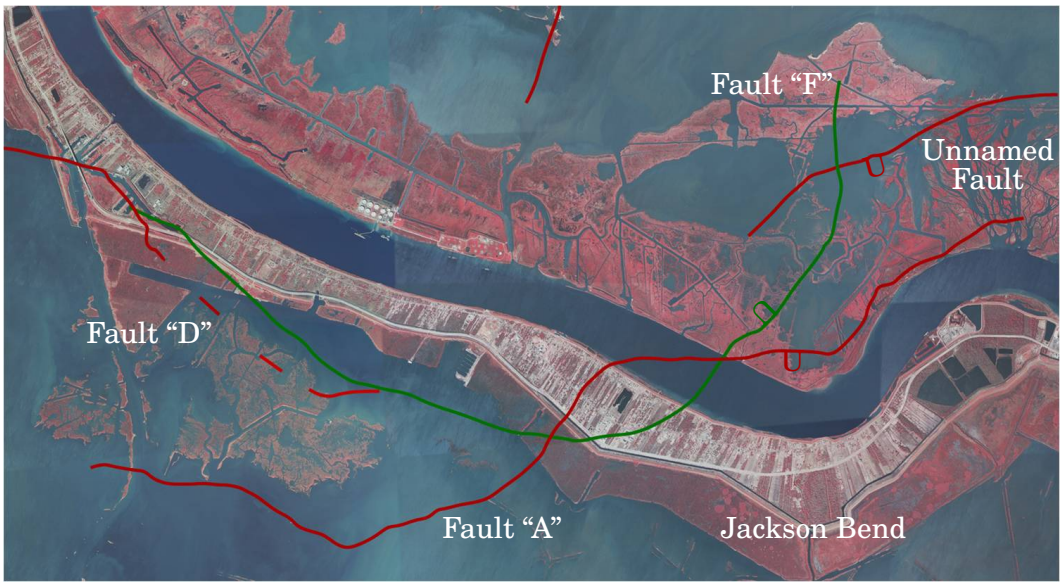

(a) $1.0s$ regional fault trace, in red, and counter-regional fault trace, in green, layered over an orthophoto. This network of complex faulting is associated with mobile salt, and the resultant fault pattern corresponds to the location of wetlands and the plan form of the Mississippi River.

(b) $.450s$ fault trace in red, and counter-regional fault trace, in green, layered over an orthophoto. Due to the shallow depth of the coherency data and the listic shape of the fault, the fault trace location better correlates to the locations of the wetlands and to the plan form of the Mississippi River.

Figure 6.14: Orthophoto Panel 5

	Offset Ratio	Dep. Rate ($mm \cdot yr^{-1}$)	F.S.R. ($mm \cdot yr^{-1}$)
Minimum offset × millennial deposition rate	0.039	3.5	0.14
Mean offset × millennial deposition rate	0.056		0.20
Maximum offset × millennial deposition rate	0.080		0.28
Minimum offset × decadal deposition rate	0.039	13	0.51
Mean offset × decadal deposition rate	0.056		0.74
Maximum offset × decadal deposition rate	0.080		1.0
Minimum offset × minimum Holocene deposition rate	0.039	1.7	0.07
Mean offset × minimum Holocene deposition rate	0.056		0.10
Maximum offset × minimum Holocene deposition rate	0.080		0.14
Minimum offset × maximum Holocene deposition rate	0.039	6.8	0.27
Mean offset × maximum Holocene deposition rate	0.056		0.38
Maximum offset × maximum Holocene deposition rate	0.080		0.55

Table 6.1: *C*alculated values of fault-related subsidence rates, $FSR = \frac{\text{fault displacement}}{\text{subsurface depth}} \times \frac{\text{depositional thickness}}{\text{time}}$. These rates characterize the magnitude of enhance subsidence associated with the vertical displacement for hanging walls of growth faults.

Chapter 7

Interpretation of Results

The information obtained using industry quality 3-D seismic, well control, high-resolution aerial imagery, and previously published depositional rates provide new insight into fault related subsidence rates and patterns. Additionally, this study confirms a significant influence of growth faulting on the modern-day surface morphology of southeastern Louisiana. However, the magnitude of fault movement and the mechanisms by which movement occurs are different than those previously proposed by other workers.

7.1 Rates of Fault Movement

The new data presented in this study provide differing results in comparison to traditional views on fault-related subsidence in coastal Louisiana. Earlier studies have recorded vertical displacement rates for faults ranging from $\sim 2.5mm \cdot yr^{-1}$ (Lopez et al. (1997)) to $\sim 16mm \cdot yr^{-1}$ (Dokka (2006)). However, long-term fault displacement rates, observed from detailed subsurface analysis of 3-D seismic data and well control, are on the order of $< 1mm \cdot yr^{-1}$, even at the upper-most limit observed (high offset ratio from salt movement combined

with high sedimentation). This discrepancy in values suggests that higher displacement rates proposed by surface mapping of faults are not representative of typical fault movement through time.

Although higher rates could be transient rates (which only occur for a short time and whose origins are not fully understood), it is likely that these high values occur because measurements made at the surface or in shallow substrate measure total subsidence, not just fault-related subsidence. Therefore rates are overprinted by other subsidence drivers such as natural compaction or fluid removal . Also contributing to higher rates are measurements skewed by on-going surficial processes such as current and wave reworking. As a wetland is converted to open water, it is quickly exposed to high energy waves which can erode the surface. This erosion can easily be mistaken for subsidence and the offset created by erosive processes incorporated into a subsidence measurement. Increased weight from man-made infrastructure such as roadways, railroads, and structures can further augment the appearance of high subsidence which can be overprinted on surface measurements. All of these scenarios occur in southeastern Louisiana and may be influencing previous attempts to quantify fault-induced subsidence.

7.2 Mechanisms of Fault Movement

This study not only challenges prior understanding of subsidence rates, but also the mechanisms by which fault movement occurs. Past workers have described fault movement as originating from the southerly movement of the SLA (Dokka (2006); Dokka et al. (2006)). This structure is suggested to be extending at rates comparable to the Basin-and-Range Province of the western United States, however concentrated mapping of the subsurface using both 3-D seismic

amplitudes and related attributes has uncovered that faulting around Breton Sound occurs at a much more local level.

Faults appear to have varying character depending upon rates of deposition (sediment loading) and proximity to mobile salt bodies. More intense faulting occurs near salt bodies, while away from the salt, sediment loading appears to be driving fault movement. No faulting patterns consistent with occurrence of the SLA were observed in roughly $1400km^2$ of 3-D seismic coverage situated within the proposed allocthon. Additionally, a proxy subsidence map generated from a continuous horizon illustrates that salt related faulting dramatically influences regional subsidence patterns through the creation of zones of enhanced subsidence above the hanging walls of both regional and counter-regional growth faults.

7.3 Fault Control on Surface Morphology

When overlain with digital orthophotos, the coherency time slices reveal the control of growth faults on the spatial extents of marshland. Wetlands are found capping the footwalls of many growth faults, while the down-thrown hanging-walls are drowned. The low rate of measured long-term fault displacement suggests that only relatively small additional subsidence along faults is necessary to convert marshland to open water.

Two bends of the lower Mississippi River are also influenced by faulting. As seen in the digital orthophoto quads, the arc-like shape of the salt derived faults set the character of the Jackson bend.

Chapter 8

Conclusions

Recent catastrophic events such as Hurricane Katrina have renewed attention to an on going debate concerning the fundamental drivers of subsidence in coastal Louisiana. As large areas of wetlands and barrier islands (imperative for protection against storm surges) are lost, many scientists are developing predictive models for coastal restoration. However, because the northern Gulf of Mexico basin has experienced not only a complex geologic history, but the compounded effects of human influence, drivers of subsidence are numerous and poorly understood. To achieve optimum results from rehabilitation efforts, each proposed subsidence driver must be independently evaluated and quantified. Subsidence related to fault movement is a critical component of that issue.

In an effort to compute fault induced subsidence rates, previous studies have heavily relied on surface measurements from benchmarks and other man-made structures. That strategy has resulted in extremely high subsidence values which have been recorded at upwards of tens of millimeters of movement per year. Those values have been used to suggest large-scale tectonic models such as the South Louisiana allochthon (SLA). I have shown that

past approaches do not adequately address subsidence rates attributed wholly to geologic faults, but rather further complicate understanding of Louisiana's subsidence problem.

Using modern subsurface technology including $\sim 1400km^2$ of 3D Kirchhoff PSTM seismic data, a second-generation coherency algorithm, and several velocity surveys from borehole check-shots, this study challenges traditional thinking about fault related subsidence. Rates of subsidence obtained from true subsurface mapping and measurement are significantly less than rates derived from surface mapping and measurements, proving that subsurface mapping and measurement is vital for obtaining realistic values and understanding of subsurface processes. This work has effectively shown that incomplete data lead to a skewed understanding of fault induced subsidence.

Problems arise when relying only on surface measurements to understand faulting, because surface measurements often record total subsidence from all contributing drivers (natural compaction, fluid removal). Additionally, surface measurements can be altered because there are surface processes at work which are independent of faulting. As land drowns, it is subjected to reworking from currents and waves, which gives the appearance that the fault has moved upwards of several centimeters to roughly a meter in a short time, when actually the fault has moved perhaps a few millimeters. Furthermore, when using man-made structures such as railroads or highways, compaction from the devices using that infrastrure undoubtedly distorts measured values. It is nearly impossible to make claims and generate values of movement related to subsurface features using only surface data, which has been influenced by surface processes. These exaggerated fault movement (subsidence) rates have creates a "sky is falling" attitude about mitigation of coastal land loss.

True subsurface measurements of six faults, both regionally and counter-regionally oriented, have revealed that fault movements in a typical coastal land loss area are on the order of $0.1-1mm{\cdot}yr^{-1}$. By multiplying $\frac{\text{fault displacement}}{\text{subsurface depth}} \times \frac{\text{depositional thickness}}{\text{time}}$ a fault related subsidence rate (FSR) was calculated for decadal and millennial time scales, as well as the entire Holocence (11,500 years). These rates (described in Table 6.1) provide minimum and maximum FSRs based on possible differences in sedimentation and fault severity. Based on those values, a minimum decadal $FSR = .51mm \cdot yr^{-1}$, an average decadal $FSR = .74mm \cdot yr^{-1}$, and a maximum decadal $FSR = 1.0mm \cdot yr^{-1}$ was calculated. For the minimum millennial time scale $FSR = .14mm \cdot yr^{-1}$, the average $FSR = .20mm \cdot yr^{-1}$, and the maximum millennial $FSR = .28mm \cdot yr^{-1}$. Finally, the Holocene minimum $FSR = .07mm \cdot yr^{-1}$., the average Holocene $FSR = .24mm \cdot yr^{-1}$, and the maximum $FSR = .55mm \cdot yr^{-1}$. These rates are much lower than most previous fault-related subsidence rates acquired by surface or shallow substrate methods, with the exception of values obtained by Lopez et al. (1997). These vaules further suggest that faulting is the result of localized influences such as salt evacuation and sediment loading, rather than large-scale tectonic models such as those proposed by Dokka (2006).

Although these fault movements are less than previously suspected, they can impact wetland morphology, as seen in the digital orthophotos. Using high resolution digital orthophoto data, coupled with seismically mapped fault traces, I have effectively shown that fault locations closely correspond with the spatial extent of wetlands and of the plan-form of the Mississippi River at the Jackson Bend.

This study has effectively proposed a systematic approach to evaluation of fault induced subsidence, which completely changes the context for examining faults. Once treated as evidence of mega-regional blocks, faults must now be

considered individually because of local influences such as salt which can alter fault character. Any engineering project aiming to rehabilitate wetlands must take each fault into consideration. One-size-fits-all methods of subsidence evaluation are inadequate to properly address the subsidence problem in southern Louisiana. However, by inputting correct values for subsidence into promising costal wetland rehabilitation models, better efforts can be made to refurbish Louisiana's dwindling marshlands. With more innovative approaches to assessing subsidence from all possible drivers, both at the surface and in the subsurface, legitimate progress can be made to mitigate coastal land loss and re-establish protection of Louisiana's population and commerce.

Appendix : Fault Data

A.1 Fault A

Table A.1: Fault "A" data

Inline (x)	Trace (y)	TWT (s)	Offset (s)	Average Depth (s)	Offset (m)	Average Depth (m)
5852	16239.6	0.39693				
5852	16252.4	0.41734	0.02041	0.407135	19.0107262	356.9059523
5852	16239.1	0.41288				
5852	16251.9	0.43329	0.02041	0.423085	19.10379143	371.8453349
5852	16242.3	0.43542				
5852	16249.75	0.4605	0.02508	0.44796	23.65326914	395.2882568
5852	16245.5	0.65312				
5852	16255.05	0.66439	0.01127	0.658755	11.30803489	600.9939184
5852	16245.5	0.68034				
5852	16255.05	0.68927	0.00893	0.684805	9.026640937	627.2901052
5852	16251.35	0.89103				
5852	16255.6	0.94546	0.05443	0.918245	58.65147544	871.5282487
5852	16250.8	0.93185				
5852	16257.2	0.98862	0.05677	0.960235	61.85443371	917.1009868
5852	16251.9	1.00456				

...

Table A.1: (. . . continued . . .)

Inline (x)	Trace (y)	TWT (s)	Offset (s)	Average Depth (s)	Offset (m)	Average Depth (m)
5852	16255.05	1.05878	0.05422	1.03167	60.1833227	995.7803391
5857	16237.5	0.41288				
5857	16250.3	0.42861	0.01573	0.420745	14.71278149	369.6490838
5857	16246	0.65525				
5857	16259.85	0.66886	0.01361	0.662055	13.66877184	604.3144566
5857	16248.15	0.70075				
5857	16259.35	0.71202	0.01127	0.706385	11.46149244	649.2198391
5857	16248.15	0.74837				
5857	16256.15	0.77091	0.02254	0.75964	23.26614601	703.9031907
5857	16253.45	0.89337				
5857	16257.2	0.9478	0.05443	0.920585	58.68788689	874.0547459
5857	16250.3	0.92739				
5857	16256.15	0.98628	0.05889	0.956835	64.1070645	913.3922763
5857	16256.65	1.30604				
5857	16261.45	1.35132	0.04528	1.32868	54.10475678	1338.432473
5867	16244.95	0.20878				
5867	16250.8	0.22026	0.01148	0.21452	10.0608077	182.1934485
5867	16243.35	0.25874				
5867	16251.9	0.27447	0.01573	0.266605	14.0196305	228.399238
5867	16241.75	0.36292				
5867	16252.4	0.3812	0.01828	0.37206	16.84345729	324.3072116
5867	16243.9	0.41734				
5867	16254.55	0.43563	0.01829	0.426485	17.1372459	375.0392371
5867	16244.4	0.44456				
5867	16254	0.4605	0.01594	0.45253	15.05404327	399.614244
5867	16249.75	0.75284				

. . .

Table A.1: (. . . continued . . .)

Inline (x)	Trace (y)	TWT (s)	Offset (s)	Average Depth (s)	Offset (m)	Average Depth (m)
5867	16259.35	0.77325	0.02041	0.763045	21.08739371	707.426881
5867	16249.2	0.82321				
5867	16259.85	0.86849	0.04528	0.84585	47.85469316	794.1308096
5867	16260.95	1.29689				
5867	16265.75	1.37386	0.07697	1.335375	92.11823517	1346.444711
5877	16246.55	0.26554				
5877	16256.15	0.27681	0.01127	0.271175	10.05930345	232.4901133
5877	16248.15	0.4082				
5877	16257.75	0.42415	0.01595	0.416175	14.89771644	365.3643033
5877	16247.1	0.42181				
5877	16256.15	0.43775	0.01594	0.42978	14.95037317	378.1376331
5877	16246.55	0.4469				
5877	16256.65	0.46731	0.02041	0.457105	19.30229169	403.9508985
5877	16246	0.46731				
5877	16255.05	0.49899	0.03168	0.48315	30.19651817	428.7521396
5877	16249.2	0.6055				
5877	16257.75	0.63505	0.02955	0.620275	29.32465811	562.5024662
5877	16252.4	0.7573				
5877	16259.85	0.79132	0.03402	0.77431	35.25865945	719.1079925
5877	16254	0.78919				
5877	16261.45	0.84128	0.05209	0.815235	54.5960177	761.8476504
5877	16253.45	0.82087				
5877	16265.75	0.87764	0.05677	0.849255	60.05329405	797.7377728
5877	16258.25	1.14722				
5877	16265.75	1.15402	0.0068	1.15062	7.77912687	1130.005424
5877	16262.55	1.33091				

. . .

Table A.1: (. . . continued . . .)

Inline (x)	Trace (y)	TWT (s)	Offset (s)	Average Depth (s)	Offset (m)	Average Depth (m)
5877	16267.35	1.41702	0.08611	1.373965	104.0070261	1392.875149
5892	16251.35	0.35845				
5892	16258.25	0.36526	0.00681	0.361855	6.254965301	314.888216
5892	16248.15	0.40608				
5892	16260.4	0.42415	0.01807	0.415115	16.87237599	364.3713057
5892	16247.1	0.42861				
5892	16261.45	0.43775	0.00914	0.43318	8.581431735	381.3379928
5892	16244.95	0.4469				
5892	16262	0.46731	0.02041	0.457105	19.30229169	403.9508985
5892	16249.2	0.4605				
5892	16262	0.47858	0.01808	0.46954	17.16302028	415.7680696
5892	16251.9	0.61464				
5892	16263.05	0.62357	0.00893	0.619105	8.858914855	561.338698
5892	16250.3	0.63505				
5892	16260.95	0.65312	0.01807	0.644085	18.05520103	586.2700087
5892	16251.9	0.75518				
5892	16262.55	0.76878	0.0136	0.76198	14.04723386	706.3244041
5892	16253.45	0.83894				
5892	16263.05	0.87764	0.0387	0.85829	41.03817448	807.3246141
5892	16252.4	0.8753				
5892	16263.6	0.90464	0.02934	0.88997	31.37838546	841.1225235
5892	16263.05	1.31964				
5892	16270.55	1.39894	0.0793	1.35929	95.44895534	1375.168809
5892	16260.95	1.35132				
5892	16271.05	1.4353	0.08398	1.39331	101.8987675	1416.309494
5912	16252.95	0.25874				

. . .

Table A.1: (. . . continued . . .)

Inline (x)	Trace (y)	TWT (s)	Offset (s)	Average Depth (s)	Offset (m)	Average Depth (m)
5912	16261.45	0.26321	0.00447	0.260975	3.976769173	223.3676397
5912	16252.95	0.4082				
5912	16262	0.42181	0.01361	0.415005	12.70754308	364.268277
5912	16253.45	0.44456				
5912	16261.45	0.45583	0.01127	0.450195	10.63608218	397.4031799
5912	16256.15	0.58743				
5912	16263.05	0.6055	0.01807	0.596465	17.80920317	538.8957464
5912	16262	0.84362				
5912	16268.95	0.8821	0.03848	0.86286	40.85515556	812.1825603
5912	16262.55	1.19272				
5912	16274.25	1.26522	0.0725	1.22897	84.56312591	1220.609446
5912	16266.8	1.24927				
5912	16275.35	1.32645	0.07718	1.28786	91.32118331	1289.856263
5912	16267.85	1.29689				
5912	16274.8	1.37407	0.07718	1.33548	92.37188139	1346.570471
5912	16267.35	1.35366				
5912	16275.85	1.43062	0.07696	1.39214	93.35517231	1414.889151
5912	16268.95	1.4353				
5912	16276.95	1.52141	0.08611	1.478355	106.576808	1520.591415
5922	16255.05	0.30169				
5922	16267.35	0.3221	0.02041	0.311895	18.45501881	269.2025588
5922	16257.75	0.39247				
5922	16271.6	0.41501	0.02254	0.40374	20.97282065	353.7353805
5922	16255.6	0.41968				
5922	16267.85	0.43542	0.01574	0.42755	14.75275563	376.0403545
5922	16258.25	0.44902				

. . .

Table A.1: (. . . continued . . .)

Inline (x)	Trace (y)	TWT (s)	Offset (s)	Average Depth (s)	Offset (m)	Average Depth (m)
5922	16264.65	0.4605	0.01148	0.45476	10.84925194	401.7273251
5922	16258.25	0.58275				
5922	16271.05	0.60104	0.01829	0.591895	18.00213264	534.3831594
5922	16258.25	0.6055				
5922	16268.95	0.62357	0.01807	0.614535	17.90255011	556.7967601
5922	16260.4	0.62591				
5922	16269.45	0.64186	0.01595	0.633885	15.89042745	576.0685066
5922	16262	0.73476				
5922	16275.85	0.76198	0.02722	0.74837	28.0092171	692.2638037
5922	16263.05	0.75964				
5922	16272.15	0.79366	0.03402	0.77665	35.28141744	721.538944
5922	16265.2	0.78919				
5922	16274.8	0.83448	0.04529	0.811835	47.42485238	758.2787942
5922	16266.8	0.83448				
5922	16273.75	0.87296	0.03848	0.85372	40.7546095	802.4725926
5922	16275.35	1.32645				
5922	16280.65	1.39214	0.06569	1.359295	79.06745677	1375.174832
5922	16273.2	1.35579				
5922	16280.15	1.43743	0.08164	1.39661	99.13650245	1420.317682
5937	16267.35	0.37886				
5937	16277.45	0.38567	0.00681	0.382265	6.294700363	333.7557502
5937	16266.8	0.43095				
5937	16276.4	0.43329	0.00234	0.43212	2.19628765	380.3398818
5937	16266.8	0.4469				
5937	16277.45	0.46263	0.01573	0.454765	14.86576577	401.7320645
5937	16268.95	0.49218				

. . .

Table A.1: (. . . continued . . .)

Inline (x)	Trace (y)	TWT (s)	Offset (s)	Average Depth (s)	Offset (m)	Average Depth (m)
5937	16277.45	0.51025	0.01807	0.501215	17.31715581	446.0674842
5937	16270.55	0.58743				
5937	16278	0.60316	0.01573	0.595295	15.49771406	537.7398809
5937	16272.15	0.64632				
5937	16278	0.66907	0.02275	0.657695	22.81988451	599.9279768
5937	16273.2	0.83682				
5937	16284.95	0.87296	0.03614	0.85489	38.28837675	803.7142308
5937	16282.8	1.32645				
5937	16290.25	1.38087	0.05442	1.35366	65.41470774	1368.392064
5937	16282.8	1.36046				
5937	16290.25	1.43977	0.07931	1.400115	96.38662283	1424.578246
5952	16270	0.37419				
5952	16282.8	0.39693	0.02274	0.38556	21.04072832	336.8128127
5952	16270.55	0.42415				
5952	16283.35	0.44009	0.01594	0.43212	14.96103638	380.3398818
5952	16274.25	0.48984				
5952	16284.4	0.51259	0.02275	0.501215	21.80217458	446.0674842
5952	16274.8	0.61677				
5952	16284.95	0.63038	0.01361	0.623575	13.51905282	565.7869815
5952	16276.4	0.64186				
5952	16287.05	0.66673	0.02487	0.654295	24.92222338	596.5110698
5952	16276.4	0.67587				
5952	16286.55	0.68948	0.01361	0.682675	13.74900069	625.1327489
5952	16278	0.70755				
5952	16287.6	0.73009	0.02254	0.71882	23.00311274	661.9163606
5952	16282.8	0.99542				

. . .

Table A.1: (. . . continued . . .)

Inline (x)	Trace (y)	TWT (s)	Offset (s)	Average Depth (s)	Offset (m)	Average Depth (m)
5952	16292.95	1.04538	0.04996	1.0204	55.29382712	983.2712521
5952	16282.25	1.02263				
5952	16291.35	1.07026	0.04763	1.046445	53.06971259	1012.234368
5952	16290.8	1.32177				
5952	16297.7	1.39214	0.07037	1.356955	84.65344191	1372.357114
5952	16289.75	1.35579				
5952	16296.65	1.43977	0.08398	1.39778	102.0060842	1421.739508
5967	16273.75	0.37652				
5967	16286	0.38779	0.01127	0.382155	10.41686631	333.6537467
5967	16276.95	0.41288				
5967	16288.15	0.42649	0.01361	0.419685	12.72575215	368.654712
5967	16276.4	0.45136				
5967	16288.65	0.47177	0.02041	0.461565	19.32831495	408.1842598
5967	16278	0.58743				
5967	16294	0.61464	0.02721	0.601035	26.85283843	543.414258
5967	16280.65	0.64186				
5967	16289.2	0.66673	0.02487	0.654295	24.92222338	596.5110698
5967	16278.55	0.71435				
5967	16291.35	0.74157	0.02722	0.72796	27.85039355	671.2765548
5967	16279.6	0.75964				
5967	16288.65	0.76878	0.00914	0.76421	9.446394323	708.6332453
5967	16285.45	0.82534				
5967	16295.6	0.86849	0.04315	0.846915	45.6167155	795.2586252
5967	16284.95	0.89783				
5967	16294.55	0.9546	0.05677	0.926215	61.30230926	880.1398194
5967	16292.4	1.32411				

. . .

Table A.1: (. . . continued . . .)

Inline (x)	Trace (y)	TWT (s)	Offset (s)	Average Depth (s)	Offset (m)	Average Depth (m)
5967	16302	1.40128	0.07717	1.362695	92.96031292	1379.27172
5967	16294	1.36493				
5967	16302	1.43743	0.0725	1.40118	88.13240203	1425.873515
5982	16267.85	0.37886				
5982	16280.65	0.39013	0.01127	0.384495	10.42440548	335.8243813
5982	16267.85	0.3946				
5982	16278.55	0.41288	0.01828	0.40374	17.00901338	353.7353805
5982	16268.95	0.43095				
5982	16279.05	0.44456	0.01361	0.437755	12.79605939	385.6495342
5982	16268.4	0.44902				
5982	16279.6	0.46497	0.01595	0.456995	15.0838469	403.8465596
5982	16269.45	0.47177				
5982	16279.6	0.48772	0.01595	0.479745	15.18758203	425.4988084
5982	16272.15	0.64186				
5982	16283.85	0.66439	0.02253	0.653125	22.5697739	595.3360102
5982	16274.8	0.71435				
5982	16284.95	0.73689	0.02254	0.72562	23.04693014	668.8779243
5982	16275.85	0.76644				
5982	16286	0.80492	0.03848	0.78568	40.00612443	730.9344864
5982	16278.55	0.87976				
5982	16288.15	0.92058	0.04082	0.90017	43.77498428	852.0650167
5982	16278.55	0.92505				
5982	16286.55	0.95906	0.03401	0.942055	36.87924288	897.308406
5982	16284.95	1.34686				
5982	16293.45	1.43062	0.08376	1.38874	101.5223961	1410.763863
5997	16263.05	0.4082				

. . .

Table A.1: (. . . continued . . .)

Inline (x)	Trace (y)	TWT (s)	Offset (s)	Average Depth (s)	Offset (m)	Average Depth (m)
5997	16278	0.42415	0.01595	0.416175	14.89771644	365.3643033
5997	16261.45	0.4469				
5997	16276.4	0.4605	0.0136	0.4537	12.84865108	400.722725
5997	16260.95	0.47624				
5997	16274.25	0.48984	0.0136	0.48304	12.96272406	428.6469879
5997	16268.4	0.66227				
5997	16276.4	0.68714	0.02487	0.674705	25.06733513	617.071805
5997	16267.85	0.71648				
5997	16279.05	0.73243	0.01595	0.724455	16.30340727	667.6843135
5997	16271.05	0.76878				
5997	16282.8	0.79366	0.02488	0.78122	25.83502312	726.2910506
5997	16272.65	0.87083				
5997	16282.8	0.90017	0.02934	0.8855	31.34089235	836.3364379
5997	16273.2	1.06579				
5997	16285.45	1.12235	0.05656	1.09407	63.7896537	1065.692985
5997	16280.15	1.30604				
5997	16286	1.38087	0.07483	1.343455	89.72991878	1356.131381
6012	16261.45	0.59423				
6012	16270.55	0.6055	0.01127	0.599865	11.11829911	542.2568757
6012	16267.35	0.70755				
6012	16276.4	0.73689	0.02934	0.72222	29.97134556	665.3955028
6012	16265.2	0.7505				
6012	16272.15	0.78005	0.02955	0.765275	30.54958244	709.7363959
6012	16264.65	0.87296				
6012	16278	0.90251	0.02955	0.887735	31.5840944	838.7287721
6012	16266.8	0.91378				

. . .

Table A.1: (. . . continued . . .)

Inline (x)	Trace (y)	TWT (s)	Offset (s)	Average Depth (s)	Offset (m)	Average Depth (m)
6012	16274.25	0.95226	0.03848	0.93302	41.62696203	887.5068709
6012	16272.65	1.16763				
6012	16280.65	1.20632	0.03869	1.186975	44.66305556	1171.829833
6012	16272.65	1.34898				
6012	16284.4	1.42382	0.07484	1.3864	90.66072935	1407.9266
6027	16258.8	0.41288				
6027	16274.25	0.42181	0.00893	0.417345	8.343840056	366.4607179
6027	16261.45	0.58743				
6027	16272.15	0.60997	0.02254	0.5987	22.22909126	541.1048253
6027	16261.45	0.6123				
6027	16271.6	0.63038	0.01808	0.62134	17.94763052	563.5621312
6027	16264.15	0.70309				
6027	16270.55	0.73689	0.0338	0.71999	34.50576905	663.1132247
6027	16264.15	0.86849				
6027	16273.75	0.90931	0.04082	0.8889	43.64346764	839.9763449
6027	16266.8	0.92292				
6027	16273.2	0.9546	0.03168	0.93876	34.32283141	893.7311735
6042	16248.7	0.43775				
6042	16257.75	0.44222	0.00447	0.439985	4.205523116	387.7532685
6042	16249.2	0.47624				
6042	16262.55	0.49218	0.01594	0.48421	15.19840672	429.7655953
6042	16249.75	0.51706				
6042	16263.6	0.55107	0.03401	0.534065	32.91244636	477.7915214
6042	16252.4	0.6055				
6042	16261.45	0.63271	0.02721	0.619105	26.99340125	561.338698
6042	16252.95	0.70309				

. . .

Table A.1: (. . . continued . . .)

Inline (x)	Trace (y)	TWT (s)	Offset (s)	Average Depth (s)	Offset (m)	Average Depth (m)
6042	16263.05	0.73243	0.02934	0.71776	29.93393633	660.8323574
6042	16254.55	0.81407				
6042	16262	0.83448	0.02041	0.824275	21.44465917	771.3525605
6042	16252.4	0.87296				
6042	16263.05	0.88444	0.01148	0.8787	12.24058164	829.0664618
6042	16258.25	1.14042				
6042	16268.95	1.22886	0.08844	1.18464	102.0345443	1169.132278
6042	16264.65	1.34005				
6042	16275.85	1.44189	0.10184	1.39097	123.5014193	1413.469197
6052	16242.3	0.58275				
6052	16251.35	0.60104	0.01829	0.591895	18.00213264	534.3831594
6052	16246	0.70755				
6052	16251.9	0.72562	0.01807	0.716585	18.42972527	659.6311226
6052	16247.6	0.86616				
6052	16258.8	0.87976	0.0136	0.87296	14.47872055	822.9399563
6052	16250.3	0.99308				
6052	16260.4	1.01136	0.01828	1.00222	20.13660187	963.1683822
6052	16251.9	1.12681				
6052	16264.15	1.14042	0.01361	1.133615	15.50353012	1110.570819

A.2 Fault B

Table A.2: Fault "B" data

Inline (x)	Trace (y)	TWT (s)	Offset (s)	Average Depth (s)	Offset (m)	Average Depth (m)
6067	15360.287	0.24721				
6067	15365.935	0.25636	0.00915	0.251785	8.116327207	215.1737449
6067	15362.626	0.32392				
6067	15367.689	0.33563	0.01171	0.329775	10.64820836	285.4714719
6067	15368.274	0.5215				
6067	15373.154	0.52418	0.00268	0.52284	2.584912258	466.9168378
6067	15366.136	0.53589				
6067	15371.984	0.54491	0.00902	0.5404	8.745246759	483.9445936
6067	15367.689	0.56321				
6067	15372.953	0.58919	0.02598	0.5762	25.45452997	518.9304494
6067	15374.908	0.88579				
6067	15381.524	0.92092	0.03513	0.903355	37.70506861	855.4879107
6067	15379.186	1.12227				
6067	15384.833	1.16788	0.04561	1.145075	52.10504831	1123.659164
6067	15382.109	1.28106				
6067	15387.373	1.32777	0.04671	1.304415	55.48943224	1309.499901
6067	15381.908	1.55925				
6067	15394.775	1.58523	0.02598	1.57224	32.85228081	1638.095665
6079	15377.431	0.25758				
6079	15382.493	0.27575	0.01817	0.266665	16.19463374	228.4529091
6079	15377.248	0.32002				
6079	15381.524	0.33954	0.01952	0.32978	17.75007292	285.4760341
6079	15379.771	0.46954				
6079	15383.663	0.47479	0.00525	0.472165	4.987670784	418.2682546

...

Table A.2: (. . . continued . . .)

Inline (x)	Trace (y)	TWT (s)	Offset (s)	Average Depth (s)	Offset (m)	Average Depth (m)
6079	15381.726	0.56967				
6079	15385.418	0.60224	0.03257	0.585955	32.0020709	528.5266387
6079	15384.833	0.76737				
6079	15388.159	0.8064	0.03903	0.786885	40.59138281	732.1900152
6079	15388.543	0.96372				
6079	15391.267	1.00019	0.03647	0.981955	39.96277914	940.870491
6079	15391.852	1.31484				
6079	15396.348	1.35253	0.03769	1.333685	45.08944658	1344.421005
6079	15402.379	1.6945				
6079	15405.889	1.71536	0.02086	1.70493	27.1692194	1808.431648
6072	15375.292	0.50467				
6072	15378.601	0.50467	0	0.50467	0	449.3896558
6072	15374.908	0.52284				
6072	15379.186	0.53065	0.00781	0.526745	7.541616071	470.6959138
6072	15375.292	0.56443				
6072	15378.802	0.59053	0.0261	0.57748	25.58165354	520.1880725
6072	15378.418	0.77517				
6072	15383.48	0.80127	0.0261	0.78822	27.15408331	733.5814762
6072	15380.172	0.87664				
6072	15386.405	0.90921	0.03257	0.892925	34.86030283	844.2895915
6072	15383.663	1.11056				
6072	15391.669	1.14056	0.03	1.12556	34.10475278	1101.393586
6072	15384.833	1.13008				
6072	15390.883	1.15483	0.02475	1.142455	28.25596213	1120.663604
6072	15387.373	1.41753				
6072	15396.933	1.44485	0.02732	1.43119	33.44510568	1462.504422

. . .

Table A.2: (. . . continued . . .)

Inline (x)	Trace (y)	TWT (s)	Offset (s)	Average Depth (s)	Offset (m)	Average Depth (m)
6072	15391.669	1.5151				
6072	15398.669	1.53462	0.01952	1.52486	24.41907059	1578.483444
6072	15397.115	1.67755				
6072	15401.995	1.69841	0.02086	1.68798	27.06813881	1786.394438
6057	15355.7	0.17064				
6057	15365.85	0.17849	0.00785	0.174565	6.789893941	147.2700689
6057	15356.75	0.24627				
6057	15362.1	0.25737	0.0111	0.25182	9.846147348	215.2049058
6057	15356.25	0.31731				
6057	15366.35	0.33478	0.01747	0.326045	15.86729774	282.0700793
6057	15354.65	0.53517				
6057	15366.9	0.54153	0.00636	0.53835	6.162544247	481.9522193
6057	15358.9	0.71188				
6057	15371.7	0.71662	0.00474	0.71425	4.831196605	657.2451504
6057	15357.3	0.86181				
6057	15372.75	0.87291	0.0111	0.86736	11.79942073	816.9718851
6057	15367.95	1.11592				
6057	15375.95	1.13161	0.01569	1.123765	17.82873431	1099.351012
6057	15362.65	1.30684				
6057	15383.4	1.32416	0.01732	1.3155	20.63028742	1322.696469
6057	15372.2	1.52455				
6057	15386.6	1.54202	0.01747	1.533285	21.89664496	1589.036997
6047	15347.2	0.24485				
6047	15363.2	0.25555	0.0107	0.2502	9.486375783	213.7629657
6047	15354.7	0.31263				
6047	15363.2	0.32358	0.01095	0.318105	9.920588939	274.8427242

. . .

Table A.2: (. . . continued . . .)

Inline (x)	Trace (y)	TWT (s)	Offset (s)	Average Depth (s)	Offset (m)	Average Depth (m)
6047	15355.8	0.68487				
6047	15372.8	0.71213	0.02726	0.6985	27.66173553	641.1917351
6047	15356.8	0.7529				
6047	15370.7	0.77736	0.02446	0.76513	25.28639001	709.5861828
6047	15360	0.8831				
6047	15374.9	0.91291	0.02981	0.898005	31.94951346	849.7399515
6047	15366.4	1.09228				
6047	15378.1	1.13585	0.04357	1.114065	49.38828997	1088.328962
6047	15367.5	1.17661				
6047	15378.1	1.21738	0.04077	1.196995	47.18095736	1183.423196
6047	15371.7	1.28515				
6047	15382.4	1.32872	0.04357	1.306935	51.79063849	1312.496872
6047	15374.9	1.51064				
6047	15384.5	1.57052	0.05988	1.54058	75.1776041	1598.191325
6037	15351.5	0.31294				
6037	15362.2	0.32582	0.01288	0.31938	11.67384408	276.0020828
6037	15353.6	0.46453				
6037	15362.2	0.48385	0.01932	0.47419	18.36581297	420.1983044
6037	15352.6	0.56755				
6037	15362.2	0.58023	0.01268	0.57389	12.41516138	516.6620092
6037	15354.7	0.68675				
6037	15363.2	0.71231	0.02556	0.69953	25.94420863	642.239427
6037	15352.6	0.77045				
6037	15365.4	0.7962	0.02575	0.783325	26.75391399	728.4819242
6037	15356.8	0.85395				
6037	15366.4	0.87658	0.02263	0.865265	24.04238261	814.7414737

. . .

Table A.2: (. . . continued . . .)

Inline (x)	Trace (y)	TWT (s)	Offset (s)	Average Depth (s)	Offset (m)	Average Depth (m)
6037	15364.3	1.09919				
6037	15372.8	1.13451	0.03532	1.11685	40.06471495	1091.490808
6037	15363.7	1.18523				
6037	15372.25	1.22815	0.04292	1.20669	49.78799562	1194.667638
6037	15368.5	1.67279				
6037	15378.1	1.68879	0.016	1.68079	20.72886792	1777.07112
6027	15343.45	0.24896				
6027	15351.95	0.25712	0.00816	0.25304	7.241094854	216.2913028
6027	15342.9	0.3075				
6027	15352.5	0.31834	0.01084	0.31292	9.804862054	270.1327501
6027	15346.65	0.48427				
6027	15353.55	0.49792	0.01365	0.491095	13.04181386	436.3560362
6027	15348.75	0.5659				
6027	15353.55	0.58082	0.01492	0.57336	14.60611538	516.1417581
6027	15353.05	0.85287				
6027	15358.35	0.87328	0.02041	0.863075	21.67104983	812.4112529
6027	15353.05	0.97531				
6027	15359.45	0.98347	0.00816	0.97939	8.935510188	938.0564881
6027	15354.65	1.1031				
6027	15363.15	1.13167	0.02857	1.117385	32.41232284	1092.098453
6027	15358.35	1.18601				
6027	15364.25	1.22134	0.03533	1.203675	40.953003	1191.167928
6027	15362.1	1.5069				
6027	15369.55	1.5546	0.0477	1.53075	59.75192064	1585.859419
6017	15336.5	0.38492				
6017	15343.95	0.38773	0.00281	0.386325	2.600634181	337.5230113

. . .

Table A.2: (. . . continued . . .)

Inline (x)	Trace (y)	TWT (s)	Offset (s)	Average Depth (s)	Offset (m)	Average Depth (m)
6017	15337.05	0.41897				
6017	15343.45	0.42854	0.00957	0.423755	8.95936777	372.4744621
6017	15335.95	0.46106				
6017	15343.95	0.46922	0.00816	0.46514	7.735877661	411.5816675
6017	15337.05	0.50187				
6017	15345.55	0.51004	0.00817	0.505955	7.840687034	450.6261175
6017	15340.25	0.68962				
6017	15348.25	0.6951	0.00548	0.69236	5.551140685	634.9525153
6017	15348.75	0.85274				
6017	15361.05	0.88539	0.03265	0.869065	34.72321957	818.7880077
6017	15354.1	0.96026				
6017	15359.45	0.9725	0.01224	0.96638	13.35774106	923.8122552
6017	15356.25	1.08946				
6017	15362.1	1.11662	0.02716	1.10304	30.70131296	1075.833732
6017	15353.05	1.17376				
6017	15363.15	1.20909	0.03533	1.191425	40.82927628	1176.975066
6017	15357.3	1.27299				
6017	15364.75	1.2948	0.02181	1.283895	25.78138078	1285.16306
6017	15353.05	1.33829				
6017	15365.85	1.3587	0.02041	1.348495	24.50338369	1362.18294
6017	15363.15	1.50703				
6017	15368.5	1.55728	0.05025	1.532155	62.96638919	1587.620337
6007	15329.05	0.30342				
6007	15343.95	0.31018	0.00676	0.3068	6.102643972	264.5832499
6007	15327.95	0.41081				
6007	15337.55	0.41629	0.00548	0.41355	5.114350694	362.9058118

. . .

Table A.2: (. . . continued . . .)

Inline (x)	Trace (y)	TWT (s)	Offset (s)	Average Depth (s)	Offset (m)	Average Depth (m)
6007	15333.85	0.45698				
6007	15349.85	0.46922	0.01224	0.4631	11.59667818	409.6425628
6007	15338.65	0.49652				
6007	15355.7	0.51144	0.01492	0.50398	14.31018681	448.7259124
6007	15336.5	0.5645				
6007	15349.85	0.57814	0.01364	0.57132	13.34508904	514.1400256
6007	15337.05	0.68426				
6007	15355.15	0.70734	0.02308	0.6958	23.40231922	638.4467869
6007	15341.85	0.85147				
6007	15361.55	0.88131	0.02984	0.86639	31.71196982	815.9390339
6007	15346.65	0.97658				
6007	15355.7	0.99151	0.01493	0.984045	16.36878595	943.1647623
6007	15348.25	1.04048				
6007	15357.3	1.06089	0.02041	1.050685	22.76571869	1016.967636
6007	15350.9	1.15603				
6007	15358.35	1.1846	0.02857	1.170315	32.84463346	1152.616888
6007	15353.05	1.27171				
6007	15358.35	1.28523	0.01352	1.27847	15.96088733	1278.748943
6007	15354.65	1.49466				
6007	15364.25	1.55179	0.05713	1.523225	71.44161133	1576.437699
5997	15334.9	0.51208				
5997	15342.35	0.5148	0.00272	0.51344	2.616183658	457.8376979
5997	15337.05	0.5231				
5997	15341.85	0.52453	0.00143	0.523815	1.379661472	467.859992
5997	15334.9	0.56086				
5997	15348.25	0.57993	0.01907	0.570395	18.65264395	513.2327663

. . .

Table A.2: (. . . continued . . .)

Inline (x)	Trace (y)	TWT (s)	Offset (s)	Average Depth (s)	Offset (m)	Average Depth (m)
5997	15335.45	0.68774				
5997	15346.65	0.69968	0.01194	0.69371	12.09961171	636.3234135
5997	15334.9	0.77622				
5997	15346.65	0.78349	0.00727	0.779855	7.546223268	724.8710372
5997	15341.85	0.97251				
5997	15349.85	0.98471	0.0122	0.97861	13.35674333	937.201138
5997	15346.1	1.157				
5997	15355.7	1.17854	0.02154	1.16777	24.74713557	1149.688829
5997	15346.1	1.17854				
5997	15353.05	1.20254	0.024	1.19054	27.7296378	1175.951353
5997	15348.75	1.52105				
5997	15357.85	1.53545	0.0144	1.52825	18.02802398	1582.727497
5997	15356.75	1.63353				
5997	15362.65	1.66726	0.03373	1.650395	43.40595384	1737.819768
5987	15348.75	0.25178				
5987	15357.3	0.25897	0.00719	0.255375	6.38512699	218.3717728
5987	15347.15	0.30681				
5987	15356.25	0.31647	0.00966	0.31164	8.734008273	268.9711916
5987	15340.75	0.3596				
5987	15346.1	0.36903	0.00943	0.364315	8.66805951	317.1560407
5987	15342.35	0.41934				
5987	15354.1	0.429	0.00966	0.42417	9.044771211	372.8642092
5987	15343.95	0.53906				
5987	15352.5	0.544	0.00494	0.54153	4.791121226	485.0433388
5987	15335.45	0.68752				
5987	15352.5	0.70437	0.01685	0.695945	17.08601385	638.5941482

. . .

Table A.2: (. . . continued . . .)

Inline (x)	Trace (y)	TWT (s)	Offset (s)	Average Depth (s)	Offset (m)	Average Depth (m)
5987	15338.1	0.78343				
5987	15351.45	0.78815	0.00472	0.78579	4.907344565	731.0490819
5987	15339.7	0.85508				
5987	15351.45	0.87193	0.01685	0.863505	17.89316344	812.8686775
5987	15339.15	0.98221				
5987	15350.9	0.99905	0.01684	0.99063	18.49455197	950.4014659
5987	15342.9	1.20008				
5987	15353.05	1.22164	0.02156	1.21086	25.03570176	1199.512283
5987	15345.05	1.2888				
5987	15353.55	1.29823	0.00943	1.293515	11.17304184	1296.557564
5987	15348.75	1.44894				
5987	15357.3	1.48016	0.03122	1.46455	38.517224	1503.524271
5987	15349.85	1.49701				
5987	15356.75	1.53048	0.03347	1.513745	41.76384661	1564.591075
5987	15354.1	1.71959				
5987	15361.05	1.75553	0.03594	1.73756	47.14550448	1851.084369
5977	15340.75	0.48403				
5977	15348.25	0.48875	0.00472	0.48639	4.503348098	431.8508741
5977	15342.35	0.53434				
5977	15349.3	0.54153	0.00719	0.537935	6.965922628	481.5490301
5977	15338.1	0.77624				
5977	15346.1	0.78815	0.01191	0.782195	12.37048713	727.3056695
5977	15337.55	0.84812				
5977	15347.15	0.86002	0.0119	0.85407	12.60461723	802.8439821
5977	15339.15	0.97727				
5977	15348.75	0.99411	0.01684	0.98569	18.47076972	944.9714118

. . .

Table A.2: (. . . continued . . .)

Inline (x)	Trace (y)	TWT (s)	Offset (s)	Average Depth (s)	Offset (m)	Average Depth (m)
5977	15342.35	1.32698				
5977	15353.05	1.34854	0.02156	1.33776	25.81785915	1349.302031
5977	15343.95	1.44423				
5977	15356.25	1.47298	0.02875	1.458605	35.42103493	1496.191111
5977	15347.15	1.52082				
5977	15356.25	1.55204	0.03122	1.53643	39.15876547	1592.981734
5967	15329.05	0.49593				
5967	15337.05	0.50087	0.00494	0.4984	4.730211004	443.3632111
5967	15331.15	0.67562				
5967	15338.65	0.68281	0.00719	0.679215	7.256320446	621.6310542
5967	15329.55	0.71403				
5967	15337.55	0.72121	0.00718	0.71762	7.325059016	660.689211
5967	15338.65	0.96289				
5967	15345.05	0.97255	0.00966	0.96772	10.54583933	925.2771603
5967	15337.55	1.04914				
5967	15345.55	1.06105	0.01191	1.055095	13.29966545	1021.896093
5967	15337.55	1.09227				
5967	15344.5	1.1163	0.02403	1.104285	27.17175419	1077.243031
5967	15343.45	1.26701				
5967	15347.7	1.28386	0.01685	1.275435	19.87746238	1275.164226
5967	15346.65	1.49701				
5967	15357.3	1.528	0.03099	1.512505	38.65831836	1563.043402
5967	15346.1	1.53048				
5967	15356.75	1.55451	0.02403	1.542495	30.18212385	1600.596916
5957	15346.65	0.26122				
5957	15354.65	0.26841	0.00719	0.264815	6.404530695	226.7985186

. . .

Table A.2: (. . . continued . . .)

Inline (x)	Trace (y)	TWT (s)	Offset (s)	Average Depth (s)	Offset (m)	Average Depth (m)
5957	15345.05	0.32119				
5957	15351.95	0.32366	0.00247	0.322425	2.240845402	278.7727698
5957	15344.5	0.34522				
5957	15350.9	0.35466	0.00944	0.34994	8.638457598	303.9283104
5957	15345.05	0.41934				
5957	15351.45	0.429	0.00966	0.42417	9.044771211	372.8642092
5957	15343.95	0.46965				
5957	15356.25	0.47684	0.00719	0.473245	6.832953808	419.2974697
5957	15343.95	0.4984				
5957	15353.55	0.50806	0.00966	0.50323	9.263103371	448.0046054
5957	15338.1	0.72346				
5957	15351.45	0.73559	0.01213	0.729525	12.41634814	672.881634
5957	15341.85	0.96783				
5957	15351.45	0.97727	0.00944	0.97255	10.31869969	930.5616048
5957	15337.05	1.10192				
5957	15348.75	1.1163	0.01438	1.10911	16.27991963	1082.708926
5957	15341.3	1.50173				
5957	15358.35	1.53048	0.02875	1.516105	35.8936303	1567.537851
5957	15347.15	1.62144				
5957	15355.15	1.64772	0.02628	1.63458	33.69999323	1717.500326
5957	15349.85	1.69579				
5957	15356.75	1.72454	0.02875	1.710165	37.48861914	1815.254303
5947	15329.55	0.7713				
5947	15340.75	0.78096	0.00966	0.77613	10.01674423	720.9985983
5947	15332.75	0.85755				
5947	15339.7	0.86474	0.00719	0.861145	7.630273413	810.3588073

. . .

Table A.2: (. . . continued . . .)

Inline (x)	Trace (y)	TWT (s)	Offset (s)	Average Depth (s)	Offset (m)	Average Depth (m)
5947	15335.95	0.98221				
5947	15346.1	0.99164	0.00943	0.986925	10.34652168	946.3282763
5947	15335.95	1.10417				
5947	15343.45	1.10911	0.00494	1.10664	5.589196241	1079.910016
5947	15339.7	1.32923				
5947	15347.7	1.34136	0.01213	1.335295	14.51699155	1346.348896
5947	15339.7	1.44176				
5947	15347.15	1.44894	0.00718	1.44535	8.818811004	1479.877163
5947	15343.95	1.52576				
5947	15350.35	1.53295	0.00719	1.529355	9.003763833	1584.111588
5947	15346.1	1.61425				
5947	15352.5	1.63582	0.02157	1.625035	27.60129568	1705.271045
5947	15348.75	1.7005				
5947	15356.25	1.73172	0.03122	1.71611	40.76244067	1823.011713
5937	15321.6	0.67822				
5937	15330.2	0.68278	0.00456	0.6805	4.60373651	622.9311427
5937	15318.4	0.71465				
5937	15331.2	0.72219	0.00754	0.71842	7.694056598	661.5072653
5937	15320.6	0.96946				
5937	15336.6	0.98013	0.01067	0.974795	11.67003929	933.020085
5937	15330.2	1.10604				
5937	15339.8	1.12582	0.01978	1.11593	22.43194551	1090.446077
5937	15336.6	1.30622				
5937	15345.1	1.31988	0.01366	1.31305	16.26120187	1319.776771
5937	15341.9	1.50811				
5937	15348.3	1.52319	0.01508	1.51565	18.82502785	1566.9696

. . .

Table A.2: (. . . continued . . .)

Inline (x)	Trace (y)	TWT (s)	Offset (s)	Average Depth (s)	Offset (m)	Average Depth (m)
5937	15343	1.68254				
5937	15348.3	1.71441	0.03187	1.698475	41.45044175	1800.029697
5927	15319.5	0.67666				
5927	15331.2	0.68278	0.00612	0.67972	6.177334324	622.141928
5927	15314.2	0.84824				
5927	15327	0.85279	0.00455	0.850515	4.814788288	799.0733417
5927	15321.6	1.09993				
5927	15333.4	1.1197	0.01977	1.109815	22.38604374	1083.508122
5927	15337.6	1.45191				
5927	15349.4	1.47468	0.02277	1.463295	28.08398916	1501.975393
5927	15335.5	1.51409				
5927	15348.3	1.53529	0.0212	1.52469	26.5196816	1578.270701
5927	15343	1.62022				
5927	15353.6	1.65209	0.03187	1.636155	40.88264451	1719.520738
5917	15328	0.85265				
5917	15336.6	0.85877	0.00612	0.85571	6.485243894	804.5846702
5917	15330.2	0.97714				
5917	15343	0.98468	0.00754	0.98091	8.259863033	939.7238201
5917	15331.2	1.03932				
5917	15343	1.04543	0.00611	1.042375	6.800699848	1007.695674
5917	15334.4	1.11671				
5917	15345.1	1.13037	0.01366	1.12354	15.52114242	1099.095043
5917	15336.6	1.30167				
5917	15355.8	1.32444	0.02277	1.313055	27.10600374	1319.782728
5917	15338.7	1.37309				
5917	15349.4	1.39429	0.0212	1.38369	25.6651291	1404.64265

. . .

Table A.2: (. . . continued . . .)

Inline (x)	Trace (y)	TWT (s)	Offset (s)	Average Depth (s)	Offset (m)	Average Depth (m)
5917	15341.9	1.44437				
5917	15348.3	1.46102	0.01665	1.452695	20.48526834	1488.911062
5917	15340.8	1.50968				
5917	15352.6	1.52476	0.01508	1.51722	18.83179623	1568.930628
5917	15340.8	1.6188				
5917	15359	1.65522	0.03642	1.63701	46.72825921	1720.617828
5907	15345.1	1.13635				
5907	15367.5	1.14702	0.01067	1.141685	12.17911047	1119.7836
5907	15337.6	1.33055				
5907	15354.7	1.34265	0.0121	1.3366	14.48560222	1347.912106
5907	15339.8	1.40041				
5907	15357.9	1.42004	0.01963	1.410225	23.91336656	1436.887157
5907	15335.5	1.43982				
5907	15355.8	1.45945	0.01963	1.449635	24.13452856	1485.14559
5907	15338.7	1.52021				
5907	15357.9	1.53998	0.01977	1.530095	24.76140225	1585.038684
5907	15337.6	1.61724				
5907	15354.7	1.64612	0.02888	1.63168	37.01014391	1713.782044
5907	15346.2	1.68098				
5907	15355.8	1.70829	0.02731	1.694635	35.48967965	1795.037088

A.3 Fault C

Table A.3: Fault "C" data

Inline (x)	Trace (y)	TWT (s)	Offset (s)	Average Depth (s)	Offset (m)	Average Depth (m)
5785	15194.15	0.54859				
5785	15202.7	0.55283	0.00424	0.55071	4.123344773	493.9828533
5785	15196.3	0.66378				
5785	15201.1	0.70481	0.04103	0.684295	41.46804673	626.7734379
5785	15195.75	0.79515				
5785	15203.2	0.8198	0.02465	0.807475	25.78121199	753.7070598
5785	15198.95	0.85659				
5785	15202.7	0.89358	0.03699	0.875085	39.4024619	825.2069545
5785	15201.6	1.22007				
5785	15209.6	1.2715	0.05143	1.245785	60.23455966	1240.281302
5785	15206.4	1.28595				
5785	15213.9	1.33719	0.05124	1.31157	60.9756836	1318.01386
5785	15209.6	1.4728				
5785	15214.4	1.53444	0.06164	1.50362	76.73593715	1551.966587
5785	15211.75	1.59396				
5785	15218.15	1.64731	0.05335	1.620635	68.20035309	1699.642364
5785	15213.35	1.65155				
5785	15217.6	1.70491	0.05336	1.67823	69.09172286	1773.755092
5785	15215.5	1.77271				
5785	15220.3	1.82607	0.05336	1.79939	70.93996496	1932.734655
5805	15191.5	0.48468				
5805	15197.9	0.48984	0.00516	0.48726	4.924435106	432.6834489
5805	15190.95	0.53803				

...

Table A.3: (. . . continued . . .)

Inline (x)	Trace (y)	TWT (s)	Offset (s)	Average Depth (s)	Offset (m)	Average Depth (m)
5805	15198.95	0.54835	0.01032	0.54319	10.01387946	486.6580817
5805	15195.25	0.92649				
5805	15201.6	0.97291	0.04642	0.9497	50.43766196	905.6201
5805	15200	1.21017				
5805	15208.55	1.26336	0.05319	1.236765	62.15870516	1229.718838
5805	15200.55	1.28399				
5805	15208.55	1.3425	0.05851	1.313245	69.65501292	1320.009093
5805	15209.1	1.56768				
5805	15212.8	1.63457	0.06689	1.601125	85.13622845	1674.750444
5825	15192.55	0.43842				
5825	15199.5	0.45228	0.01386	0.44535	13.06120188	392.8202745
5825	15191.5	0.52095				
5825	15198.95	0.52272	0.00177	0.521835	1.706690976	465.9449459
5825	15188.85	0.64973				
5825	15200.55	0.68584	0.03611	0.667785	36.32508473	610.0874574
5825	15193.65	0.74596				
5825	15204.3	0.789	0.04304	0.76748	44.52303713	712.0214065
5825	15190.95	0.80109				
5825	15198.45	0.84058	0.03949	0.820835	41.45306013	767.7329154
5825	15195.75	1.09315				
5825	15203.2	1.12249	0.02934	1.10782	33.20565008	1081.246931
5825	15198.45	1.20147				
5825	15204.8	1.25482	0.05335	1.228145	62.21421414	1219.646343
5825	15202.7	1.3475				
5825	15208.55	1.39908	0.05158	1.37329	62.29038817	1392.059377

. . .

Table A.3: (. . . continued . . .)

Inline (x)	Trace (y)	TWT (s)	Offset (s)	Average Depth (s)	Offset (m)	Average Depth (m)
5845	15183.5	0.45389				
5845	15192.55	0.45744	0.00355	0.455665	3.355870061	402.5852784
5845	15182.95	0.48323				
5845	15190.95	0.49516	0.01193	0.489195	11.39196972	434.5359799
5845	15187.75	0.79593				
5845	15195.75	0.84751	0.05158	0.82172	54.15710772	768.6638115
5845	15190.45	0.83381				
5845	15196.3	0.87668	0.04287	0.855245	45.42279878	804.091044
5845	15189.9	0.86991				
5845	15199.5	0.89909	0.02918	0.8845	31.16163889	835.2665011
5845	15190.45	0.887				
5845	15197.9	0.92665	0.03965	0.906825	42.59572264	859.2203674
5845	15190.95	0.93003				
5845	15195.75	0.96791	0.03788	0.94897	41.15061767	904.8257232
5845	15192.55	1.06752				
5845	15202.15	1.1104	0.04288	1.08896	48.29839762	1059.926243
5845	15192.05	1.1947				
5845	15201.6	1.2445	0.0498	1.2196	57.95272055	1209.682291
5845	15193.1	1.24628				
5845	15204.8	1.28399	0.03771	1.265135	44.37436739	1263.018111
5862	15180.8	0.25524				
5862	15188.8	0.26488	0.00964	0.26006	8.573776985	222.5507427
5862	15181.35	0.44788				
5862	15189.35	0.45586	0.00798	0.45187	7.534960153	398.9891183

. . .

Table A.3: (. . . continued . . .)

Inline (x)	Trace (y)	TWT (s)	Offset (s)	Average Depth (s)	Offset (m)	Average Depth (m)
5862	15184	0.48159				
5862	15189.9	0.49604	0.01445	0.488815	13.79675065	434.1720916
5862	15183.5	0.48957				
5862	15188.3	0.51199	0.02242	0.50078	21.48313516	445.6494479
5862	15184.55	0.6339				
5862	15188.3	0.67408	0.04018	0.65399	40.26086873	596.2047134
5862	15187.2	1.09291				
5862	15200.55	1.11067	0.01776	1.10179	20.06932792	1074.419216
5862	15191.5	1.18923				
5862	15200.55	1.24221	0.05298	1.21572	61.59454978	1205.164784
5862	15193.6	1.255				
5862	15200.55	1.30647	0.05147	1.280735	60.79567028	1281.425896
5862	15195.75	1.33687				
5862	15203.75	1.38984	0.05297	1.363355	63.81856997	1380.067378
5862	15197.9	1.38503				
5862	15201.1	1.438	0.05297	1.411515	64.54785992	1438.459816
5862	15200.55	1.55509				
5862	15203.75	1.60972	0.05463	1.582405	69.23958844	1650.967958
5882	15175.5	0.29543				
5882	15180.8	0.3034	0.00797	0.299415	7.178154679	257.9008179
5882	15176.55	0.47196				
5882	15182.95	0.48159	0.00963	0.476775	9.161504708	422.6637866
5882	15180.3	0.65165				
5882	15185.1	0.68055	0.0289	0.6661	29.05821791	608.3888455
5882	15185.6	0.92285				

. . .

Table A.3: (. . . continued . . .)

Inline (x)	Trace (y)	TWT (s)	Offset (s)	Average Depth (s)	Offset (m)	Average Depth (m)
5882	15189.35	0.95656	0.03371	0.939705	36.53128649	894.7568023
5882	15186.15	0.98064				
5882	15189.35	1.0127	0.03206	0.99667	35.26529531	957.050048
5882	15188.3	1.25184				
5882	15193.1	1.29353	0.04169	1.272685	49.14772348	1271.918386
5882	15194.15	1.56156				
5882	15200	1.62567	0.06411	1.593615	81.46025959	1665.197559
5892	15177.1	0.39807				
5892	15187.75	0.41898	0.02091	0.408525	19.48475615	358.2050091
5892	15179.75	0.52975				
5892	15185.6	0.55549	0.02574	0.54262	24.97228405	486.1035337
5892	15182.95	0.63721				
5892	15187.75	0.66926	0.03205	0.653235	32.10758814	595.4464693
5892	15174.95	0.84098				
5892	15191.5	0.85543	0.01445	0.848205	15.28137852	796.6251427
5892	15185.1	0.99509				
5892	15190.95	1.03196	0.03687	1.013525	40.73384795	975.6580702
5892	15187.75	1.06086				
5892	15197.9	1.1042	0.04334	1.08253	48.73685614	1052.680378
5892	15184.55	1.18291				
5892	15196.3	1.20684	0.02393	1.194875	27.6784159	1180.967934
5892	15187.2	1.25334				
5892	15195.2	1.30316	0.04982	1.27825	58.8113198	1278.489007
5902	15172.8	0.24411				

. . .

Table A.3: (. . . continued . . .)

Inline (x)	Trace (y)	TWT (s)	Offset (s)	Average Depth (s)	Offset (m)	Average Depth (m)
5902	15179.75	0.24727	0.00316	0.24569	2.797509629	209.7525968
5902	15173.9	0.26337				
5902	15181.35	0.273	0.00963	0.268185	8.587251349	229.8129187
5902	15176	0.28414				
5902	15180.3	0.29708	0.01294	0.29061	11.62179685	249.9536966
5902	15174.95	0.49438				
5902	15182.95	0.49769	0.00331	0.496035	3.167194968	441.0929751
5902	15178.7	0.64684				
5902	15185.6	0.67408	0.02724	0.66046	27.34520918	602.7091441
5902	15182.95	0.97899				
5902	15190.95	1.01435	0.03536	0.99667	38.89522277	957.050048
5902	15185.6	1.16997				
5902	15194.15	1.20849	0.03852	1.18923	44.49164283	1174.436435
5902	15187.2	1.25334				
5902	15195.75	1.29518	0.04184	1.27426	49.34339518	1273.777104
5902	15188.8	1.28555				
5902	15201.1	1.3176	0.03205	1.301575	38.04797357	1306.124523
5902	15185.6	1.3176				
5902	15199.5	1.33521	0.01761	1.326405	21.03061327	1335.712762
5922	15170.7	0.23764				
5922	15176.55	0.24095	0.00331	0.239295	2.924251457	204.0759454
5922	15170.15	0.27782				
5922	15176	0.28745	0.00963	0.282635	8.627032551	242.7746887
5922	15176	0.64518				
5922	15184	0.66926	0.02408	0.65722	24.15070017	599.4504177

. . .

Table A.3: (. . . continued . . .)

Inline (x)	Trace (y)	TWT (s)	Offset (s)	Average Depth (s)	Offset (m)	Average Depth (m)
5922	15184.55	0.79929				
5922	15190.4	0.82187	0.02258	0.81058	23.63626102	756.962295
5922	15186.7	0.84911				
5922	15190.95	0.86837	0.01926	0.85874	20.42612735	807.8027047
5922	15189.9	1.04159				
5922	15193.6	1.06567	0.02408	1.05363	26.87958281	1020.25825
5922	15190.4	1.11534				
5922	15194.15	1.14423	0.02889	1.129785	32.87777152	1106.204923
5922	15189.9	1.25169				
5922	15197.9	1.29187	0.04018	1.27178	47.35721142	1270.850679
5922	15191.5	1.28871				
5922	15198.4	1.32724	0.03853	1.307975	45.8111641	1313.734242
5922	15196.3	1.5438				
5922	15202.15	1.59512	0.05132	1.56946	64.85448118	1634.580358
5942	15176.55	0.26171				
5942	15188.3	0.27616	0.01445	0.268935	12.88843384	230.4842175
5942	15176	0.38046				
5942	15185.6	0.39174	0.01128	0.3861	10.43883086	337.3141121
5942	15183.5	0.7576				
5942	15191.5	0.77521	0.01761	0.766405	18.21137906	710.9072268
5942	15189.9	0.91472				
5942	15193.1	0.9388	0.02408	0.92676	26.00621094	880.7293492
5942	15194.15	1.12181				
5942	15198.4	1.14589	0.02408	1.13385	27.43181652	1110.838836
5942	15195.75	1.16997				

. . .

Table A.3: (. . . continued . . .)

Inline (x)	Trace (y)	TWT (s)	Offset (s)	Average Depth (s)	Offset (m)	Average Depth (m)
5942	15198.95	1.1957	0.02573	1.182835	29.67180692	1167.048076
5942	15196.3	1.25981				
5942	15200	1.29036	0.03055	1.275085	36.03590321	1274.751
5942	15202.15	1.55991				
5942	15207.45	1.60159	0.04168	1.58075	52.80667648	1648.870177
5942	15202.15	1.62086				
5942	15208.55	1.67067	0.04981	1.645765	64.03281206	1731.863702
5942	15203.75	1.70589				
5942	15209.6	1.76684	0.06095	1.736365	79.9323915	1849.516982
5952	15182.4	0.43178				
5952	15190.95	0.45104	0.01926	0.44141	18.128288	389.0983219
5952	15187.2	0.63886				
5952	15191.5	0.65331	0.01445	0.646085	14.44642767	588.2737641
5952	15189.35	0.79448				
5952	15195.2	0.81856	0.02408	0.80652	25.17847994	752.7064022
5952	15191.5	0.91322				
5952	15196.3	0.9373	0.02408	0.92526	25.99588496	879.1069934
5952	15194.15	1.04475				
5952	15198.95	1.07049	0.02574	1.05762	28.76193792	1024.720425
5952	15194.7	1.1057				
5952	15201.6	1.1346	0.0289	1.12015	32.80954813	1095.240189
5952	15194.7	1.12497				
5952	15201.1	1.14905	0.02408	1.13701	27.45356992	1114.444329
5952	15194.7	1.13942				
5952	15200	1.16199	0.02257	1.150705	25.82038572	1130.102774

. . .

Table A.3: (. . . continued . . .)

Inline (x)	Trace (y)	TWT (s)	Offset (s)	Average Depth (s)	Offset (m)	Average Depth (m)
5952	15197.9	1.26147				
5952	15202.65	1.29353	0.03206	1.2775	37.8391901	1277.602967
5972	15188.3	0.24576				
5972	15195.75	0.24892	0.00316	0.24734	2.799000207	211.2191356
5972	15186.7	0.43825				
5972	15192	0.44156	0.00331	0.439905	3.114081237	387.6777739
5972	15183.5	0.44954				
5972	15192.55	0.46082	0.01128	0.45518	10.66159496	402.1254624
5972	15184	0.64202				
5972	15193.6	0.65647	0.01445	0.649245	14.45948152	591.4420105
5972	15189.9	0.90359				
5972	15204.25	0.94693	0.04334	0.92526	46.78827467	879.1069934
5972	15190.95	1.05604				
5972	15204.8	1.08012	0.02408	1.06808	26.97905647	1036.439697
5972	15194.7	1.11865				
5972	15203.75	1.14273	0.02408	1.13069	27.41006311	1107.236176
5972	15201.6	1.3626				
5972	15206.95	1.38668	0.02408	1.37464	29.08941256	1393.69105
5972	15203.2	1.45561				
5972	15208.55	1.47804	0.02243	1.466825	27.68727643	1506.333136
5972	15204.25	1.55509				
5972	15212.25	1.59196	0.03687	1.573525	46.63646949	1639.721286
5972	15205.35	1.61288				
5972	15212.25	1.65788	0.045	1.63538	57.71575955	1718.526479

. . .

Table A.3: (. . . continued . . .)

Inline (x)	Trace (y)	TWT (s)	Offset (s)	Average Depth (s)	Offset (m)	Average Depth (m)
5992	15183.5	0.23764				
5992	15192.55	0.24892	0.01128	0.24328	9.978275439	207.6119493
5992	15184	0.26969				
5992	15191.5	0.27616	0.00647	0.272925	5.77818748	234.0582098
5992	15181.35	0.40454				
5992	15193.1	0.41898	0.01444	0.41176	13.46911142	361.2304757
5992	15185.6	0.44141				
5992	15194.7	0.4527	0.01129	0.447055	10.6448226	394.4322817
5992	15186.15	0.50086				
5992	15193.6	0.51199	0.01113	0.506425	10.68287205	451.0784812
5992	15186.7	0.54254				
5992	15195.2	0.56181	0.01927	0.552175	18.74789455	495.4116872
5992	15188.3	0.60681				
5992	15196.8	0.62125	0.01444	0.61403	14.30410366	556.2952246
5992	15188.3	0.65				
5992	15197.9	0.66129	0.01129	0.655645	11.3180646	597.8673903
5992	15192.55	0.79779				
5992	15201.1	0.81058	0.01279	0.804185	13.36491572	750.2608577
5992	15191.5	0.85708				
5992	15204.25	0.87951	0.02243	0.868295	23.84932946	817.9677212
5992	15194.15	0.90359				
5992	15203.75	0.92285	0.01926	0.91322	20.72609689	866.1080074
5992	15193.1	0.95822				
5992	15203.2	0.97899	0.02077	0.968605	22.67990114	926.2449328
5992	15196.8	1.04806				
5992	15206.4	1.06417	0.01611	1.056115	17.99442144	1023.036793

. . .

Table A.3: (. . . continued . . .)

Inline (x)	Trace (y)	TWT (s)	Offset (s)	Average Depth (s)	Offset (m)	Average Depth (m)
5992	15197.35	1.09938				
5992	15207.45	1.1203	0.02092	1.10984	23.68836576	1083.536465
5992	15201.1	1.24386				
5992	15208	1.26629	0.02243	1.255075	26.32947436	1251.184064
5992	15202.15	1.36095				
5992	15210.65	1.38668	0.02573	1.373815	31.07659705	1392.693855
5992	15202.65	1.40745				
5992	15212.25	1.42521	0.01776	1.41633	21.66631947	1444.334027
5992	15206.95	1.44929				
5992	15213.35	1.47337	0.02408	1.46133	29.68618569	1499.551155
5992	15210.65	1.56803				
5992	15215.45	1.59527	0.02724	1.58165	34.51885766	1650.010868
6012	15188.8	0.49438				
6012	15196.3	0.49438	0	0.49438	0	439.5052335
6012	15187.75	0.62923				
6012	15196.8	0.64037	0.01114	0.6348	11.10130659	576.9824363
6012	15187.75	0.79116				
6012	15202.65	0.81043	0.01927	0.800795	20.11751916	746.7131197
6012	15186.7	0.89546				
6012	15202.15	0.91803	0.02257	0.906745	24.24627978	859.1342781
6012	15187.75	1.01902				
6012	15205.35	1.04791	0.02889	1.033465	32.08225758	997.7760179
6012	15195.75	1.07846				
6012	15204.8	1.09773	0.01927	1.088095	21.70022832	1058.950805
6012	15200.55	1.24702				

. . .

Table A.3: (. . . continued . . .)

Inline (x)	Trace (y)	TWT (s)	Offset (s)	Average Depth (s)	Offset (m)	Average Depth (m)
6012	15209.05	1.26147	0.01445	1.254245	16.95871595	1250.208979
6012	15202.15	1.37208				
6012	15210.65	1.38172	0.00964	1.3769	11.65165758	1396.423748
6012	15208	1.54862				
6012	15213.35	1.56954	0.02092	1.55908	26.37509482	1621.474237
6022	15184.55	0.48957				
6022	15190.95	0.49107	0.0015	0.49032	1.432834022	435.6135211
6022	15183.5	0.5281				
6022	15189.35	0.53442	0.00632	0.53126	6.110976168	475.0707115
6022	15183.5	0.63871				
6022	15192	0.64684	0.00813	0.642775	8.120296983	584.9581639
6022	15182.4	0.8008				
6022	15194.7	0.81524	0.01444	0.80802	15.10491518	754.2782317
6022	15186.15	0.85377				
6022	15194.15	0.8634	0.00963	0.858585	10.21263695	807.6380226
6022	15188.3	0.89395				
6022	15198.95	0.9084	0.01445	0.901175	15.50019579	853.1447714
6022	15188.8	0.97583				
6022	15199.5	0.99027	0.01444	0.98305	15.82745778	942.072359
6022	15194.7	1.11865				
6022	15203.2	1.12828	0.00963	1.123465	10.94185806	1099.009724
6022	15200.55	1.3465				
6022	15210.65	1.3626	0.0161	1.35455	19.35684894	1369.462745
6022	15206.95	1.57601				
6022	15212.25	1.59046	0.01445	1.583235	18.31776246	1652.020311

. . .

Table A.3: (. . . continued . . .)

Inline (x)	Trace (y)	TWT (s)	Offset (s)	Average Depth (s)	Offset (m)	Average Depth (m)
6042	15204.25	0.89079				
6042	15213.85	0.89395	0.00316	0.89237	3.381707924	843.6945725
6042	15199.5	0.99659				
6042	15209.05	1.00623	0.00964	1.00141	10.616851	962.2748916
6042	15199.5	1.11218				
6042	15210.65	1.12181	0.00963	1.116995	10.92404599	1091.655489
6042	15202.15	1.20684				
6042	15211.75	1.21963	0.01279	1.213235	14.86056826	1202.273728
6042	15204.25	1.35764				
6042	15211.2	1.36892	0.01128	1.36328	13.58996901	1379.976956
6042	15203.75	1.43304				
6042	15213.85	1.4508	0.01776	1.44192	21.79624575	1475.663715
6042	15206.4	1.5423				
6042	15215.45	1.5584	0.0161	1.55035	20.25805133	1610.475122
6042	15210.15	1.68361				
6042	15221.35	1.71236	0.02875	1.697985	37.38851111	1799.392387
6062	15212.8	1.37374				
6062	15220.8	1.38172	0.00798	1.37773	9.64714531	1397.427713
6062	15213.35	1.48932				
6062	15225.05	1.49248	0.00316	1.4909	3.922408435	1536.147706
6062	15215.45	1.54064				
6062	15226.15	1.55178	0.01114	1.54621	14.00387693	1605.266604
6062	15216	1.60641				

. . .

Table A.3: (. . . continued . . .)

Inline (x)	Trace (y)	TWT (s)	Offset (s)	Average Depth (s)	Offset (m)	Average Depth (m)
6062	15225.05	1.6177	0.01129	1.612055	14.40495936	1688.682231
6062	15216	1.68497				
6062	15225.05	1.70423	0.01926	1.6946	25.0284133	1794.991602
6062	15216.55	1.77015				
6062	15225.05	1.78941	0.01926	1.77978	25.49741853	1906.72102

A.4 Fault D

Table A.4: Fault "D" data

Inline (x)	Trace (y)	TWT (s)	Offset (s)	Average Depth (s)	Offset (m)	Average Depth (m)
5745	16081.3	0.35378				
5745	16093.55	0.36526	0.01148	0.35952	10.53668355	312.7372144
5745	16082.35	0.4014				
5745	16094.6	0.41054	0.00914	0.40597	8.510333551	355.8175967
5745	16081.3	0.46497				
5745	16095.7	0.48304	0.01807	0.474005	17.17659299	420.0219306
5745	16083.95	0.60997				
5745	16094.1	0.63718	0.02721	0.623575	27.02817247	565.7869815
5745	16081.8	0.62804				
5745	16101	0.65759	0.02955	0.642815	29.51507049	584.9982131
5745	16084.5	0.71648				
5745	16094.6	0.75964	0.04316	0.73806	44.28417095	681.6474396
5745	16091.4	0.97947				
5745	16098.35	1.0271	0.04763	1.003285	52.48202599	964.3434402
5745	16090.35	1.05431				
5745	16099.95	1.10427	0.04996	1.07929	56.13492736	1049.033717
5745	16092.5	1.12915				
5745	16099.4	1.19931	0.07016	1.16423	80.53526588	1145.619065
5745	16096.2	1.28796				
5745	16102.6	1.36493	0.07697	1.326445	91.92173782	1335.760569
5745	16097.25	1.48526				
5745	16107.4	1.58497	0.09971	1.535115	125.0272341	1591.332004
5745	16099.4	1.52821				
5745	16105.8	1.63472	0.10651	1.581465	134.9651279	1649.776374

...

Table A.4: (. . . continued . . .)

Inline (x)	Trace (y)	TWT (s)	Offset (s)	Average Depth (s)	Offset (m)	Average Depth (m)
5750	16080.75	0.27447				
5750	16091.4	0.28808	0.01361	0.281275	12.18722281	241.5522323
5750	16081.8	0.35611				
5750	16091.4	0.36526	0.00915	0.360685	8.401188044	313.8102188
5750	16083.95	0.41947				
5750	16088.75	0.43542	0.01595	0.427445	14.94910523	375.9416385
5750	16084.5	0.4875				
5750	16088.75	0.50345	0.01595	0.495475	15.25930747	440.5556463
5750	16082.35	0.57595				
5750	16092.5	0.60082	0.02487	0.588385	24.45361412	530.9212783
5750	16082.35	0.63038				
5750	16098.85	0.65312	0.02274	0.64175	22.70619676	583.93206
5750	16083.4	0.65759				
5750	16097.25	0.68927	0.03168	0.67343	31.91982293	615.7839281
5750	16082.35	0.86849				
5750	16097.8	0.8889	0.02041	0.878695	21.76218958	829.061121
5750	16088.2	1.0339				
5750	16096.2	1.09067	0.05677	1.062285	63.51064475	1029.943207
5750	16095.15	1.29009				
5750	16102.05	1.36939	0.0793	1.32974	94.77904845	1339.70018
5750	16096.75	1.40787				
5750	16106.85	1.48739	0.07952	1.44763	97.72200589	1482.679785
5750	16095.7	1.4555				
5750	16109	1.53948	0.08398	1.49749	104.399942	1544.33745
5750	16093.55	1.47825				
5750	16107.4	1.57796	0.09971	1.528105	124.8274134	1582.5459

. . .

Table A.4: (. . . continued . . .)

Inline (x)	Trace (y)	TWT (s)	Offset (s)	Average Depth (s)	Offset (m)	Average Depth (m)
5750	16098.35	1.5348				
5750	16107.4	1.62792	0.09312	1.58136	117.9950708	1649.643287
5750	16099.4	1.57796				
5750	16110.05	1.68447	0.10651	1.631215	136.4799696	1713.186059
5760	16081.3	0.37206				
5760	16094.6	0.39013	0.01807	0.381095	16.69663372	332.6709789
5760	16085	0.42861				
5760	16091.95	0.44456	0.01595	0.436585	14.99078167	384.5463454
5760	16086.6	0.57595				
5760	16091.95	0.60316	0.02721	0.589555	26.76353787	532.0748503
5760	16086.1	0.64186				
5760	16092.5	0.6712	0.02934	0.65653	29.42035629	598.7568143
5760	16085	0.84575				
5760	16097.8	0.86616	0.02041	0.855955	21.62950598	804.8447776
5760	16082.35	0.87976				
5760	16097.25	0.90017	0.02041	0.889965	21.82794789	841.1171667
5760	16083.95	0.97735				
5760	16097.25	0.98628	0.00893	0.981815	9.784880261	940.7168521
5760	16095.15	1.26968				
5760	16099.4	1.35132	0.08164	1.3105	97.12676021	1316.73971
5760	16095.7	1.30816				
5760	16099.95	1.39214	0.08398	1.35015	100.8625735	1364.17168
5770	16077	0.23153				
5770	16093.55	0.24513	0.0136	0.23833	12.01129941	203.220351
5770	16077.55	0.2564				
5770	16093	0.26767	0.01127	0.262035	10.02985558	224.3142873

. . .

Table A.4: (. . . continued . . .)

Inline (x)	Trace (y)	TWT (s)	Offset (s)	Average Depth (s)	Offset (m)	Average Depth (m)
5770	16079.7	0.27915				
5770	16093	0.29042	0.01127	0.284785	10.10315306	244.7083189
5770	16080.2	0.34718				
5770	16095.7	0.35611	0.00893	0.351645	8.176113974	305.4941702
5770	16080.75	0.37652				
5770	16089.8	0.38333	0.00681	0.379925	6.290144751	331.5865959
5770	16081.3	0.39247				
5770	16089.3	0.39927	0.0068	0.39587	6.311904946	346.3982056
5770	16081.3	0.42181				
5770	16088.75	0.44009	0.01828	0.43095	17.15120974	379.2385633
5770	16085	0.63718				
5770	16093.55	0.65993	0.02275	0.648555	22.76044005	590.7499681
5770	16085	0.68714				
5770	16093.55	0.7235	0.03636	0.70532	36.96673501	648.1344803
5770	16086.1	0.75964				
5770	16096.2	0.79812	0.03848	0.77888	39.93131993	723.8570655
5770	16088.75	0.84362				
5770	16097.25	0.90017	0.05655	0.871895	60.18658022	821.804272
5770	16088.75	0.8889				
5770	16095.7	0.94546	0.05656	0.91718	60.92945334	870.378883
5770	16089.3	0.97735				
5770	16098.85	1.02497	0.04762	1.00116	52.44207838	961.9991605
5770	16089.8	1.01583				
5770	16098.85	1.0726	0.05677	1.044215	63.21737936	1009.746983
5770	16089.3	1.0339				
5770	16097.8	1.09301	0.05911	1.063455	66.14825817	1031.254069

. . .

Table A.4: (. . . continued . . .)

Inline (x)	Trace (y)	TWT (s)	Offset (s)	Average Depth (s)	Offset (m)	Average Depth (m)
5770	16091.95	1.2244				
5770	16102.6	1.30136	0.07696	1.26288	90.51128106	1260.362953
5770	16093.55	1.26755				
5770	16103.65	1.34452	0.07697	1.306035	91.47263243	1311.426318
5770	16095.7	1.3105				
5770	16102.05	1.38768	0.07718	1.34909	92.6721754	1362.897836
5785	16081.3	0.25406				
5785	16091.95	0.26321	0.00915	0.258635	8.13424545	221.278999
5785	16082.35	0.35399				
5785	16092.5	0.3676	0.01361	0.360795	12.49662136	313.9115525
5785	16078.1	0.38567				
5785	16089.3	0.39693	0.01126	0.3913	10.43706114	342.1456735
5785	16084.5	0.58275				
5785	16096.2	0.6055	0.02275	0.594125	22.40643985	536.5844037
5785	16082.35	0.63505				
5785	16094.6	0.65312	0.01807	0.644085	18.05520103	586.2700087
5785	16085	0.73243				
5785	16096.75	0.74837	0.01594	0.7404	16.3658459	684.054328
5785	16085.55	0.81173				
5785	16101	0.83448	0.02275	0.823105	23.89567311	770.1210835
5785	16087.15	0.85489				
5785	16100.45	0.88444	0.02955	0.869665	31.43144348	819.4273086
5785	16085.55	0.8753				
5785	16099.95	0.90017	0.02487	0.887735	26.58194341	838.7287721
5785	16094.1	1.02944				
5785	16103.15	1.09513	0.06569	1.062285	73.48977019	1029.943207

. . .

Table A.4: (. . . continued . . .)

Inline (x)	Trace (y)	TWT (s)	Offset (s)	Average Depth (s)	Offset (m)	Average Depth (m)
5785	16093.55	1.22206				
5785	16107.4	1.28329	0.06123	1.252675	71.83287636	1248.365074
5785	16095.15	1.3037				
5785	16107.95	1.38534	0.08164	1.34452	97.92076127	1357.409532
5785	16102.05	1.56435				
5785	16112.2	1.65513	0.09078	1.60974	115.7665115	1685.728616
5796	16088.2	0.44902				
5796	16097.25	0.46263	0.01361	0.455825	12.86636663	402.7369849
5796	16089.8	0.69841				
5796	16094.1	0.71882	0.02041	0.708615	20.76980496	651.4935106
5796	16090.35	0.83001				
5796	16098.85	0.87976	0.04975	0.854885	52.70736506	803.7089238
5796	16094.1	1.0339				
5796	16101.55	1.09067	0.05677	1.062285	63.51064475	1029.943207
5796	16097.25	1.18804				
5796	16107.4	1.25607	0.06803	1.222055	79.214886	1212.542868
5796	16095.15	1.21759				
5796	16107.95	1.28775	0.07016	1.25267	82.3091371	1248.359203
5796	16099.95	1.28563				
5796	16108.45	1.36046	0.07483	1.323045	89.29329989	1331.698644
5801	16089.3	0.26321				
5801	16101.55	0.26767	0.00446	0.26544	3.973565583	227.3573257
5801	16088.75	0.40374				
5801	16101.55	0.42181	0.01807	0.412775	16.86028789	362.1803452
5801	16086.6	0.42181				
5801	16102.05	0.44456	0.02275	0.433185	21.35972311	381.3427016

. . .

Table A.4: (. . . continued . . .)

Inline (x)	Trace (y)	TWT (s)	Offset (s)	Average Depth (s)	Offset (m)	Average Depth (m)
5801	16088.75	0.44009				
5801	16099.95	0.4605	0.02041	0.450295	19.26255663	397.4978405
5801	16088.75	0.57595				
5801	16098.35	0.59423	0.01828	0.58509	17.95672787	527.6746301
5801	16089.8	0.64632				
5801	16100.45	0.66673	0.02041	0.656525	20.46586966	598.7517887
5801	16089.8	0.65993				
5801	16098.85	0.678	0.01807	0.668965	18.18372742	611.2774692
5801	16092.5	0.80492				
5801	16102.6	0.83894	0.03402	0.82193	35.72179431	768.8847347
5801	16092.5	0.83682				
5801	16103.15	0.87976	0.04294	0.85829	45.53434657	807.3246141
5801	16097.25	1.19272				
5801	16106.85	1.26075	0.06803	1.226735	79.30590459	1218.00076
5801	16101	1.26522				
5801	16108.45	1.33771	0.07249	1.301465	86.0538079	1305.993832
5801	16099.95	1.29009				
5801	16105.8	1.36259	0.0725	1.32634	86.58124574	1335.635078
5811	16090.9	0.39247				
5811	16099.4	0.4014	0.00893	0.396935	8.291735196	347.3900736
5811	16090.35	0.57595				
5811	16099.4	0.59189	0.01594	0.58392	15.65277793	526.52254
5811	16098.35	0.92292				
5811	16103.65	0.97054	0.04762	0.94673	51.70108983	902.3891272
5811	16099.4	1.02029				
5811	16105.25	1.06792	0.04763	1.044105	53.03785006	1009.624323

. . .

Table A.4: (. . . continued . . .)

Inline (x)	Trace (y)	TWT (s)	Offset (s)	Average Depth (s)	Offset (m)	Average Depth (m)
5811	16098.35	1.09301				
5811	16104.2	1.15402	0.06101	1.123515	69.32203096	1099.066603
5811	16101.55	1.19484				
5811	16107.4	1.25841	0.06357	1.226625	74.10466497	1217.872405
5811	16100.45	1.25607				
5811	16106.85	1.34452	0.08845	1.300295	104.9705437	1304.603973
5826	16091.4	0.6123				
5826	16110.6	0.63038	0.01808	0.62134	17.94763052	563.5621312
5826	16098.35	0.93653				
5826	16105.8	0.97947	0.04294	0.958	46.75835534	914.6626858
5826	16100.45	1.04304				
5826	16107.95	1.08833	0.04529	1.065685	50.71157658	1033.753625
5826	16103.15	1.19718				
5826	16109	1.26075	0.06357	1.228965	74.14719071	1220.603608
5826	16103.65	1.26755				
5826	16109	1.33325	0.0657	1.3004	77.97330873	1304.728688
5826	16105.25	1.44423				
5826	16115.4	1.52353	0.0793	1.48388	98.27344602	1527.43713
5826	16091.4	0.6123				
5826	16110.6	0.63038	0.01808	0.62134	17.94763052	563.5621312
5826	16098.35	0.93653				
5826	16105.8	0.97947	0.04294	0.958	46.75835534	914.6626858
5826	16100.45	1.04304				
5826	16107.95	1.08833	0.04529	1.065685	50.71157658	1033.753625
5826	16103.15	1.19718				
5826	16109	1.26075	0.06357	1.228965	74.14719071	1220.603608

. . .

Table A.4: (. . . continued . . .)

Inline (x)	Trace (y)	TWT (s)	Offset (s)	Average Depth (s)	Offset (m)	Average Depth (m)
5826	16103.65	1.26755				
5826	16109	1.33325	0.0657	1.3004	77.97330873	1304.728688
5826	16105.25	1.44423				
5826	16115.4	1.52353	0.0793	1.48388	98.27344602	1527.43713
5846	16102.05	0.43542				
5846	16111.15	0.43775	0.00233	0.436585	2.189875943	384.5463454
5846	16115.95	1.01583				
5846	16121.8	1.04751	0.03168	1.03167	35.1642874	995.7803391
5846	16114.85	1.28329				
5846	16128.2	1.32411	0.04082	1.3037	48.48402668	1308.649899
5846	16123.95	1.47144				
5846	16131.95	1.52353	0.05209	1.497485	64.7557362	1544.331231
5856	16111.65	0.60316				
5856	16127.65	0.60104	-0.00212	0.6021	-2.092818098	544.4681103
5856	16114.35	0.66439				
5856	16126.6	0.67587	0.01148	0.67013	11.55607526	612.4527413
5856	16119.15	0.90251				
5856	16128.75	0.90485	0.00234	0.90368	2.51174205	855.8373474
5856	16122.85	1.04985				
5856	16131.4	1.06792	0.01807	1.058885	20.19799627	1026.136068
5856	16125.55	1.11788				
5856	16131.95	1.13361	0.01573	1.125745	17.88309063	1101.604154
5856	16128.2	1.21993				
5856	16134.05	1.24247	0.02254	1.2312	26.30475378	1223.213708
5856	16128.2	1.3037				
5856	16135.65	1.31964	0.01594	1.31167	18.9690817	1318.132956

. . .

Table A.4: (. . . continued . . .)

Inline (x)	Trace (y)	TWT (s)	Offset (s)	Average Depth (s)	Offset (m)	Average Depth (m)
5856	16129.25	1.34005				
5856	16136.75	1.37173	0.03168	1.35589	38.10064368	1371.075205
5856	16134.6	1.47825				
5856	16142.05	1.51226	0.03401	1.495255	42.25788411	1541.558516
5856	16136.75	1.53948				
5856	16144.2	1.5803	0.04082	1.55989	51.47366704	1622.495869
5867	16131.95	0.61911				
5867	16136.2	0.63038	0.01127	0.624745	11.19845917	566.9522333
5867	16130.85	0.67353				
5867	16137.8	0.68714	0.01361	0.680335	13.73989615	622.764179
5867	16132.45	0.70521				
5867	16140.45	0.71435	0.00914	0.70978	9.304171824	652.6818864
5867	16133	0.82534				
5867	16139.4	0.83894	0.0136	0.83214	14.32001369	779.6409012
5867	16134.6	0.9614				
5867	16143.65	0.96821	0.00681	0.964805	7.428814168	922.0910963
5867	16134.6	1.05219				
5867	16148.45	1.05665	0.00446	1.05442	4.97953465	1021.14138
5867	16142.6	1.39894				
5867	16150.6	1.43977	0.04083	1.419355	49.84588492	1448.027835
5867	16144.7	1.47825				
5867	16153.8	1.50546	0.02721	1.491855	33.78234442	1537.333772
5867	16144.7	1.49185				
5867	16154.3	1.53034	0.03849	1.511095	47.99864037	1561.284078
5867	16146.3	1.54862				
5867	16154.3	1.57349	0.02487	1.561055	31.36913791	1623.965581

. . .

Table A.4: (. . . continued . . .)

Inline (x)	Trace (y)	TWT (s)	Offset (s)	Average Depth (s)	Offset (m)	Average Depth (m)
5877	16152.7	0.42415				
5877	16162.85	0.42861	0.00446	0.42638	4.178768074	374.9405528
5877	16148.45	0.57148				
5877	16157.5	0.57595	0.00447	0.573715	4.37641449	516.4902193
5877	16151.65	0.6055				
5877	16159.1	0.60997	0.00447	0.607735	4.41988809	550.049482
5877	16143.65	1.05219				
5877	16155.4	1.06111	0.00892	1.05665	9.96475591	1023.63522
5877	16139.4	1.15636				
5877	16157.5	1.17911	0.02275	1.167735	26.13706736	1149.648574
5877	16142.05	1.18124				
5877	16154.85	1.19718	0.01594	1.18921	18.4110404	1174.41331
5877	16154.3	1.41936				
5877	16166.6	1.43296	0.0136	1.42616	16.62954444	1456.346865
5877	16153.25	1.49866				
5877	16168.7	1.51907	0.02041	1.508865	25.4391123	1558.502753
5877	16156.45	1.54394				
5877	16170.3	1.56435	0.02041	1.554145	25.70331253	1615.253868
5877	16159.1	1.57796				
5877	16168.2	1.59157	0.01361	1.584765	17.25887663	1653.960701
5882	16150.6	1.14042				
5882	16162.85	1.1519	0.01148	1.14616	13.11835925	1124.900261
5882	16155.9	1.19718				
5882	16170.85	1.20632	0.00914	1.20175	10.58966149	1188.934802
5882	16157	1.34218				
5882	16169.25	1.36046	0.01828	1.35132	21.96095881	1365.578087

. . .

Table A.4: (. . . continued . . .)

Inline (x)	Trace (y)	TWT (s)	Offset (s)	Average Depth (s)	Offset (m)	Average Depth (m)
5882	16162.3	1.39894				
5882	16173	1.40575	0.00681	1.402345	8.280635766	1427.290775
5882	16163.9	1.41936				
5882	16171.9	1.42616	0.0068	1.42276	8.308162676	1452.188764
5882	16163.4	1.501				
5882	16175.1	1.5146	0.0136	1.5078	16.94695815	1557.17495
5882	16165	1.56669				
5882	16175.65	1.58264	0.01595	1.574665	20.18018292	1641.163864
5882	16175.1	1.7776				
5882	16185.75	1.80013	0.02253	1.788865	29.88493486	1918.759159
5882	16150.6	1.14042				
5882	16162.85	1.1519	0.01148	1.14616	13.11835925	1124.900261
5882	16155.9	1.19718				
5882	16170.85	1.20632	0.00914	1.20175	10.58966149	1188.934802
5882	16157	1.34218				
5882	16169.25	1.36046	0.01828	1.35132	21.96095881	1365.578087
5882	16162.3	1.39894				
5882	16173	1.40575	0.00681	1.402345	8.280635766	1427.290775
5882	16163.9	1.41936				
5882	16171.9	1.42616	0.0068	1.42276	8.308162676	1452.188764
5882	16163.4	1.501				
5882	16175.1	1.5146	0.0136	1.5078	16.94695815	1557.17495
5882	16165	1.56669				
5882	16175.65	1.58264	0.01595	1.574665	20.18018292	1641.163864
5882	16175.1	1.7776				
5882	16185.75	1.80013	0.02253	1.788865	29.88493486	1918.759159

. . .

Table A.4: (. . . continued . . .)

Inline (x)	Trace (y)	TWT (s)	Offset (s)	Average Depth (s)	Offset (m)	Average Depth (m)
5892	16189.5	1.06792				
5892	16201.75	1.08152	0.0136	1.07472	15.26315697	1043.895187
5892	16193.75	1.12915				
5892	16207.1	1.13595	0.0068	1.13255	7.743999079	1109.356386
5892	16194.3	1.17443				
5892	16208.7	1.18358	0.00915	1.179005	10.54175114	1162.628702
5892	16193.75	1.22886				
5892	16205.5	1.24481	0.01595	1.236835	18.63975042	1229.800719
5892	16195.35	1.28775				
5892	16211.9	1.30136	0.01361	1.294555	16.12971979	1297.790975
5892	16195.9	1.35132				
5892	16208.15	1.36259	0.01127	1.356955	13.55754285	1372.357114
5892	16193.75	1.4353				
5892	16208.7	1.45337	0.01807	1.444335	22.18917377	1478.629978
5892	16195.35	1.501				
5892	16208.7	1.51907	0.01807	1.510035	22.52857022	1559.961837
5892	16198.05	1.55075				
5892	16210.85	1.57796	0.02721	1.564355	34.34630704	1628.130802
5892	16199.65	1.60071				
5892	16210.3	1.62112	0.02041	1.610915	26.03455474	1687.227561
5892	16200.7	1.63239				
5892	16210.3	1.65046	0.01807	1.641425	23.20731146	1726.286216
5892	16198.55	1.65726				
5892	16209.75	1.67767	0.02041	1.667465	26.36451329	1759.831282
5897	16195.9	1.28329				
5897	16212.45	1.29456	0.01127	1.288925	13.3383592	1291.117619

. . .

Table A.4: (. . . continued . . .)

Inline (x)	Trace (y)	TWT (s)	Offset (s)	Average Depth (s)	Offset (m)	Average Depth (m)
5897	16195.35	1.30604				
5897	16212.45	1.32177	0.01573	1.313905	18.72922591	1320.795493
5897	16196.45	1.34686				
5897	16208.7	1.35132	0.00446	1.34909	5.355246207	1362.897836
5897	16192.15	1.43296				
5897	16210.3	1.44891	0.01595	1.440935	19.57040274	1474.454348
5897	16196.95	1.501				
5897	16211.35	1.51673	0.01573	1.508865	19.60594005	1558.502753
5897	16198.05	1.54862				
5897	16209.25	1.57116	0.02254	1.55989	28.4227451	1622.495869
5897	16202.3	1.62558				
5897	16210.3	1.6528	0.02722	1.63919	34.94126976	1723.416024
5897	16204.95	1.67087				
5897	16210.3	1.70488	0.03401	1.687875	44.13068577	1786.258179
5902	16195.35	1.28116				
5902	16216.7	1.29689	0.01573	1.289025	18.61734323	1291.236072
5902	16196.95	1.30604				
5902	16216.7	1.31964	0.0136	1.31284	16.18895991	1319.52659
5902	16196.45	1.34218				
5902	16210.3	1.35366	0.01148	1.34792	13.78051588	1361.49217
5902	16198.05	1.43296				
5902	16212.45	1.44891	0.01595	1.440935	19.57040274	1474.454348
5902	16200.7	1.48739				
5902	16210.85	1.501	0.01361	1.494195	16.90648445	1540.241038
5902	16199.65	1.55075				
5902	16212.45	1.57349	0.02274	1.56212	28.6894404	1625.309474

. . .

Table A.4: (. . . continued . . .)

Inline (x)	Trace (y)	TWT (s)	Offset (s)	Average Depth (s)	Offset (m)	Average Depth (m)
5902	16204.45	1.59837				
5902	16213.5	1.61878	0.02041	1.608575	26.02090128	1684.242815
5902	16204.95	1.62346				
5902	16213.5	1.6528	0.02934	1.63813	37.65374145	1722.055265
5907	16205.5	0.92058				
5907	16217.25	0.92058	0	0.92058	0	874.0493458
5907	16203.35	1.21079				
5907	16214.55	1.21759	0.0068	1.21419	7.902705933	1203.384571
5907	16199.65	1.3173				
5907	16216.15	1.33538	0.01808	1.32634	21.59157135	1335.635078
5907	16200.7	1.4353				
5907	16217.75	1.45337	0.01807	1.444335	22.18917377	1478.629978
5907	16200.15	1.49866				
5907	16215.65	1.52141	0.02275	1.510035	28.36330783	1559.961837
5907	16202.85	1.55308				
5907	16216.7	1.57349	0.02041	1.563285	25.7566427	1626.779922
5907	16206.55	1.5939				
5907	16216.7	1.62346	0.02956	1.60868	37.6872098	1684.376713
5907	16204.95	1.62792				
5907	16214.55	1.65726	0.02934	1.64259	37.69115068	1727.782874
5917	16206.05	1.28775				
5917	16222.05	1.29689	0.00914	1.29232	10.82631576	1295.140707
5917	16206.05	1.32411				
5917	16224.15	1.35132	0.02721	1.337715	32.58332099	1349.248104
5917	16206.55	1.41702				
5917	16222.55	1.4421	0.02508	1.42956	30.69121393	1460.508245

. . .

Table A.4: (. . . continued . . .)

Inline (x)	Trace (y)	TWT (s)	Offset (s)	Average Depth (s)	Offset (m)	Average Depth (m)
5917	16206.55	1.46018				
5917	16224.15	1.48505	0.02487	1.472615	30.74034405	1513.488477
5917	16207.65	1.49866				
5917	16222.05	1.52821	0.02955	1.513435	36.86985407	1564.204116
5917	16207.1	1.55308				
5917	16225.2	1.58476	0.03168	1.56892	40.02998788	1633.897783
5917	16208.7	1.61431				
5917	16224.7	1.64387	0.02956	1.62909	37.85968681	1710.46325
5932	16199.1	0.83214				
5932	16208.7	0.84128	0.00914	0.83671	9.635832705	784.464946
5932	16199.1	0.88657				
5932	16207.1	0.89337	0.0068	0.88997	7.27242744	841.1225235
5932	16199.65	0.96374				
5932	16209.25	0.97501	0.01127	0.969375	12.3088114	927.0871304
5932	16202.85	1.16083				
5932	16211.35	1.16997	0.00914	1.1654	10.49468101	1146.963764
5932	16204.95	1.30136				
5932	16217.75	1.3105	0.00914	1.30593	10.86187791	1311.301435
5932	16206.05	1.41255				
5932	16221.5	1.43296	0.02041	1.422755	24.93667674	1452.182651
5932	16207.1	1.45571				
5932	16222.55	1.47825	0.02254	1.46698	27.82405766	1506.524563
5932	16208.15	1.49185				
5932	16222.05	1.52141	0.02956	1.50663	36.82482476	1555.716607
5932	16209.75	1.55755				
5932	16219.9	1.57583	0.01828	1.56669	23.08645796	1631.079877

. . .

Table A.4: (. . . continued . . .)

Inline (x)	Trace (y)	TWT (s)	Offset (s)	Average Depth (s)	Offset (m)	Average Depth (m)
5932	16210.85	1.62558				
5932	16222.05	1.65046	0.02488	1.63802	31.92917968	1721.914072
5932	16210.85	1.6664				
5932	16225.2	1.69808	0.03168	1.68224	41.05629067	1778.950163
5932	16212.45	1.70488				
5932	16223.65	1.7389	0.03402	1.72189	44.47447913	1830.563433
5937	16203.9	0.8028				
5937	16211.9	0.8096	0.0068	0.8062	7.109579901	752.3711611
5937	16206.55	0.86169				
5937	16212.45	0.87083	0.00914	0.86626	9.713045176	815.8006308
5937	16206.55	0.91846				
5937	16211.35	0.93653	0.01807	0.927495	19.51925503	881.5245365
5937	16205.5	0.96821				
5937	16215.65	0.97947	0.01126	0.97384	12.31226253	931.974098
5937	16202.85	1.20632				
5937	16217.75	1.21525	0.00893	1.210785	10.3694197	1199.425106
5937	16204.45	1.2312				
5937	16216.7	1.24247	0.01127	1.236835	13.17053211	1229.800719
5937	16204.45	1.28329				
5937	16218.85	1.29689	0.0136	1.29009	16.10050864	1292.49778
5937	16205.5	1.32645				
5937	16220.45	1.34218	0.01573	1.334315	18.82100748	1345.175309
5937	16205.5	1.43296				
5937	16223.1	1.46018	0.02722	1.44657	33.44236765	1481.376628
5937	16206.55	1.49185				
5937	16221.5	1.52353	0.03168	1.50769	39.47544746	1557.037824

. . .

Table A.4: (. . . continued . . .)

Inline (x)	Trace (y)	TWT (s)	Offset (s)	Average Depth (s)	Offset (m)	Average Depth (m)
5937	16207.65	1.55542				
5937	16222.05	1.57349	0.01807	1.564455	22.80969586	1628.257069
5937	16210.85	1.63026				
5937	16222.55	1.65046	0.0202	1.64036	25.93672156	1724.918364
5937	16211.35	1.67321				
5937	16220.95	1.69808	0.02487	1.685645	32.25495233	1783.365021
5947	16207.65	1.21079				
5947	16216.7	1.21759	0.0068	1.21419	7.902705933	1203.384571
5947	16207.1	1.28563				
5947	16215.65	1.29923	0.0136	1.29243	16.10960648	1295.271112
5947	16204.95	1.33325				
5947	16216.15	1.34686	0.01361	1.340055	16.30675241	1352.05305
5947	16205.5	1.4353				
5947	16215.1	1.45784	0.02254	1.44657	27.69254103	1481.376628
5947	16209.25	1.501				
5947	16215.65	1.51907	0.01807	1.510035	22.52857022	1559.961837
5947	16207.1	1.55075				
5947	16218.3	1.56903	0.01828	1.55989	23.05092194	1622.495869
5947	16206.55	1.60985				
5947	16217.25	1.63706	0.02721	1.623455	34.80603381	1703.249205
5947	16210.85	1.67554				
5947	16219.35	1.69808	0.02254	1.68681	29.24058397	1784.876293
5947	16210.3	1.70276				
5947	16217.75	1.73444	0.03168	1.7186	41.3855915	1826.263801
5972	16215.65	1.33325				
5972	16226.3	1.34898	0.01573	1.341115	18.85158635	1353.324178

. . .

Table A.4: (. . . continued . . .)

Inline (x)	Trace (y)	TWT (s)	Offset (s)	Average Depth (s)	Offset (m)	Average Depth (m)
5972	16214.55	1.44657				
5972	16225.2	1.46698	0.02041	1.456775	25.135177	1493.935824
5972	16213.5	1.52353				
5972	16224.15	1.54182	0.01829	1.532675	22.92123155	1588.272206
5972	16214.55	1.60517				
5972	16223.65	1.61431	0.00914	1.60974	11.65571619	1685.728616
5972	16213.5	1.64153				
5972	16223.1	1.6528	0.01127	1.647165	14.49256105	1733.664031
5972	16212.95	1.72083				
5972	16224.15	1.74358	0.02275	1.732205	29.80825041	1844.063796
5987	16216.7	1.33325				
5987	16223.1	1.34005	0.0068	1.33665	8.140766214	1347.972008
5987	16214.55	1.41936				
5987	16220.95	1.42382	0.00446	1.42159	5.447685505	1450.758646
5987	16214.05	1.61665				
5987	16227.9	1.63919	0.02254	1.62792	28.86111241	1708.964651
5987	16215.1	1.65046				
5987	16224.7	1.66874	0.01828	1.6596	23.57199507	1749.679211
5987	16216.15	1.71169				
5987	16226.3	1.72997	0.01828	1.72083	23.89197609	1829.177806
5987	16221.5	1.87263				
5987	16228.95	1.89538	0.02275	1.884005	30.7955227	2046.231526
6002	16220.45	1.33538				
6002	16227.35	1.34218	0.0068	1.33878	8.1449069	1350.524521
6002	16218.85	1.42169				
6002	16226.3	1.4285	0.00681	1.425095	8.32492644	1455.044048

. . .

Table A.4: (. . . continued . . .)

Inline (x)	Trace (y)	TWT (s)	Offset (s)	Average Depth (s)	Offset (m)	Average Depth (m)
6002	16215.65	1.49185				
6002	16230	1.50312	0.01127	1.497485	14.0103119	1544.331231
6002	16217.75	1.55989				
6002	16228.4	1.56903	0.00914	1.56446	11.53740212	1628.263382
6002	16216.15	1.59837				
6002	16233.2	1.61665	0.01828	1.60751	23.29977865	1682.884887
6002	16215.65	1.62792				
6002	16229.5	1.6528	0.02488	1.64036	31.94582339	1724.918364
6002	16216.7	1.71637				
6002	16232.7	1.73444	0.01807	1.725405	23.64113968	1835.160506
6002	16218.85	1.73678				
6002	16230.55	1.75931	0.02253	1.748045	29.62201829	1864.854092
6002	16219.9	1.79567				
6002	16229.5	1.82054	0.02487	1.808105	33.1256228	1944.330548
6002	16220.45	1.81374				
6002	16230.55	1.84095	0.02721	1.827345	36.39205228	1970.006948
6002	16220.95	1.87497				
6002	16234.8	1.90665	0.03168	1.89081	42.94524209	2055.447536
6002	16222.55	1.93173				
6002	16239.6	1.96788	0.03615	1.949805	49.61443816	2135.895054
6002	16223.1	1.98148				
6002	16238	2.03145	0.04997	2.006465	69.39125096	2214.08797
6017	16216.15	1.60071				
6017	16226.8	1.61198	0.01127	1.606345	14.36104441	1681.399823
6017	16215.1	1.62112				
6017	16225.75	1.63472	0.0136	1.62792	17.41398087	1708.964651

. . .

Table A.4: (. . . continued . . .)

Inline (x)	Trace (y)	TWT (s)	Offset (s)	Average Depth (s)	Offset (m)	Average Depth (m)
6017	16218.85	1.68001				
6017	16225.75	1.69128	0.01127	1.685645	14.61653851	1783.365021
6017	16215.65	1.73678				
6017	16227.35	1.75251	0.01573	1.744645	20.66621734	1860.385529
6017	16217.25	1.78206				
6017	16230	1.79333	0.01127	1.787695	14.9453301	1917.20753
6017	16220.95	1.81608				
6017	16231.1	1.83861	0.02253	1.827345	30.13277979	1970.006948
6032	16216.7	1.74124				
6032	16224.7	1.75251	0.01127	1.746875	14.81381346	1863.31601
6032	16216.15	1.7844				
6032	16223.65	1.79333	0.00893	1.788865	11.84520498	1918.759159
6032	16215.1	1.82054				
6032	16224.15	1.84776	0.02722	1.83415	36.45838095	1979.113579
6032	16217.25	1.8705				
6032	16226.8	1.89304	0.02254	1.88177	30.49685459	2043.207532
6032	16219.35	1.92493				
6032	16227.9	1.95214	0.02721	1.938535	37.25697648	2120.450622
6032	16219.9	1.99509				
6032	16228.4	2.03145	0.03636	2.01327	50.5623479	2223.540382
6072	16219.9	1.87731				
6072	16228.95	1.90452	0.02721	1.890915	36.88655027	2055.58984
6072	16220.95	1.90452				
6072	16232.15	1.943	0.03848	1.92376	52.5257583	2100.257513
6072	16223.65	1.96788				
6072	16232.7	2.0223	0.05442	1.99509	75.39381244	2198.316981

A.5 Fault E

Table A.5: Fault "E" data

Inline (x)	Trace (y)	TWT (s)	Offset (s)	Average Depth (s)	Offset (m)	Average Depth (m)
5174	15554.18	0.60997				
5174	15557.16	0.61677	0.0068	0.61337	6.734721466	555.6398614
5174	15553.74	0.65079				
5174	15558.22	0.66227	0.01148	0.65653	11.51144138	598.7568143
5174	15554.38	0.68034				
5174	15558.44	0.69394	0.0136	0.68714	13.75625833	629.6565733
5174	15555.02	0.7641				
5174	15558.86	0.78005	0.01595	0.772075	16.52054428	716.7875724
5174	15556.52	0.86616				
5174	15558.86	0.8821	0.01594	0.87413	16.97524377	824.1879804
5179	15550.34	0.24726				
5179	15553.96	0.25194	0.00468	0.2496	4.148378433	213.2291027
5179	15549.7	0.28362				
5179	15553.54	0.29042	0.0068	0.28702	6.100302288	246.7197849
5179	15549.9	0.31763				
5179	15553.74	0.33804	0.02041	0.327835	18.5480257	283.7018905
5179	15553.96	0.678				
5179	15558.86	0.68948	0.01148	0.68374	11.60074195	626.2112662
5189	15551.4	0.31317				
5189	15555.02	0.3221	0.00893	0.317635	8.08928956	274.4154691
5189	15551.4	0.36058				
5189	15553.96	0.36526	0.00468	0.36292	4.299991346	315.8698074
5189	15552.04	0.5262				
5189	15555.88	0.54427	0.01807	0.535235	17.49289808	478.9270643

...

Table A.5: (. . . continued . . .)

Inline (x)	Trace (y)	TWT (s)	Offset (s)	Average Depth (s)	Offset (m)	Average Depth (m)
5189	15555.24	0.81407				
5189	15558.66	0.83235	0.01828	0.82321	19.20111594	770.2315848
5189	15556.52	0.91612				
5189	15560.36	0.92972	0.0136	0.92292	14.67296343	876.5773929
5189	15558.44	0.97969				
5189	15560.78	1.00903	0.02934	0.99436	32.25397946	954.5060735
5199	15549.9	0.35611				
5199	15553.1	0.36058	0.00447	0.358345	4.101196699	311.6553896
5199	15550.76	0.41054				
5199	15553.96	0.42649	0.01595	0.418515	14.90838634	367.5575208
5199	15551.82	0.50813				
5199	15554.38	0.52854	0.02041	0.518335	19.65955716	462.5624839
5199	15555.66	0.75518				
5199	15558.02	0.80046	0.04528	0.77782	46.97406886	722.7550022
5199	15557.58	0.93185				
5199	15560.78	0.99542	0.06357	0.963635	69.32524471	920.8129767
5199	15559.72	1.07472				
5199	15563.34	1.14956	0.07484	1.11214	84.79286557	1086.14477
5199	15562.28	1.24247				
5199	15566.54	1.32177	0.0793	1.28212	93.69948952	1283.063513
5199	15562.5	1.26522				
5199	15566.76	1.35132	0.0861	1.30827	102.3779134	1314.085282
5199	15563.34	1.41021				
5199	15568.68	1.45337	0.04316	1.43179	52.8438146	1463.239401
5199	15564.84	1.4555				
5199	15571.66	1.55075	0.09525	1.503125	118.5637115	1551.350135

. . .

Table A.5: (. . . continued . . .)

Inline (x)	Trace (y)	TWT (s)	Offset (s)	Average Depth (s)	Offset (m)	Average Depth (m)
5199	15565.48	1.501				
5199	15571.02	1.5939	0.0929	1.54745	116.8157121	1606.826133
5199	15565.26	1.53948				
5199	15571.66	1.63239	0.09291	1.585935	117.8504908	1655.444977
5214	15553.54	0.49218				
5214	15556.52	0.51025	0.01807	0.501215	17.31715581	446.0674842
5214	15557.58	0.59189				
5214	15559.3	0.60104	0.00915	0.596465	9.01794184	538.8957464
5214	15557.16	0.77325				
5214	15560.78	0.80046	0.02721	0.786855	28.29829408	732.1587522
5214	15558.86	0.92505				
5214	15562.28	0.99095	0.0659	0.958	71.76002834	914.6626858
5214	15560.78	1.04751				
5214	15565.26	1.13361	0.0861	1.09056	97.01914111	1061.73108
5214	15563.98	1.24481				
5214	15570.38	1.3173	0.07249	1.281055	85.63084247	1281.804214
5214	15565.9	1.34218				
5214	15571.02	1.43296	0.09078	1.38757	110.0007143	1409.345037
5214	15567.82	1.5078				
5214	15573.16	1.59624	0.08844	1.55202	111.3230963	1612.577518
5224	15552.04	0.3357				
5224	15555.24	0.34251	0.00681	0.339105	6.210674628	293.9967962
5224	15558.02	0.58956				
5224	15560.58	0.60316	0.0136	0.59636	13.4033086	538.791999
5224	15559.72	0.75284				
5224	15563.34	0.79812	0.04528	0.77548	46.94377839	720.323274

. . .

Table A.5: (. . . continued . . .)

Inline (x)	Trace (y)	TWT (s)	Offset (s)	Average Depth (s)	Offset (m)	Average Depth (m)
5224	15560.14	0.85723				
5224	15564.42	0.92058	0.06335	0.888905	67.73192972	839.9817001
5224	15560.14	0.89571				
5224	15564.2	0.9614	0.06569	0.928555	70.97839338	882.6716072
5224	15561	0.92505				
5224	15564.84	0.99542	0.07037	0.960235	76.67247666	917.1009868
5224	15563.34	1.06345				
5224	15565.9	1.10193	0.03848	1.08269	43.27343117	1052.860537
5224	15570.6	1.54628				
5224	15575.92	1.63005	0.08377	1.588165	106.3103801	1658.275058
5234	15554.18	0.28808				
5234	15557.8	0.31317	0.02509	0.300625	22.60590622	258.9946454
5234	15559.3	0.64186				
5234	15562.5	0.67587	0.03401	0.658865	34.12584915	601.1045532
5234	15560.14	0.76878				
5234	15564.62	0.796	0.02722	0.78239	28.27394896	727.5086257
5234	15561.42	0.89337				
5234	15566.76	0.96374	0.07037	0.928555	76.0351582	882.6716072
5234	15561.64	0.92972				
5234	15565.68	0.99776	0.06804	0.96374	74.20197396	920.9276639
5249	15562.28	0.35611				
5249	15565.68	0.36526	0.00915	0.360685	8.401188044	313.8102188
5249	15565.04	0.60997				
5249	15569.1	0.63952	0.02955	0.624745	29.36241957	566.9522333
5249	15565.68	0.64186				
5249	15568.24	0.6712	0.02934	0.65653	29.42035629	598.7568143

. . .

Table A.5: (. . . continued . . .)

Inline (x)	Trace (y)	TWT (s)	Offset (s)	Average Depth (s)	Offset (m)	Average Depth (m)
5249	15572.72	1.21993				
5249	15577.64	1.29689	0.07696	1.25841	90.41293514	1255.103999
5259	15562.28	0.28808				
5259	15566.32	0.29956	0.01148	0.29382	10.32106256	252.8483961
5259	15567.18	0.64186				
5259	15570.8	0.67587	0.03401	0.658865	34.12584915	601.1045532
5259	15569.74	0.80492				
5259	15574	0.85042	0.0455	0.82767	47.85072563	774.9281469
5259	15575.72	1.21993				
5259	15582.32	1.30136	0.08143	1.260645	95.71633917	1257.732767
5274	15569.32	0.37652				
5274	15572.72	0.37652	0	0.37652	0	328.4329729
5274	15568.88	0.41054				
5274	15573.58	0.41968	0.00914	0.41511	8.534215852	364.3666225
5274	15568.88	0.43542				
5274	15573.8	0.44009	0.00467	0.437755	4.390712515	385.6495342
5274	15569.1	0.46263				
5274	15574	0.47177	0.00914	0.4672	8.670324063	413.5409811
5274	15570.16	0.50579				
5274	15573.16	0.52386	0.01807	0.514825	17.38746305	459.1738477
5274	15569.96	0.5194				
5274	15573.8	0.53747	0.01807	0.528435	17.45777029	472.3327578
5274	15573.58	0.64186				
5274	15576.56	0.6712	0.02934	0.65653	29.42035629	598.7568143
5274	15575.92	0.80046				
5274	15579.34	0.84128	0.04082	0.82087	42.84958328	767.7697263

. . .

Table A.5: (. . . continued . . .)

Inline (x)	Trace (y)	TWT (s)	Offset (s)	Average Depth (s)	Offset (m)	Average Depth (m)
5274	15580.2	1.14276				
5274	15585.52	1.20632	0.06356	1.17454	73.14659559	1157.481866
5284	15567.4	0.25406				
5284	15571.44	0.26321	0.00915	0.258635	8.13424545	221.278999
5284	15568.46	0.37206				
5284	15574.22	0.37886	0.0068	0.37546	6.272228233	327.4518996
5284	15571.44	0.51493				
5284	15577.42	0.5262	0.01127	0.520565	10.86280501	464.7171937
5284	15573.58	0.64186				
5284	15577.42	0.6712	0.02934	0.65653	29.42035629	598.7568143
5284	15575.92	0.8096				
5284	15580.62	0.84808	0.03848	0.82884	40.48091302	776.161139
5284	15579.76	1.14722				
5284	15584.46	1.20632	0.0591	1.17677	68.05158195	1160.051695
5294	15570.8	0.45583				
5294	15574.22	0.46731	0.01148	0.46157	10.87160169	408.1890089
5294	15570.6	0.50813				
5294	15573.8	0.52173	0.0136	0.51493	13.08671136	459.2751664
5294	15570.16	0.65079				
5294	15577	0.66227	0.01148	0.65653	11.51144138	598.7568143
5294	15574.44	0.81407				
5294	15578.48	0.84128	0.02721	0.827675	28.61582449	774.9334153
5294	15578.28	0.99542				
5294	15580.62	1.0339	0.03848	1.01466	42.52505611	976.9140132
5294	15577.64	1.04538				
5294	15581.48	1.08599	0.04061	1.065685	45.47134301	1033.753625

. . .

Table A.5: (. . . continued . . .)

Inline (x)	Trace (y)	TWT (s)	Offset (s)	Average Depth (s)	Offset (m)	Average Depth (m)
5294	15578.06	1.09513				
5294	15582.1	1.1132	0.01807	1.104165	20.43190603	1077.107176
5294	15578.28	1.1587				
5294	15583.6	1.20399	0.04529	1.181345	52.20908503	1165.328295
5304	15568.04	0.64866				
5304	15574.86	0.66439	0.01573	0.656525	15.77305878	598.7517887
5304	15568.68	0.82087				
5304	15575.92	0.84362	0.02275	0.832245	23.95511756	779.7516716
5304	15573.58	0.99095				
5304	15578.92	1.00903	0.01808	0.99999	19.90476271	960.7089744
5304	15575.92	1.16083				
5304	15581.48	1.20399	0.04316	1.18241	49.76681932	1166.55747

A.6 Fault F

Table A.6: Fault "F" data

Inline (x)	Trace (y)	TWT (s)	Offset (s)	Average Depth (s)	Offset (m)	Average Depth (m)
5850	16105.8	0.94648				
5850	16095.15	0.95567	0.00919	0.951075	9.98900912	907.1167681
5850	16106.3	1.03521				
5850	16095.65	1.03837	0.00316	1.03679	3.51217418	1001.475163
5850	16102.05	1.4424				
5850	16095.15	1.45475	0.01235	1.448575	15.18023247	1483.84183
5850	16103.65	1.52195				
5850	16091.4	1.55267	0.03072	1.53731	38.53935154	1594.08601
5850	16101	1.68419				
5850	16089.25	1.70889	0.0247	1.69654	32.11140432	1797.513367
5850	16099.4	1.73933				
5850	16087.15	1.76689	0.02756	1.75311	36.27527363	1871.517017
5855	16112.2	0.58207				
5855	16106.85	0.58207	0	0.58207	0	524.7016516
5855	16112.2	0.6464				
5855	16106.85	0.65271	0.00631	0.649555	6.314699583	591.752972
5855	16113.25	0.68315				
5855	16105.8	0.68315	0	0.68315	0	625.613738
5855	16111.65	0.72307				
5855	16103.65	0.73226	0.00919	0.727665	9.402058057	670.9740778
5855	16111.65	0.90369				
5855	16102.05	0.88847	-0.01522	0.89608	-16.30398895	847.6737469
5855	16111.65	1.03837				
5855	16102.6	1.04756	0.00919	1.042965	10.23042595	1008.353326

...

Table A.6: (. . . continued . . .)

Inline (x)	Trace (y)	TWT (s)	Offset (s)	Average Depth (s)	Offset (m)	Average Depth (m)
5855	16110.6	1.18827				
5855	16098.85	1.20377	0.0155	1.19602	17.93300706	1182.293849
5855	16109	1.26494				
5855	16097.25	1.28016	0.01522	1.27255	17.94204516	1271.7591
5855	16109	1.32007				
5855	16096.75	1.32926	0.00919	1.324665	10.97051867	1333.633623
5855	16107.9	1.46078				
5855	16095.65	1.48548	0.0247	1.47313	30.53385359	1514.12538
5855	16104.2	1.52223				
5855	16094.6	1.5498	0.02757	1.536015	34.57735574	1592.461044
5855	16099.95	1.69367				
5855	16091.4	1.71808	0.02441	1.705875	31.79953055	1809.66267
5867	16128.7	0.57513				
5867	16118.6	0.59135	0.01622	0.58324	15.92457948	525.8531276
5867	16128.7	0.94203				
5867	16115.9	0.94422	0.00219	0.943125	2.375428559	898.4707192
5867	16123.9	0.95606				
5867	16116.45	0.96768	0.01162	0.96187	12.66614158	918.8856079
5867	16122.85	1.0262				
5867	16117.5	1.03781	0.01161	1.032005	12.88802403	996.1527224
5867	16125	1.10795				
5867	16112.7	1.12198	0.01403	1.114965	15.9071606	1089.350503
5867	16121.8	1.20614				
5867	16110.6	1.21776	0.01162	1.21195	13.49688873	1200.779442
5867	16120.7	1.29031				
5867	16109.5	1.29031	0	1.29031	0	1292.758454

. . .

Table A.6: (. . . continued . . .)

Inline (x)	Trace (y)	TWT (s)	Offset (s)	Average Depth (s)	Offset (m)	Average Depth (m)
5867	16115.9	1.47486				
5867	16105.25	1.49349	0.01863	1.484175	23.08901503	1527.802891
5867	16116.45	1.53798				
5867	16103.15	1.5542	0.01622	1.54609	20.38928951	1605.115705
5867	16121.25	1.56363				
5867	16104.2	1.59869	0.03506	1.58116	44.42354505	1649.389796
5872	16128.2	0.57227				
5872	16120.75	0.59025	0.01798	0.58126	17.64234655	523.9047033
5872	16123.4	0.9501				
5872	16118.05	0.96476	0.01466	0.95743	15.9612229	914.0410639
5872	16125	1.04137				
5872	16116.45	1.06212	0.02075	1.051745	23.15124936	1018.15175
5872	16121.8	1.2065				
5872	16115.4	1.23029	0.02379	1.218395	27.6764477	1208.278845
5872	16116.45	1.46318				
5872	16109	1.48392	0.02074	1.47355	25.64103775	1514.644852
5872	16114.85	1.54284				
5872	16107.4	1.56331	0.02047	1.553075	25.77261187	1613.906087
5872	16111.65	1.69607				
5872	16105.8	1.69911	0.00304	1.69759	3.953085369	1798.878686
5882	16146.85	0.56951				
5882	16139.4	0.58721	0.0177	0.57836	17.35293056	521.0529579
5882	16142.05	0.72274				
5882	16134.6	0.74625	0.02351	0.734495	24.09839489	677.9835208
5882	16134.05	1.06488				
5882	16124.45	1.08563	0.02075	1.075255	23.29071091	1044.496437

. . .

Table A.6: (. . . continued . . .)

Inline (x)	Trace (y)	TWT (s)	Offset (s)	Average Depth (s)	Offset (m)	Average Depth (m)
5882	16128.7	1.28616				
5882	16118.05	1.30663	0.02047	1.296395	24.27052985	1299.973915
5882	16122.85	1.46318				
5882	16113.8	1.49277	0.02959	1.477975	36.61979966	1520.120897
5882	16121.25	1.55473				
5882	16114.85	1.5929	0.03817	1.573815	48.2839901	1640.088223
5892	16160.2	0.56646				
5892	16154.85	0.57836	0.0119	0.57241	11.64641779	515.2094318
5892	16161.25	0.58721				
5892	16155.4	0.58997	0.00276	0.58859	2.713952461	531.1233718
5892	16147.4	1.04442				
5892	16142.05	1.08563	0.04121	1.065025	46.13539229	1033.013699
5892	16146.3	1.16252				
5892	16140.45	1.19488	0.03236	1.1787	37.27926222	1162.276947
5892	16144.7	1.28616				
5892	16135.1	1.3188	0.03264	1.30248	38.75683335	1307.199879
5892	16136.7	1.47203				
5892	16127.65	1.51628	0.04425	1.494155	54.96730714	1540.191328
5892	16132.45	1.56635				
5892	16125.5	1.61945	0.0531	1.5929	67.45974018	1664.288897
5892	16130.85	1.6402				
5892	16122.85	1.71986	0.07966	1.68003	103.1865435	1776.08648
5907	16169.75	0.57531				
5907	16163.9	0.59302	0.01771	0.584165	17.39212481	526.7637575
5907	16167.65	0.73159				
5907	16162.3	0.76395	0.03236	0.74777	33.2926957	691.6451482

. . .

Table A.6: (. . . continued . . .)

Inline (x)	Trace (y)	TWT (s)	Offset (s)	Average Depth (s)	Offset (m)	Average Depth (m)
5907	16161.8	0.98218				
5907	16158.05	1.00293	0.02075	0.992555	22.80013369	952.5193027
5907	16161.8	1.04718				
5907	16155.9	1.09448	0.0473	1.07083	53.03176104	1039.52592
5907	16159.65	1.14454				
5907	16154.3	1.19765	0.05311	1.171095	61.06814254	1153.514656
5907	16157	1.32433				
5907	16147.9	1.38352	0.05919	1.353925	71.15289558	1368.710839
5907	16151.65	1.47784				
5907	16144.7	1.53703	0.05919	1.507435	73.7504747	1556.719955
5907	16151.1	1.57243				
5907	16142.05	1.64324	0.07081	1.607835	90.26135616	1683.299244
5922	16185.75	0.25391				
5922	16183.1	0.25668	0.00277	0.255295	2.459853445	218.3004678
5922	16186.85	0.36593				
5922	16184.15	0.38668	0.02075	0.376305	19.14453252	328.2339559
5922	16193.75	0.41323				
5922	16188.45	0.41904	0.00581	0.416135	5.426625255	365.3268259
5922	16186.3	0.56646				
5922	16182.55	0.58112	0.01466	0.57379	14.35338735	516.5638425
5922	16179.9	0.73159				
5922	16177.75	0.7551	0.02351	0.743345	24.15787609	687.0857178
5922	16177.25	0.95286				
5922	16174.05	0.97057	0.01771	0.961715	19.30363584	918.7163911
5922	16174.05	1.11495				
5922	16167.65	1.18299	0.06804	1.14897	77.80493367	1128.116085

. . .

Table A.6: (. . . continued . . .)

Inline (x)	Trace (y)	TWT (s)	Offset (s)	Average Depth (s)	Offset (m)	Average Depth (m)
5922	16173.5	1.15339				
5922	16168.15	1.22697	0.07358	1.19018	85.00687529	1175.534991
5922	16169.25	1.32433				
5922	16162.3	1.38629	0.06196	1.35531	74.50727317	1370.377212
5922	16165	1.4748				
5922	16157	1.54865	0.07385	1.511725	92.10734049	1562.07009
5922	16163.9	1.54256				
5922	16155.4	1.60756	0.065	1.57506	82.24632993	1641.663791
5937	16202.85	0.42208				
5937	16193.75	0.42208	0	0.42208	0	370.9018829
5937	16197.5	0.57531				
5937	16192.15	0.58997	0.01466	0.58264	14.39047771	525.2625786
5937	16190.55	0.88814				
5937	16185.25	0.91165	0.02351	0.899895	25.21005471	851.7696114
5937	16188.95	1.05631				
5937	16179.35	1.11827	0.06196	1.08729	69.75980146	1058.043219
5937	16188.45	1.11522				
5937	16178.3	1.18299	0.06777	1.149105	77.49879943	1128.270638
5937	16186.85	1.15644				
5937	16178.3	1.22144	0.065	1.18894	75.07137087	1174.101137
5937	16182.05	1.32156				
5937	16172.45	1.39237	0.07081	1.356965	85.18295391	1372.369152
5952	16212.4	0.44255				
5952	16206.55	0.45444	0.01189	0.448495	11.21542977	395.7943846
5952	16210.3	0.57836				
5952	16203.35	0.59606	0.0177	0.58721	17.39771223	529.7631672

. . .

Table A.6: (. . . continued . . .)

Inline (x)	Trace (y)	TWT (s)	Offset (s)	Average Depth (s)	Offset (m)	Average Depth (m)
5952	16207.1	0.74348				
5952	16200.15	0.7728	0.02932	0.75814	30.25199669	702.3519479
5952	16204.95	0.89976				
5952	16198.05	0.95591	0.05615	0.927835	60.65881523	881.8924301
5952	16198.55	1.16225				
5952	16192.7	1.20346	0.04121	1.182855	47.52356105	1167.071164
5952	16200.7	1.23001				
5952	16190.05	1.23001	0	1.23001	0	1221.823814
5952	16197.5	1.32156				
5952	16186.85	1.39514	0.07358	1.35835	88.54433971	1374.03672
5952	16194.3	1.39237				
5952	16186.3	1.47175	0.07938	1.43206	97.19662769	1463.570175
5952	16191.65	1.58682				
5952	16177.75	1.67533	0.08851	1.631075	113.4115557	1713.006634
5972	16218.8	0.42208				
5972	16212.4	0.42789	0.00581	0.424985	5.441324776	373.6297584
5972	16220.95	0.46634				
5972	16212.95	0.47214	0.0058	0.46924	5.505338721	415.4824586
5972	16222.55	0.72578				
5972	16210.8	0.75814	0.03236	0.74196	33.23894694	685.6597832
5972	16213.5	1.06793				
5972	16202.3	1.13265	0.06472	1.10029	73.10777058	1072.722381
5972	16210.3	1.13569				
5972	16202.3	1.20927	0.07358	1.17248	84.63455489	1155.109197
5972	16211.35	1.16805				
5972	16202.3	1.25075	0.0827	1.2094	95.99760359	1197.815515

. . .

Table A.6: (. . . continued . . .)

Inline (x)	Trace (y)	TWT (s)	Offset (s)	Average Depth (s)	Offset (m)	Average Depth (m)
5972	16211.9	1.23582				
5972	16201.25	1.31852	0.0827	1.27717	97.59984064	1277.213159
5972	16208.7	1.33318				
5972	16199.65	1.41588	0.0827	1.37453	99.90165263	1393.55808
5972	16209.75	1.40703				
5972	16196.95	1.49554	0.08851	1.451285	108.8622864	1487.175662
5972	16205.5	1.48945				
5972	16197.5	1.57216	0.08271	1.530805	103.6088761	1585.928341
5972	16203.9	1.60175				
5972	16192.15	1.67837	0.07662	1.64006	98.37321123	1724.533111
5972	16201.25	1.63411				
5972	16191.1	1.71654	0.08243	1.675325	106.6637532	1769.994429
5972	16199.65	1.68418				
5972	16189.5	1.76384	0.07966	1.72401	104.1881089	1833.335643
5987	16233.75	0.38059				
5987	16224.15	0.38059	0	0.38059	0	332.2028856
5987	16232.15	0.39829				
5987	16219.9	0.42208	0.02379	0.410185	22.17974263	359.7571188
5987	16230.55	0.44863				
5987	16221.5	0.4514	0.00277	0.450015	2.614049798	397.2327981
5987	16230	0.4868				
5987	16222	0.49566	0.00886	0.49123	8.465577895	436.4853949
5987	16220.95	0.74625				
5987	16216.15	0.7847	0.03845	0.765475	39.75283953	709.9435962
5987	16216.15	1.09448				
5987	16208.15	1.13873	0.04425	1.116605	50.1912279	1091.212568

. . .

Table A.6: (. . . continued . . .)

Inline (x)	Trace (y)	TWT (s)	Offset (s)	Average Depth (s)	Offset (m)	Average Depth (m)
5987	16215.1	1.17414				
5987	16205.5	1.25075	0.07661	1.212445	88.99506193	1201.355007
5987	16214.55	1.23886				
5987	16202.85	1.31852	0.07966	1.27869	94.04674713	1279.008892
5987	16211.9	1.33318				
5987	16202.3	1.42473	0.09155	1.378955	110.7082708	1398.909826
5987	16204.95	1.5929				
5987	16197.5	1.69884	0.10594	1.64587	136.1934252	1731.998708
5997	16232.15	0.41019				
5997	16219.9	0.42485	0.01466	0.41752	13.69845965	366.6247449
5997	16218.8	1.07069				
5997	16212.95	1.14454	0.07385	1.107615	83.57567399	1081.014642
5997	16216.15	1.1769				
5997	16208.7	1.25656	0.07966	1.21673	92.63571961	1206.340322
5997	16212.4	1.44824				
5997	16202.3	1.53371	0.08547	1.490975	106.0930506	1536.240843
5997	16207.1	1.58986				
5997	16195.35	1.69303	0.10317	1.641445	132.5018806	1726.311907
5997	16207.1	1.62526				
5997	16192.15	1.72262	0.09736	1.67394	125.9445034	1768.202323
5997	16208.15	1.67533				
5997	16192.15	1.77573	0.1004	1.72553	131.3577894	1835.324051
6012	16232.7	0.62933				
6012	16224.75	0.665	0.03567	0.647165	35.67219478	589.3562639
6012	16229.55	0.74667				
6012	16223.925	0.78933	0.04266	0.768	44.13628513	712.5604762

. . .

Table A.6: (. . . continued . . .)

Inline (x)	Trace (y)	TWT (s)	Offset (s)	Average Depth (s)	Offset (m)	Average Depth (m)
6012	16225.5	0.88167				
6012	16218.3	0.94933	0.06766	0.9155	72.85447065	868.5664531
6012	16223.1	1.10933				
6012	16211.925	1.18733	0.078	1.14833	89.18009727	1127.383459
6012	16223.925	1.17667				
6012	16211.925	1.262	0.08533	1.219335	99.29284568	1209.373614
6012	16222.35	1.255				
6012	16209.525	1.344	0.089	1.2995	105.6030443	1303.659803
6012	16218.3	1.34033				
6012	16208.7	1.429	0.08867	1.384665	107.3703283	1405.823905
6012	16218.3	1.454				
6012	16204.725	1.56067	0.10667	1.507335	132.9072924	1556.595305
6012	16219.125	1.51433				
6012	16201.5	1.614	0.09967	1.564165	125.8048186	1627.890902
6012	16215.15	1.59267				
6012	16200.75	1.69933	0.10666	1.646	137.1230005	1732.165861
6012	16213.5	1.63167				
6012	16200.75	1.742	0.11033	1.686835	143.1291661	1784.908728
6012	16212.75	1.67433				
6012	16201.5	1.79867	0.12434	1.7365	163.0695003	1849.69403
6022	16238.325	0.47667				
6022	16223.925	0.49433	0.01766	0.4855	16.84489811	430.9993819
6022	16235.925	0.576				
6022	16227.9	0.601	0.025	0.5885	24.5822595	531.0346463
6022	16231.125	0.832				
6022	16223.1	0.85333	0.02133	0.842665	22.52343633	790.7598726

. . .

Table A.6: (. . . continued . . .)

Inline (x)	Trace (y)	TWT (s)	Offset (s)	Average Depth (s)	Offset (m)	Average Depth (m)
6022	16223.1	1.255				
6022	16217.55	1.27267	0.01767	1.263835	20.7861955	1261.487245
6022	16215.9	1.60333				
6022	16207.125	1.71333	0.11	1.65833	141.8046718	1748.041552
6027	16251.15	0.46967				
6027	16239.9	0.473	0.00333	0.471335	3.162818182	417.4775086
6027	16234.35	0.793				
6027	16227.15	0.80367	0.01067	0.798335	11.13177636	744.1406963
6027	16227.15	1.255				
6027	16222.35	1.28	0.025	1.2675	29.4350725	1265.804339
6027	16223.925	1.34033				
6027	16217.55	1.35467	0.01434	1.3475	17.21191912	1360.987667
6032	16240.725	0.61167				
6032	16234.35	0.633	0.02133	0.622335	21.17990356	564.5524377
6032	16223.1	1.614				
6032	16212.75	1.71333	0.09933	1.663665	128.2011138	1754.924085
6032	16212.75	1.87				
6032	16199.925	1.99433	0.12433	1.932165	170.0109967	2111.737099
6042	16242.3	0.523				
6042	16235.925	0.54433	0.02133	0.533665	20.63920982	477.4033906
6042	16232.7	1.20167				
6042	16223.925	1.29767	0.096	1.24967	112.5413433	1244.837767
6042	16231.95	1.25867				
6042	16225.5	1.36533	0.10666	1.312	126.9386856	1318.525993
6042	16234.35	1.34033				
6042	16222.35	1.454	0.11367	1.397165	138.0489788	1420.992089

. . .

Table A.6: (. . . continued . . .)

Inline (x)	Trace (y)	TWT (s)	Offset (s)	Average Depth (s)	Offset (m)	Average Depth (m)
6042	16231.95	1.47167				
6042	16217.55	1.56433	0.09266	1.518	115.7338077	1569.905156
6042	16227.15	1.61033				
6042	16217.55	1.724	0.11367	1.667165	146.8228933	1759.443722
6047	16243.125	0.523				
6047	16236.75	0.54067	0.01767	0.531835	17.08849779	475.6282714
6047	16243.125	0.61167				
6047	16231.95	0.633	0.02133	0.622335	21.17990356	564.5524377
6047	16238.325	0.896				
6047	16228.725	0.96367	0.06767	0.929835	73.14255612	884.057174
6047	16235.925	1.16967				
6047	16223.1	1.28	0.11033	1.224835	128.5571592	1215.7842
6047	16231.95	1.33667				
6047	16219.95	1.454	0.11733	1.395335	142.4325622	1418.768697
6047	16230.3	1.47167				
6047	16217.55	1.589	0.11733	1.530335	146.9607728	1585.339397
6047	16230.3	1.60333				
6047	16217.55	1.724	0.12067	1.663665	155.7437673	1754.924085
6047	16219.125	1.99067				
6057	16243.125	0.626				
6057	16235.925	0.64	0.014	0.633	13.94416856	575.1847678
6057	16232.7	1.28				
6057	16224.75	1.37933	0.09933	1.329665	118.716696	1339.610473
6057	16235.925	1.344				
6057	16224.75	1.45767	0.11367	1.400835	138.1682391	1425.453886
6057	16232.7	1.47167				

. . .

Table A.6: (. . . continued . . .)

Inline (x)	Trace (y)	TWT (s)	Offset (s)	Average Depth (s)	Offset (m)	Average Depth (m)
6057	16219.125	1.582	0.11033	1.526835	138.0825836	1580.955615
6057	16226.325	1.60333				
6057	16217.55	1.72067	0.11734	1.662	151.3900216	1752.775249

Bibliography

D.I. Andrews. The Louann salt and its relationship to Gulf Coast salt domes. *Gulf Coast Association of Geological Societies Transactions*, 10:215–240, 1960. 4

A. Aslan, W.J. Autin, and M.D. Blum. Causes of river avulsion: Insight from the Late Holocene avulsion history of the Mississippi River, U.S.A. *Journal of Sedimentary Research*, 75:650–664, 2005. 7

Andrew Beall, Paul F. Connor Jr., Sarah Fearnley, Shea Penland, and S. Jeffress Williams. Changes in louisiana's shoreline: 1855-2002. *Journal of Coastal Research*, Special Issue:7–39, Spring 2005. 1, 8

D.S. Biedenharn, C.R. Thorne, and C.C. Watson. Recent morphological evolution of the Lower Mississippi River. *Geomorphology*, 35:227–249, 2000. 7, 8

R. Boyd, J. Suter, and S. Penland. Sequence stratigraphy of the Mississippi Delta. *Gulf Coast Association of Geological Societies Transactions*, 39:331–340, 1989. 7

R.T. Buffler, J.S. Watkins, J. Schaub, and J.L. Worzel. *Structure and early geological history of the deep central Gulf of Mexico basin*, pages 3–16. Louisiana State University, 1980. 3

Satinder Chopra. Coherence cube and beyond. *First Break Technical Article*, 20(1):27–33, 2002. 35

J.M. Coleman. Dynamic changes and processes in the Mississippi River Delta. *Geological Society of America Bulletin*, 100:999–1015, 1988. 7, 8

J.M. Coleman, H.H. Roberts, and W.R. Bryant. *Late Quaternary Sedimentation*, pages 325–388. Volume J of , Salvador (1991b), 1991. 6, 7

J.W. Day, D.F. Boesch, E.J. Clairain, G.P. Kemp, S.B. Laska, W.J. Mitsch, K. Orth, H. Mashriqui, D.J. Reed, L. Shabman, C.A. Simenstad, B.J. Streever, R.J. Twilley, C.C. Watson, J.T. Wells, and D.F. Whigham. Restoration of the Mississippi Delta: Lessons from Hurricanes Katrina and Rita. *Science*, 315: 1679–1684, 2007. 8

F.A. Diegel, J.F. Karlo, D.C. Schuster, R.C. Shoup, and P.R. Tauvers. *Cenozoic structural evolution and tectono-stratigraphic framework of the northern Gulf coast continental margin*, pages 19–09–151. Volume 65 of , Jackson et al. (1995), 1995. 4, 7

T.H. Dixon, F. Amelung, A. Ferretti, F. Rocca, R. Dokka, G. Sella, S.W. Kim, S. Wdowinski, and D. Whitman. Subsidence and flooding in New Orleans. *Nature*, 441:587–588, 2006. 28

Milton B. Dobrin and Carl H. Savit. *Introduction to Geophysical Prospecting*. McGraw-Hill Book Company, Fourth edition, 1988. 38

R.K. Dokka. Modern-day tectonic subsidence in coastal Louisiana. *Geology*, 34 (4):281–284, 2006. 2, 13, 15, 18, 22, 23, 46, 70, 71, 75

R.K. Dokka, G.F. Sella, and T.H. Dixon. Tectonic control of subsidence and southward displacement of southeast louisiana with respect to stable north

america. *Geophysical Research Letters*, 33:L23308, 2006. 2, 7, 10, 13, 15, 18, 21, 22, 23, 28, 61, 71

J.A. Dunbar and D.S. Sawyer. Continental rifting at pre-existing lithospheric weaknesses. *Nature*, 333:450–452, 1988. 3

H.N. Fisk. Geological investigation of the alluvial valley of the Lower Mississippi River. Technical report, Mississippi River Commission, Vicksburg, Miss, 1944. 6, 7

H.N. Fisk, E. McFarlan, C.R. Kolb, and L.J. Wilbert. Sedimentary framework of the modern Mississippi Delta. *Journal of Sedimentary Research*, 24(2): 76–99, 1954. 6, 7, 8

Sherwood M. Gagliano. Effects of earthquakes, fault movements, and subsidence on the south louisiana landscape. *The Louisiana Civil Engineer Journal of the Louisiana Section of The American Society of Civil Engineers*, 13 (2):5–7, 19–22, 2005a. 7, 10, 13

Sherwood M. Gagliano. Effects of geological faults on levee failures in South Louisiana. In *Testimony of Sherwood Gagliano, Ph.D.*, pages 1–28, Washington, D.C., November 2005b. U.S. Senate Committee on Environment and Public Works, Senator James M. Inhofe, Chairman. 1, 10, 13, 14, 15, 25

Sherwood M. Gagliano. Effects of natural fault movement on land submergence in coastal louisiana. In *Proceedings of the 14^{th} Biennial Coastal Zone Conference*, pages 1–5, New Orleans, La., July 2005c. Federal Geographic Data Committee. 2, 10, 13

Sherwood M. Gagliano, E. Burton Kemp, III, Karen M. Wicker, Kathleen S. Wiltenmuth, and Robert W. Sabate. Neo-tectonic framework of southeast louisiana and applications to coastal restoration. In Gregory W. Stone,

John H. Wrenn, and Samuel J. Bentley, editors, *Transactions of the 53rd annual convention; 50th GCSSEPM anniversary*, volume 53, pages 262–276, Louisiana State University, Department of Oceanography and Coastal Sciences, Baton Rouge, LA, United States, October 2003. 13, 15, 23, 24, 26, 61

Sherwood M. Gagliano, Klaus J. Meyer-Arendt, and Karen M. Wicker. Land loss in the mississippi river deltaic plain. *Gulf Coast Association of Geological Societies Transactions*, 31:295–300, 1981. 1, 8

William E. Galloway, Patricia E. Ganey-Curry, Xiang Li, and Richard T. Buffler. Cenozoic depositional history of the gulf of mexico basin. *AAPG Bulletin*, 84 (11):1743–1774, November 2000. 5, 6

Juan L. González and Torbjörn E. Törnqvist. Coastal louisiana in crisis: Subsidence or sea level rise? *EOS, Transactions American Geophysical Union*, 87 (45):493, November 2006. 60

Rutger Gras, Keith Tushingham, , and George A. Jamieson. Interpretation of the evolution of a salt body in the gulf of mexico. *The Leading Edge*, 17(10): 1378–1385, October 1998. 6

M. Hickey and R. Sabate. Tectonic map of Gulf coast region, U.S.A., 1972. 13, 22, 23

C.C. Humphris. *Salt movement on continental slope*, volume 7 of *Studies in Geology*, pages 69–85. American Association of Petroleum Geologists, 1978. 3

M. P. A. Jackson, B. C. Vendeville, and D. D. Schultz-Ela. Structural dynamics of salt systems. *Annual Reviews of Earth and Planetary Sciences*,

22:93–117, 1994a. URL http://dx.doi.org/10.1146/annurev.ea.22.050194.000521. 6

M.P.A. Jackson, D.G. Roberts, and S. Snelson, editors. *Salt tectonics: a global perspective*, volume 65 of *AAPG Memoir*. American Association of Petroleum Geologists, 1995. 159, 165

M.P.A. Jackson, B. C. Vendeville, and D. D. Schultz-Ela. Salt-related structures in the Gulf of Mexico; a field guide for geophysicists. *The Leading Edge*, 13 (8):837–842, August 1994b. 6

Mark Kulp, Paul Howell, Sandra Adiau, Shea Penland, Jack Kindinger, and W.S. Jeffress. Latest Quaternary Stratigraphic Framework of the Mississippi River Delta Region. *Gulf Cost Association of Geological Societies Transactions*, 52:573–582, 2002. ISSN 0533-6562. 6, 7

Schlumberger Limited. Online oilfield glassary, 2008. 35, 38

John A. Lopez, Shea Penland, and Jeff Williams. Confirmation of active geologic faults in lake pontchartrain in southeast louisiana. *Coast Association of Geological Societies Transactions* 47^{th} *Annual Convention*, 47:299–303, 1997. 10, 11, 13, 15, 16, 28, 60, 70, 75

Steven J. Maione. Discovery of ring faults associated with salt withdrawal basins, early cretaceous age, in the east texas basin. *The Leading Edge*, 20 (8):819–829, August 2001. 4

Kurt J. Marfurt, R. Lynn Kirlin, Steven L. Farmer, and Michael S. Bahorich. 3-d seismic attributes using a semblance-based coherency algorithm. *Geophysics*, 63(4):1150–1165, 1998. ISSN 0016-8033. 35, 36

Barry C. McBride. The evolution of allochthonous salt along a megaregional profile across the northern gulf of mexico basin. *AAPG Bulletin*, 82(5B):1037–1054, May 1998. 22, 23, 24

E. McFarlan. Radiocarbon dating of late quaternary deposits, south louisiana. *The Geological Society of America Bulletin*, 72(1):129–158, January 1961. 6

T.A. Meckel, U.S. ten Brink, and S.J. Williams. Numerical constraints of current rates of subsidence due to compaction of shallow sediments in the Louisiana coastal plain. In *Fall Meet. Suppl.*, pages Abstract G21D–06. American Geophysical Union, 2005. 2

T.A. Meckel, U.S Ten Brink, and S.J. Williams. Sediment compaction rates and subsidence in deltaic plains: numerical constraints and stratigraphic influences. *Basin Research*, 19(1):19–31(13), January 2007. 7, 28

T.A. Meckel, U.S. ten Brink, and S.Jeffress Williams. Current subsidence rates due to compaction of holocene sediments in southern louisiana. *Geophysical Research Letters*, 33:L.11403, 2006. 2, 11, 12, 60

J.P. Morgan and P.B. Larimore. Changes in the louisiana shoreline. *Coast Association of Geological Societies Transactions*, 7:303–310, 1957. 1, 6

R.A. Morton, N.A. Purcell, and R. Peterson. Field evidence of subsidence and faulting induced by hydrocarbon production in coastal southeast texas. *Gulf Coast Association of Geological Societies Transactions*, 51:239–248, 2001. 2, 10, 12, 28

Robert A. Morton, Julie C. Bernier, John A. Barras, and Nicholas F. Ferina. Rapid subsidence and historical wetland loss in the Mississippi Delta Plain: Likely causes and future implications. Open File Report 1216, USGS, 2005.

URL http://pubs.usgs.gov/of/2005/1216/ofr-2005-1216.pdf. 1, 2, 12, 60

Robert A. Morton, Noreen A. Buster, and M. Dennis Krohn. Subsurface controls on historical subsidence rates and associated wetland loss in Southcentral Louisiana. *Gulf Coast Association of Geological Societies Transactions*, 52: 767–778, October 2002. 28

Fernando A. Neves, Mohammad S. Zahrani, and Stephen W. Bremkamp. Detection of potential fractures and small faults using seismic attributes. *The Leading Edge*, 23(9):903–906, September 2004. 34, 35

Chris Paola. Quantitative models of sedimentary basin filling. *Sedimentology*, 47(Suppl. 1):121–178, 2000. 60

Shea Penland, Ron Boyd, and John R. Suter. Transgressive depostional systems of the mississippi delta plain: A model for barrier shoreline and shelf sand development. *Journal of Sedimentary Petrology*, 58(6):932–949, November 1988. 7

Harry H. Roberts, Alan Bailey, and Gerald J. Kuecher. Subsidence in the mississippi river delta–important influences of valley filling by cyclic deposition, primary consolidation phenomena, and early diagenesis. *Gulf Coast Association of Geological Societies Transactions*, 44:619–629, 1994. 28

W.F. Ruddiman and H.E. Wright, editors. *North America and adjacent oceans during the last deglaciation: The Geology of North America*, volume k–3. Geological Society of America, Boulder, Colorado, 1987. 6

A. Salvador. *Origin and development of the Gulf of Mexico basin*, pages 389–444. Volume J of , Salvador (1991b), 1991a. 3, 4, 5, 6, 7

Amos Salvador, editor. *The Gulf of Mexico Basin: The Geology of North America*, volume J. Geological Society of America, Boulder, Colorado, 1991b. 159, 164, 165

D.C. Schuster. *Deformation of allochthonous salt and evolution of related salt-structural systems, Eastern Louisiana Gulf Coast*, pages 177–198. Volume 65 of , Jackson et al. (1995), 1995. 6, 14

Kurt D. Shinkle and Roy K. Dokka. Rates of vertical displacement at benchmarks in the Lower Mississippi Valley and the Northern Gulf Coast. NOAA Technical Report 50, U.S. Department of Commerce, National Oceanic and Atmospheric Administration, National Ocean Service, July 2004. 17, 18, 19, 22, 28, 60

G.A. Snedden, J.E. Cable, and W.J. Wiseman Jr. Subtidal Sea Level Variability in a Shallow Mississippi River Deltaic Estuary, Louisiana. *Estuaries and Coasts*, 30(5):802–812, 2007. vii

N.F. Sohl, E.R. Martinez, P. Salmeron-Urena, and F. Soto-Jaramillo. *Upper Creatceous*, pages 205–244. Volume J of , Salvador (1991b), 1991. 4

D.J. Stanley, A.G. Warne, and J.B. Dunbar. Eastern mississippi delta: late wisconsin unconformity, overlying transgressive facies, sea level and subsidence. *Engineering Geology*, 45(1):359–381(23), December 1996. 60

G.W. Stone, Sheremet. A., X. Zhang, and D. Braud. Wave and storm protection provided by louisiana's gulf shoreline: Barrier islands and shell reefs. Technical Series 04–003, University of New Orleans, Pontchartrain Institute for Environmental Sciences, 2004. 8

S.C. Strover, S. Ge, P. Weimer, and B.C. McBride. The effects of salt evolution, structural development, and fault propogation on Late Mesozoic-Cenozoic oil

migration: A two-deminsional fluid-flow study along a mega-regional profile in the Northern Gulf of Mexico Basin. *American Association of Petroluem Geologists Bulletin*, 85:11, 2001. 23

John Suppe. *Principles of Structural Geology*. Prentice-Hall, Inc, First edition, 1985. 13

Torbjörn E. Törnqvist, Scott J. Bick, Klaas van der Borg, and Arie F.M. de Jong. How stable is the mississippi delta? *Geology*, 34(8):697–700, August 2006. 2, 28

Torbjörn E. Törnqvist, Davin J. Wallace, Joep E. A. Storms, Jakob Wallinga, Remke L. van Dam, Martijn Blaauw, Mayke S. Derksen, Cornelis J. W. Klerks, Camiel Meijneken, and Els M. A. Snijders. Mississippi delta subsidence primarily caused by compaction of holocene strata. *Nature Geoscience*, 1:173–176, February 2008. URL `http://www.nature.com/ngeo/journal/v1/n3/full/ngeo129.html`. 2, 7, 8, 10, 12, 28

R.E. Turner and D.R. Cahoon. Causes of wetland loss in the coastal central gulf of mexico. Executive Summary and Technical Narrative 1–3, US Department of the Interior, Minerals Management Service, January 1988. 1

USGS. 100+ years of land change for Southeast Coastal Louisiana, 2003. 8

W.E. Wallace. Fault and salt map of South Louisiana. *Gulf Coast Association of Geological Societies*, 16:373, 1966. 23

S.J. Williams, S. Penland, and A. H. Sallenger Jr. Louisiana barrier island erosion study: Atlas of shoreline changes in louisiana from 1853-1989. Miscellaneous Investigations I-2150-A, U.S. Geological Survey in cooperation with the Louisiana Geological Survey, 1992. 1, 7, 8

D.M. Worrall and S. Snelson. *Evolution of the northern Gulf of Mexico, with an emphasis on Cenozoic growth faulting and the role of salt*, volume A, pages 97–138. Geological Society of America, Boulder, Colorado, 1989. 6, 7

D.A. Yurewicz, T.B. Marler, K.A. Meyerholtz, and F.X. Siroky. *Early Cretaceous carbonate platform, north rim of the Gulf of Mexico, Mississippi and Louisiana*, pages 81–96. Memoir 56. American Association of Petroleum Geologists, 1993. 4

Vita

Terra Jane George, daughter of Terry Lee and Kathy Lee George, was born on March 20, 1983 in Okmulgee, Oklahoma. Upon receipt of her diploma in 2001 from Morris High School, in Morris, Oklahoma, she entered Oklahoma State University in Stillwater, Oklahoma. While at Oklahoma State, she held internship positions with the Natural Resources Conservation Service, Lamamco Drilling Company, and Chesapeake Energy Corporation, and in May 2006, she completed a Bachelor of Science in Geology. In August 2006, she entered the Jackson School of Geosciences at University of Texas at Austin to pursue a Master of Science in Geosciences. She also held an internship position with ConocoPhillips Co. in Summer 2007.

Permanent Address: 118 E. 8th St.
Okmulgee OK 74447

This thesis was typeset with LaTeX 2_ε[1] by the author with the help of Aymeric-Pierre B. Peyret.

[1] LaTeX 2_ε is an extension of LaTeX. LaTeX is a collection of macros for TeX. TeX is a trademark of the American Mathematical Society. The macros used in formatting this thesis were written by Dinesh Das, Department of Computer Sciences, The University of Texas at Austin, and extended by Bert Kay, James A. Bednar, and Ayman El-Khashab.